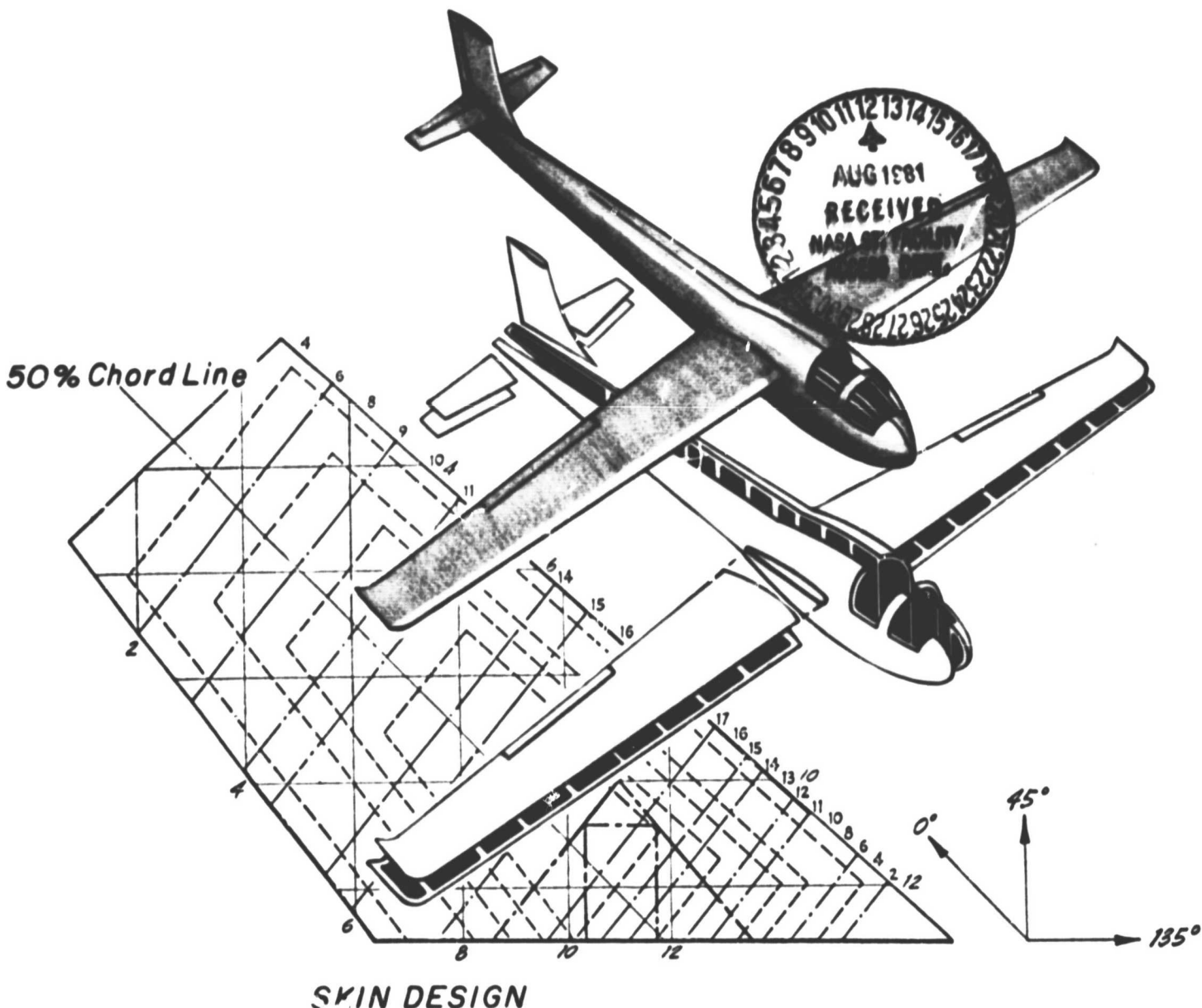**N O T I C E**

THIS DOCUMENT HAS BEEN REPRODUCED FROM
MICROFICHE. ALTHOUGH IT IS RECOGNIZED THAT
CERTAIN PORTIONS ARE ILLEGIBLE, IT IS BEING RELEASED
IN THE INTEREST OF MAKING AVAILABLE AS MUCH
INFORMATION AS POSSIBLE

COMPOSITE STRUCTURAL PROGRAM

RENSSELAER POLYTECHNIC INSTITUTE   TROY, N.Y. 12181

50% Chord Line

SKIN DESIGN

0°   45°   135°

SPONSORED BY
NASA/AFOSR

Semi-Annual Progress Report

September 30, 1980 through April 30, 1981

COMPOSITE STRUCTURAL MATERIALS

Air Force Office of Scientific Research

and

National Aeronautics and Space Administration

Grant No. NGL 33-018-(03

Co-Principal Investigators:

George S. Ansell
Dean, School of Engineering

Robert G. Loewy
Institute Professor

and

Stephen E. Wiberley
Professor of Chemistry

Rensselaer Polytechnic Institute

Troy, New York   12181

40th Semi-Annual Report   July 1981

CONTENTS

LIST OF TABLES

LIST OF FIGURES

INTRODUCTION

INTRODUCTION

The promise of filamentary composite materials, whose development may be considered as entering its second generation, continues to generate intense interest. Such interest is well founded, since it is based on the possibility of using relatively brittle materials with high modulus, high strength, but low density in composites with good durability and high tolerance to damage and which, when they do fail, do so in a non-catastrophic manner. Such fiber reinforced composite materials offer substantially improved performance and potentially lower costs for aerospace hardware.

Much progress has been achieved since the initial developments in the mid 1960's. Only a very few applications to primary aircraft structure have been made, however, and those are in a material-substitution mode and - with the exception of experiments only just now being conducted on large passenger airplanes - on military aircraft.

To fulfill the promise of composite materials more completely, requires a strong technology base. NASA and AFOSR have realized that to fully exploit composites in sophisticated aerospace structures the technology base must be improved. This, in turn, calls for expanding fundamental knowledge and the means by which it can be successfully applied in design and manufacture. Not the least of this effort is to learn how to design structures specifically to capitalize on the unique properties of composite materials.

It also calls for expanding the body of engineers and scientists competent i- these areas. As part of their approach to accomplishing this, NASA and AFOSR have funded the current composites program at Rensselaer. The purpose of the RPI composites program is to develop advanced technology in the areas of physical properties, structural concepts and analysis, manufacturing, reliability and life prediction. Concommitant goals are to educate engineers to design and use composite materials as normal or conventional materials. A multifaceted program has been instututed to achieve these objectives. The major elements of the program are:

1. **CAPCOMP** (**C**omposite **A**ircraft **P**rogram **C**omponent). CAPCOMP is primarily a graduate level project being conducted in parallel with a composite structures program sponsored by NASA and performed by a private, aerospace manufacturing contractor. The first component redesign is being done in conjunction with the Boeing Commercial Airplane Company. The main spar/rib region on the Boeing 727 elevator, near its actuator attachment point, was selected, with Boeing's advice and the concurrence of NASA/AFOSR, for study in CAPCOMP. The magnitude of the project - studying, designing, fabricating and testing of a relatively small but highly stressed region on the elevator - is both consistent with Rensselaer's capabilities and a significant challenge. The selection of a portion of a full-scale flight hardware structure assures relevance to this project's direction.

Visits to Boeing were conducted by Professor Hoff and several of his students, and the first serious design work began on two alternative designs. Each was pursued to the point of preliminary analysis and testing. One of these was selected for more detailed analysis, redesign, complete fabrication and testing. Successful completion of the test of the first CAPCOMP structural parts is reported in Part I, as well as progress on additional test specimens and choice of a second possible aircraft component for redesign, as CAPCOMP Phase II.

2. CAPGLIDE (Composite Aircraft Program Glider). This undergraduate demonstration project has as its objectives the design, fabrication and testing of a foot-launched, ultralight glider using composite structures. A flight vehicle was selected to maximize student interest and to provide the students with a broad-based engineering experience. For those students continuing with graduate work at RPI, CAPGLIDE is intended to provide natural progression to CAPCOMP. The progress on the CAPGLIDE project to date has been very good. Seven professors and approximately 46 students were actively engaged in the project during this period; that is, the Fall 1980 and Spring 1981 semesters. High point of the project to date was initial flight testing of the glider, dubbed "RP-1", and first public flight demonstration on September 16, 1980. Since then, design and construction of the RP-2 has begun. A description of the status

of the CAPGLIDE project at the end of the current reporting period is given in Part II.

3. <u>COMPAD</u> (<u>Comp</u>uter <u>A</u>ided <u>D</u>esign). A major thrust of the composites program is to develop effective and efficient tools for the analysis and design of composite structures. Rensselaer and NASA Langley have jointly implemented the use of the SPAR code on minicomputers, and the work at Rensselaer has made "virtual memory" available to those using SPAR. Special RPI software has been developed to make existing programs more useful, particularly as regards graphics. Attention for the past year has focused on interactive graphics preprocessor and postprocessor capabilities for use in finite element analyses. During the current period efforts have begun on finite element applications to investigate moisture effects and the micromechanics of failure in composites. Details are reported in Part III.

4. <u>Composites Fabrication and Test Facility.</u> Structural design engineers, educated only by course work and design projects limited to paper, often fail to sense or appreciate problems involved in fabrication. The actual fabrication and testing of composite structural components provides this training and the final validation for the designs in our CAP projects. RPI's Composites Fabrication and Test Facility is located in the laboratory and high bay areas of the Jonsson Engineering Center. Equipment is available for compression molding parts as large as 19" x 19" and vacuum

bagging parts of much larger size. Panels, approximately 4' x 20', have been made by vacuum bagging. A pressure vessel for long narrow parts, such as spars, has been designed and built. All of these techniques and facilities have been used in the CAPGLIDE part of the project, described in Part II. A second vessel capable of fabricating shorter but wider parts at higher pressures has been designed and used in the CAPCOMP part of the program. Special loading devices and other test equipment were used on CAPCOMP in the current period. More information is contained in Part I.

5. INSURE (Innovative and Supporting Research). The criteria for selecting research projects to be conducted under this program include the following: (a) they must anticipate critical problem areas which may occur in the CAP or NASA/AFOSR programs or (b) solutions to existing problems are not yet satisfactorily in hand. During the reporting period six such projects were conducted as part of the program. Results from the ongoing projects are reported in Part IV.

6. Curriculum Revisions. The goal of educating engineers to think of composites as normal or conventional materials has required changes in curriculum. Since the initiation of this program, almost all Rensselaer engineers take introductory courses which incorporate the concepts of anisotropy and composite materials. In addition, six specialized courses in composites have been offered during the past

three years to develop those special skills required of students involved in the composites program. A new course was introduced in the Fall of '78 semester on composite design and analysis using programmable hand calculators, a central mini and full frame computers. A new graduate level advanced topics course with the title "Advanced Finite Elements" was offered for the first time in September 1979.

The additions of the SAP and SPAR computer codes and the growing availability of interactive computer graphics under our COMPAD program element have reached the point where our engineering students are using these facilities as everyday working tools for design, analysis and visualization purposes. We have thus achieved one of the principal goals of the curriculum development activities.

7. _Technical Interchange_. Technical meetings, on- and off-campus, provide important opportunities for interchange of technical information. Because of the large number of composites meetings, a central catalog with all upcoming meetings is being maintained and distributed periodically. In this way we help assure that a Rensselaer staff member will participate in important meetings. The calendar for this reporting period is shown in Table 1. Meetings attended by RPI composites program faculty/staff during the reporting period are shown in Table 2. Some meetings particularly relevant to composites, held on-campus with special

TABLE 1

CALENDAR OF COMPOSITES-RELATED MEETINGS

(September 30, 1980 through April 30, 1981)

1980

10/6-8	Symposium on Computational Methods in Nonlinear Structural and Solid Mechanics, Washington, D. C. "Sponsored by George Washington University and NASA Langley."
10/7-9	12th National SAMPE Technical Conference, Seattle, WA.
10/13-16	1980 SAE Aerospace Congress and Exposition, Los Angeles, CA.
10/20-23	Flywheel Technology Symposium, Tamarron, CO. "Sponsored by ASME."
10/22-24	National Specialists Meeting "Rotor System Design", Philadelphia, PA. "Sponsored by AHS."
10/28-30	Mechanics of Composites Review, Dayton, OH.
11/5-7/80	Ultrasonics Symposium, Boston, MA.
11/12-13	Mechanical Testing for Deformation Modeling Development, Bal Harbour, FL. "Sponsored by ASTM."
11/13-14	Damage in Composite Materials: Basic Mechanisms, Accumulation, Tolerance and Characterization, Bal Harbour, FL. "Sponsored by ASTM."
11/18-19	Large Space Structures Conference, Hampton, VA.
12/2-3	Technology Conference: Reinforced Plastics, El Segundo, CA.
12/15-17	1980 SES National Meeting, Atlanta, GA.

1981

1/12-15	19th Aerospace Sciences Meeting, St. Louis, MO. "Sponsored by AIAA."
1/19-23	Gordon Research Conference, Ventura, CA.
1/22	Society for Experimental Stress Analysis, Schenectady, NY.
1/27-29	5th Conference on Fiber Composites and Structural Design, New Orleans, LA. "Sponsored by DOD and NASA."
2/16-20	SPI Reinforced Plastics/Composites Institute Conference, Washington, D. D.
2/22-24	DOD Manufacturing Technology Composites Review, Orlando, FL.

TABLE 1 (continued)

1981

2/23-25	Society for Rheology Meeting, Williamsburg, VA.
3/9-12	International Technology Status and Export Control of Composite Materials and Technology, Washington, D. C.
3/9-13	2nd USA/USSR Symposium, Fracture of Composite Materials, Bethlehem, PA.
3/17	Nondestructive Seminar, Schenectady, NY. "Sponsored by American Society of Nondestructive Testing and Schenectady Community College."
3/27	26th Annual Structural Engineering Conference, Lawrence, KS.
3/29-4/3	5th International Conference on Fracture, Cannes, France.
3/30	National American Chemical Society Meeting, Atlanta, GA.
4/6	Southeastern Section Meeting of ASEE, Chattanooga, TN.
4/6-7	Interfaces in Composite Materials, Liverpool, UK.
4/6-8	22nd Structures, Structural Dynamics and Materials Conference, Atlanta, GA. "Sponsored by AIAA, ASME, ASCE and AHS."
4/9-10	Dynamics Specialists Conference, Atlanta, GA. "Sponsored by AIAA."
4/28-30	26th Annual SAMPE Symposium and Exhibition, Los Angeles, CA.

TABLE 2

COMPOSITES-RELATED TECHNICAL MEETINGS ATTENDED OFF-CAMPUS

for the period September 30, 1980 through April 30, 1981

1980

10/6-8   Symposium on Computational Methods in Nonlinear Structural and Solid Mechanics (Prof. Shephard), Washington, D. C.

10/28-30   Mechanics of Composites Review (Students T. Vinopal, S. Ward, A. Alksninis and C. Ellis), Dayton, OH.

11/5-7   Ultrasonics Symposium (Prof. Das, Students R. Webster and R. Werner), Boston, MA

> Professor Das presented the paper, "Ultrasonic Imaging for Nondestructive Evaluation of Composite Material with Digital Image Enhancement".

11/13-14   ASTM Meeting on Damage in Composite Materials: Basic Mechanisms, Accumulation, Tolerance and Characterization (Prof. Krempl), Bal Harbour, FL.

> Professor Krempl presented the paper, "The Role of Servocontrol Testing in the Development of the Theory Viscoplascity Based on Total Strain and Overstress".

11/18-19   Large Space Structures Conference (Student C. Rubeiz), Hampton, VA.

12/15-17   1980 SES National Meeting (Profs. Brunelle and Scarton), Atlanta, GA.

> Professor Brunelle presented the paper, "The Use of Affine Transformations in the Solution of Composite Structures Problems".

> Professor Scarton presented the paper "Acoustic Emission from Bovine Tibia".

1981

1/19-23   Gordon Research Conference (Profs. Diefendorf, Vice-Chairman and Sternstein, Discussion Leader), Ventura, CA.

TABLE 2 (continued)

1981

1/22   Society for Experimental Stress Analysis (Prof.
            Scarton), Schenectady, NY.

            Professor Scarton presented the paper,
            "Acoustic Emission in Composite Mate-
            rials".

1/26-27   NASA/DOD sponsored 5th Conference on Fiber Compos-
            ites and Structural Design (Prof. Loewy), New
            Orleans, LA.

2/22-24   DOD Manufacturing Technology Composites Review
            (Prof. Diefendorf), Orlando, FL.

2/23-25   Society of Rheology Meeting (Prof. Sternstein),
            Williamsburg, VA.

            Professor Sternstein presented the paper,
            "Delamination Failure in Carbon-Epoxy
            Laminates".

3/9-12   International Technology Status and Export Control
            of Composite Materials and Technology (Prof.
            Diefendorf), Washington, D. C.

3/17   American Society of Nondestructive Testing and
            Schenectady Community College sponsored Nondestruc-
            tive Seminar (Prof. Scarton), Schenectady, NY.

            Professor Scarton presented the paper,
            "Acoustic Emission Testing: Theory and
            Application".

3/27   26th Annual Structural Engineering Conference
            (Prof. Shephard), Lawrence KS.

            Professor Shephard presented the paper,
            "Computer Graphics in Structural Engi-
            neering".

3/30   National American Chemical Society Meeting (Prof.
            Sternstein), Atlanta, GA.

            Professor Sternstein presented the paper,
            "Viscoelastic Characterization of Solids".

4/6   Southeastern Section Meeting of ASEE (Prof.
            Shephard), Chattanooga, TN.

            Professor Shephard presented the paper,
            "Computing at RPI - A Case Study" (with
            L. J. Feeser).

speakers, are listed in Table 3. A list of composite-related visits to relevant organizations by RPI faculty/staff/students, with the purpose of each visit outlined, is presented in Table 4.

In summary, the NASA/AFOSR Composites Aircraft Program is a multi-faceted program whereby aeronautical, mechanical and materials engineers must interact to achieve its goals. "Hard-nosed" engineering of composite aircraft structures is balanced against research aimed at solving present and future problems. In the following sections, detailed descriptions of the CAPCOMP, CAPGLIDE, COMPAD and INSURE programs are presented.

TABLE 3

COMPOSITES-RELATED MEETINGS/TALKS HELD AT RPI

(September 30, 1980 through April 30, 1981)

Topic	Date	Speaker(s)
Wavefront Analysis in the Nonseparable Elastodynamic Quarter Plane Problems	10/9/80	Julius Miklowitz Prof. of Applied Mechanics California Institute of Technology
Nonlinear Optimization of Framed Structures	11/6/80	C. S. Krishnamoorthy University of Southern California
Analysis of Steady State Elastic Wave by Global-Local Finite Elements	11/11/80	Daniel B. Goetschel Research Engineer California Research and Technology
Materials Behavior - Its Role in Life Prediction	1/27/81	Louis F. Coffin, Jr. General Electric Research and Development Center
Properties of the Strength Distribution for Composite Materials	2/3/81	David G. Harlow Prof. of Mechanical Engineering and Mechanics Drexel University
Continuum Modeling of Large Space Structures	2/20/81	Taft Broome Visiting Professor of Civil Engineering Rensselaer Polytechnic Institute
Advanced Composites Activities at Boeing Aerospace	2/24/81	Herbert Voss Manager, Structures Department and Dominic Reilly Research Engineer Boeing Aerospace Company
Laser Speckle Doppler Velocimeter Technique Applied to Measure Torsional Vibrations of Rotating Surfaces	3/4/81	Seetha R. Mannava Doctoral thesis dissertation Department of Mechanical Engineering, Aeronautical Engineering and Mechanics Rensselaer Polytechnic Institute
Dynamics and Control of Flexible Spacecraft: More Appropriate Techniques	3/24/81	Hari B. Hablani Research Associate Johnson Space Center

<u>TABLE 3 (continued)</u>

Topic	Date	Speaker(s)
The Next Generation of Commercial Aircraft - The Technological Imperative	4/7/81	John Swihart Vice President, Domestic and Canadian Sales Boeing Commercial Airplane Company
Recent Development in Computational Methods for Structure-Medium Interaction Problems	4/14/81	K. C. Park Staff Scientist Lockheed Palo Alto Research Laboratory
Polyhedral Chain Space Trusses	4/17/81	Martin Rooney Professor of Civil Engineering Rensselaer Polytechnic Institute
The Use of Affine Transformations in the Analysis of Stability and Vibrations of Orthotropic Plates	4/17/81	Gabriel A. Oyibo Doctoral thesis dissertation Department of Mechanical Engineering, Aeronautical Engineering and Mechanics Rensselaer Polytechnic Institute
Molecular Orientation in Polymers: A Study of Hot-Drawn Polymethylmethacrylate	4/20/81	Jay Rosenthal Doctoral thesis dissertation Department of Chemical and Environment Engineering Rensselaer Polytechnic Institute
Fracture Mechanics Application to Problems in Industry	4/28/81	Kenal Arin General Electric Company

TABLE 4

COMPOSITES-RELATED VISITS TO RELEVANT ORGANIZATIONS

by RPI Faculty/Staff/Students

(September 30, 1980 through April 30, 1981)

Visited	Date	By	Purpose
Lockheed California Co. W. Stauffer M. Melcon	11/12/80	Prof. R. G. Loewy	To discuss possible CAPCOMP redesign projects
Peckert Boatworks Bennington, VT	1/8/81	Student C. Muser	To discuss new fabrication techniques
NASA Langley Dr. N. Johnston	2/26/81	Prof. S. S. Sternstein	To discuss long range planning for advanced composites
BASF Ludwigshafen, Germany	3/8/81	Prof. R. J. Diefendorf	Presented a Seminar in "High Performance Composites"
NASA Langley	3/31/81	Prof. S. S. Sternstein	Presented two seminars: "Viscoelastic Properties of Composites" and "Delamination Failure in Composites"
General Motors Research Labs., Warren, MI	4/2/81	Prof. M. S. Shephard	To present the talk "Finite Element Grid Optimization - An Overview"
University of Massachusetts Polymer Science and Engineering Division	4/10/81	Prof. R. J. Diefendorf	Presented a Seminar in "Discotic Liquid Crystals"

PART I

CAPCOMP (Composite Aircraft Program Component)

CAPCOMP (Composite Aircraft Program Component)
(D. Goetschel, N. Hoff, R. Loewy, H. Scarton)

CAPCOMP is a program to design flight critical struc-
tures to take the maximum advantage of composite materials.
By combining the efforts of experienced faculty with bright
and well trained but inexperienced graduate students in an
environment relatively free of traditional design and manu-
facturing processes, we intend to devise new and hopefully
useful design concepts.

There is sufficient information available to prove that
many structural elements can be made lighter by using ad-
vanced composites today than by using metals. But if such
elements have to be joined by methods other than adhesive
bonding, difficulties and uncertainties arise which can be
eliminated only through conservative designs with their at-
tendent penalties in weight or by extensive and expensive
programs of "cut and try". This stands as one important im-
pediment to full adoption of composites by the aerospace in-
dustry.

On the basis of these considerations Rensselaer Poly-
technic Institute began, as the first task aimed at new
structural concepts, the design using composites of a joint
used in an airplane elevator. To make the design realistic,
an existing metal airframe component was chosen for redesign
in composites. The existing design chosen was that of the
Boeing 727 elevator actuator attachment. We conceive of

this work as carrying forward a Structures Demonstration
Program using the actuator attachment joint of the 727 ele-
vator, paralleling that of NASA and its aerospace contractor,
the Boeing Commercial Airplane Company. Our design, fabri-
cation and test effort emphasizes designs using advanced
composite construction for the purpose of minimizing the
weight of the structure, but on a scale consistent with the
university context and funding level. The staff of RPI is
very grateful to the Boeing Company and its engineers for
their wholehearted support of this work at RPI.

One of two different designs was reported previously
(July and December 1979) as suitable for replacing the large-
ly metal attachment produced by Boeing. This so-called
"Berg Design" makes use of quasi-isotropic, graphite-epoxy
laminates and was selected for further analysis, redesign,
fabrication and testing. The second design, called the
"Muser Design", which made a deliberate attempt to use uni-
axial graphite-epoxy tape to as great an extent as possible,
was suspended. It led, however, to more generic research ef-
forts to maximize the load carrying ability of pin-loaded
holes in composite membranes and plates. These efforts are
directed at improving the design of the attachment of the rib
flanges to the elevator skin through mechanical (i.e., pin-
type) fasteners and at maximizing the efficiency of the mov-
able, heavily loaded, actuator attachment points in CAPCOMP.
In addition, however, these generic effects were, and continue

to be motivated by the general and widespread utility that will result from improvements in pin-loaded hole designs for composites.

These efforts have been jointly directed by Dr. Nicholas J. Hoff, in part-time arrangement and by Drs. Daniel Goetschel, Robert Loewy and Henry Scarton.

1. The Elevator and Its Attachment

To place the progress reported here in proper context, some descriptions used in earlier reports are repeated. The conventional aluminum alloy elevator of the Boeing 727 is shown in the upper half of Figure I-1. The lower half of the figure is the new version of the elevator redesigned by Boeing in graphite epoxy; it is evident from the pictures that the latter is composed of fewer parts than the former. However, the actuator fitting of the new design is still manufactured of aluminum alloy. This fitting is shown in Figure I-2. The fitting is attached to outboard and inboard portions of a new graphite-epoxy spar and to a graphite-epoxy Nomex-honeycomb rib as indicated in Figure I-3.

The attachment was designed by Boeing to carry loads up to 19,000 pounds. The direction of the load varies as the elevator rotates over an angle of 28 degrees from the full-down to the full-up position.

2. Berg's Design (CAPCOMP I)
(R. Loewy, H. Scarton)

Berg's design for the elevator rib is shown in Figure I-4

UPPER SKIN PANEL

CONTROL TAB

BALANCE PANELS

BALANCE WEIGHT

LOWER SKIN PANEL
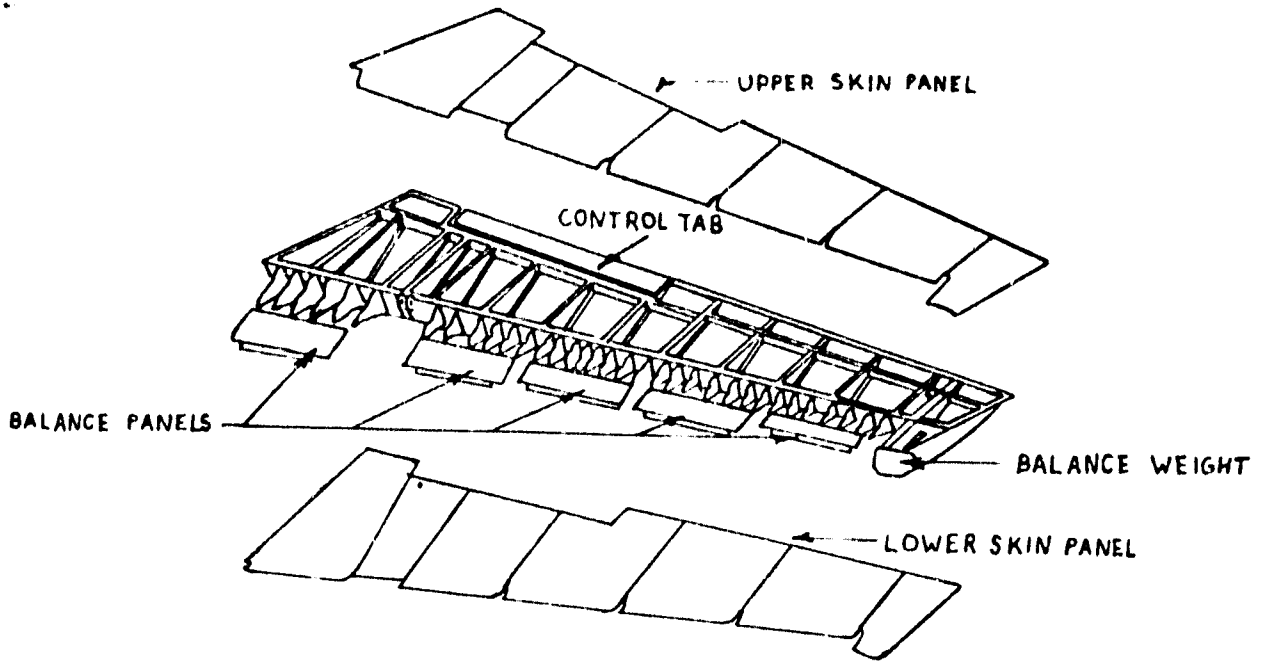
Conventional Aluminum Elevator

UPPER HONEYCOMB SKIN

CONTROL TAB

ACTUATOR FITTING

EXISTING ALUMINUM STRUCTURE

HONEYCOMB AREAS

LOWER SKIN
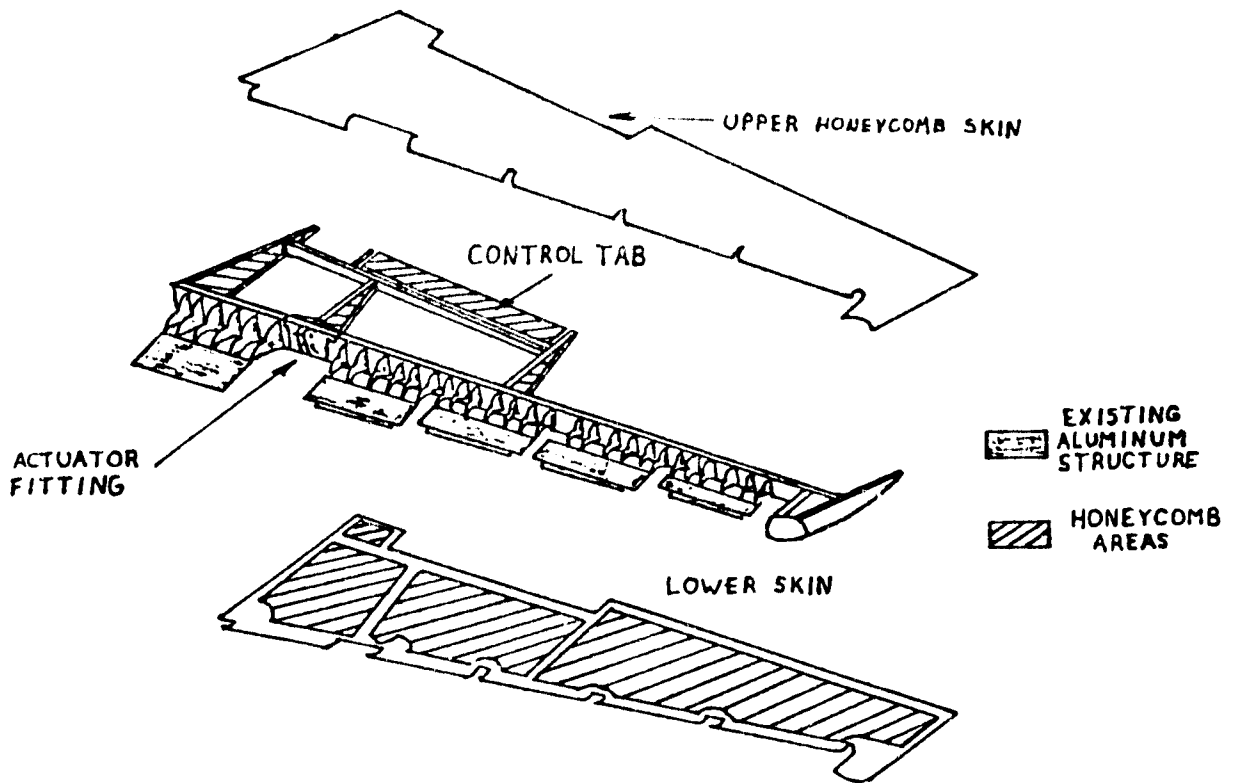
Advanced Composite Elevator

BOEING ELEVATOR ASSEMBLY

Figure I-1

ALUMINUM ACTUATOR FITTING   (Boeing Design)

Figure I-2

actuator rib
(graphite epoxy)

outboard spar
(graphite epoxy)

actuator fitting
(aluminum alloy)

inboard spar
(graphite epoxy)
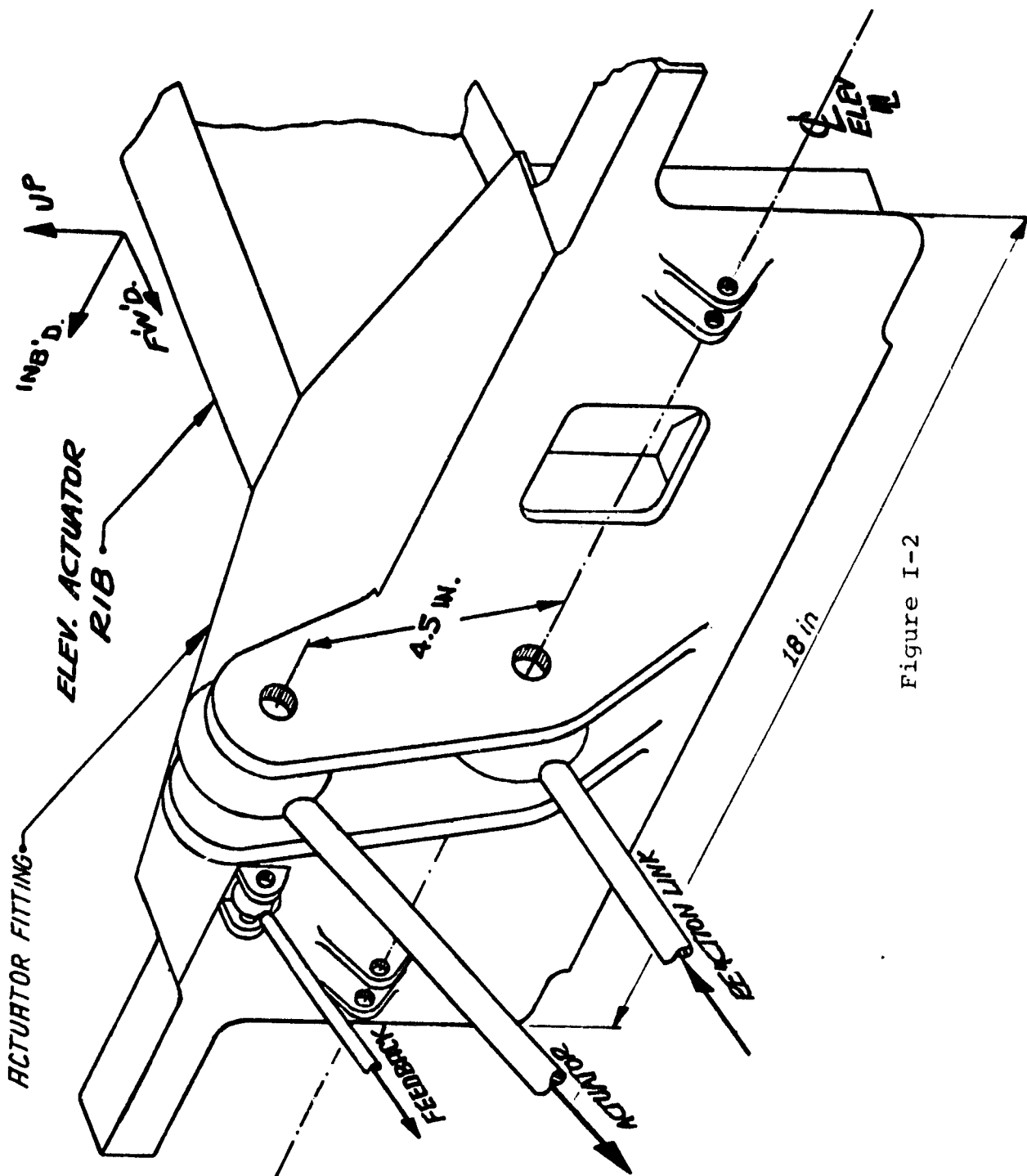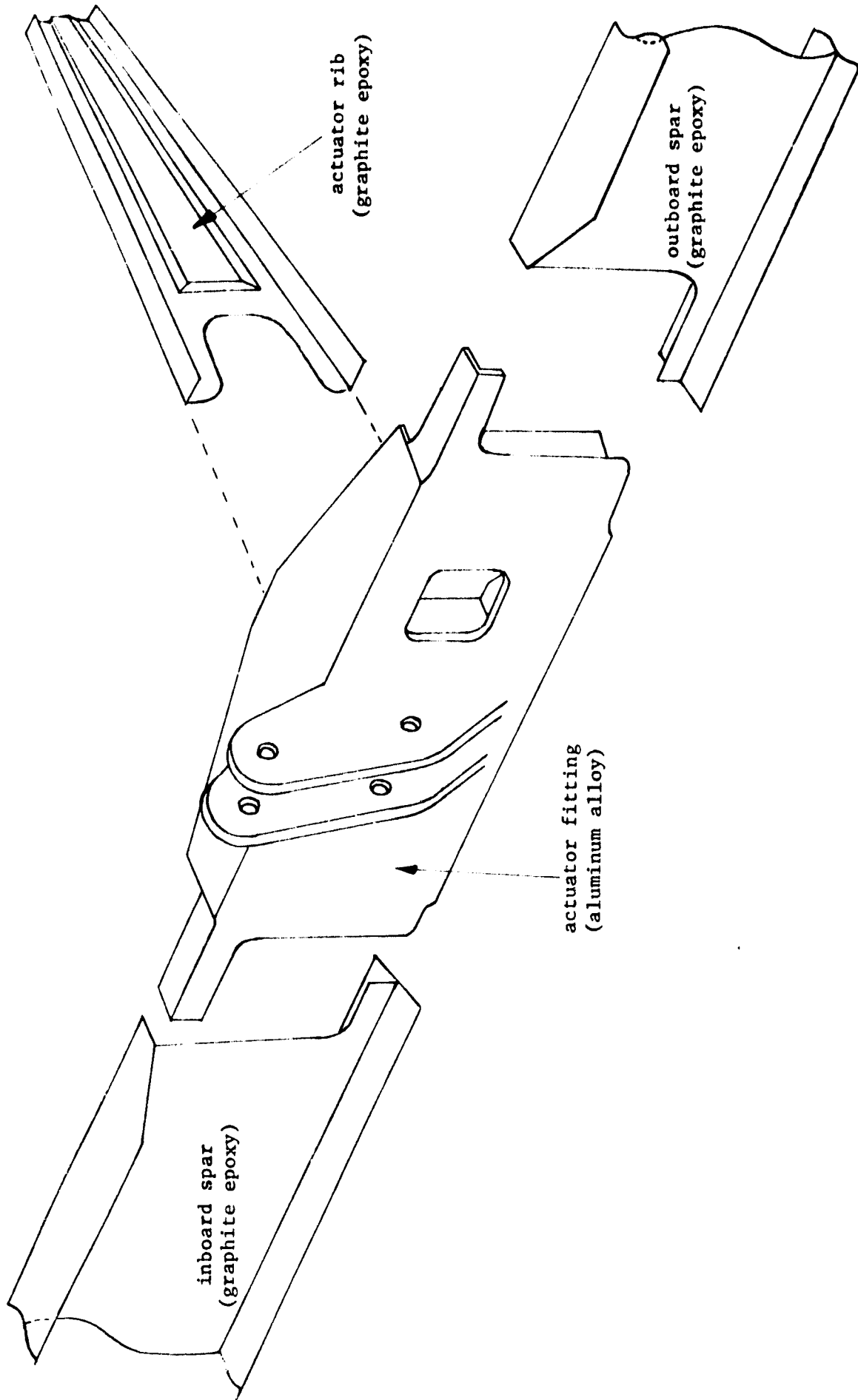
COMPOSITE ELEVATOR ACTUATOR ASSEMBLY (Boeing Design)

Figure I-3

ACTUATOR
FITTING
(Aluminum)

EXISTING
COMPOSITE RIB

PRESENT DESIGN

WEB OF
ELEVATOR SPAR

SANDWICH CORE

PROPOSED DESIGN   (Berg)
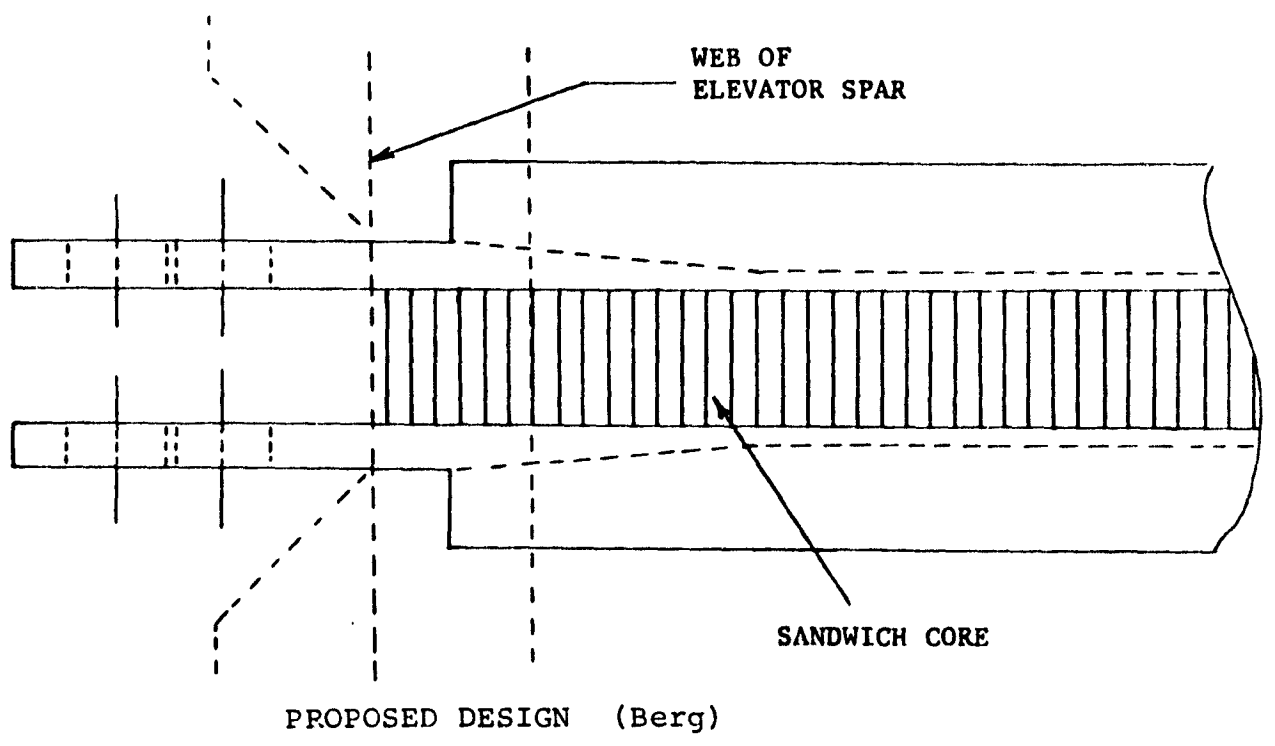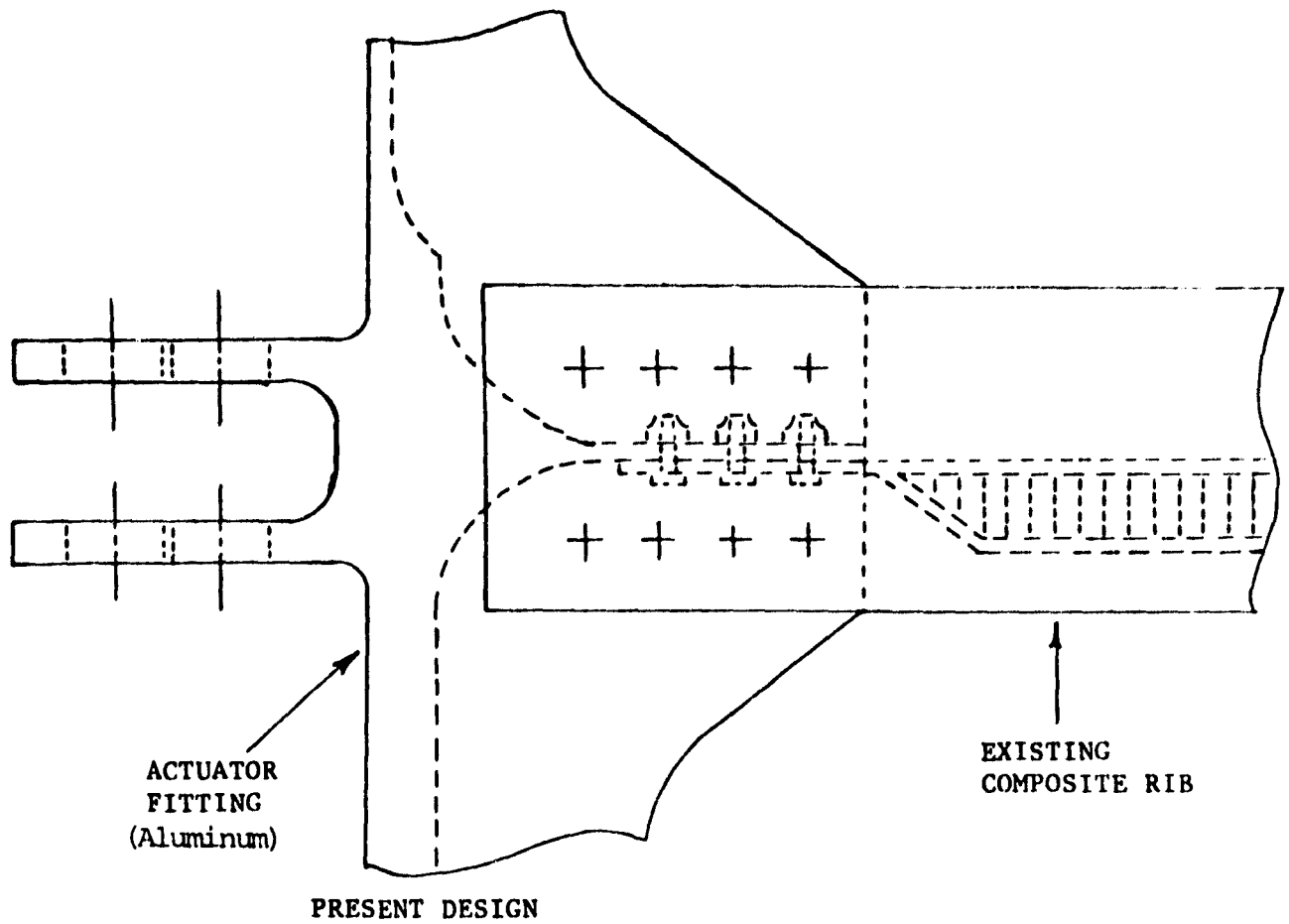
ACTUATOR LUG TO RIB TRANSITION - TOP VIEW

Figure I-4

and I-5. The first of these figures compares the Boeing composite design with Berg's design; both are shown. Figure I-5 shows both how the spar and new actuator rib would be assembled and also the build-up of thickness in the lug areas anticipated as needed to provide the required bearing strength. These ribs are fabricated from Fiberite HY-E 1048 AE/104 Graphite-Epoxy Composite (6.9 μm dia. fibers). Note that the edges of some of the layers are bent 90° to form flanges to which the upper and lower skins of the elevator can be attached. Attachment of flanges to elevator skins is by means of titanium Hi-Loc fasteners. The right-hand and left-hand graphite-epoxy webs are stabilized by a layer of Nomex-honeycomb between them to form one complete rib.

The design analyses described in the previous reports led to an elevator attachment rib with a variable thickness web. The distribution of thickness was chosen using successive finite element calculations to produce a relatively uniform stress level. It is shown in Figure I-6.

The Berg design, composite 727 aircraft elevator actuator attachment rib is shown in various stages of assembly in Figures I-7a, -7b and -7c. It was fabricated by undergraduate student Francis DeTaranto. The laminate stacking sequence and thicknesses were given in Reference [1]*. They consist of integer multiple layers of $(0°, +45°, -45°, 90°)_{2s}$ laminates.

As noted in earlier reports, the Boeing Commercial

---

*References in this section refer to the list on page 54.
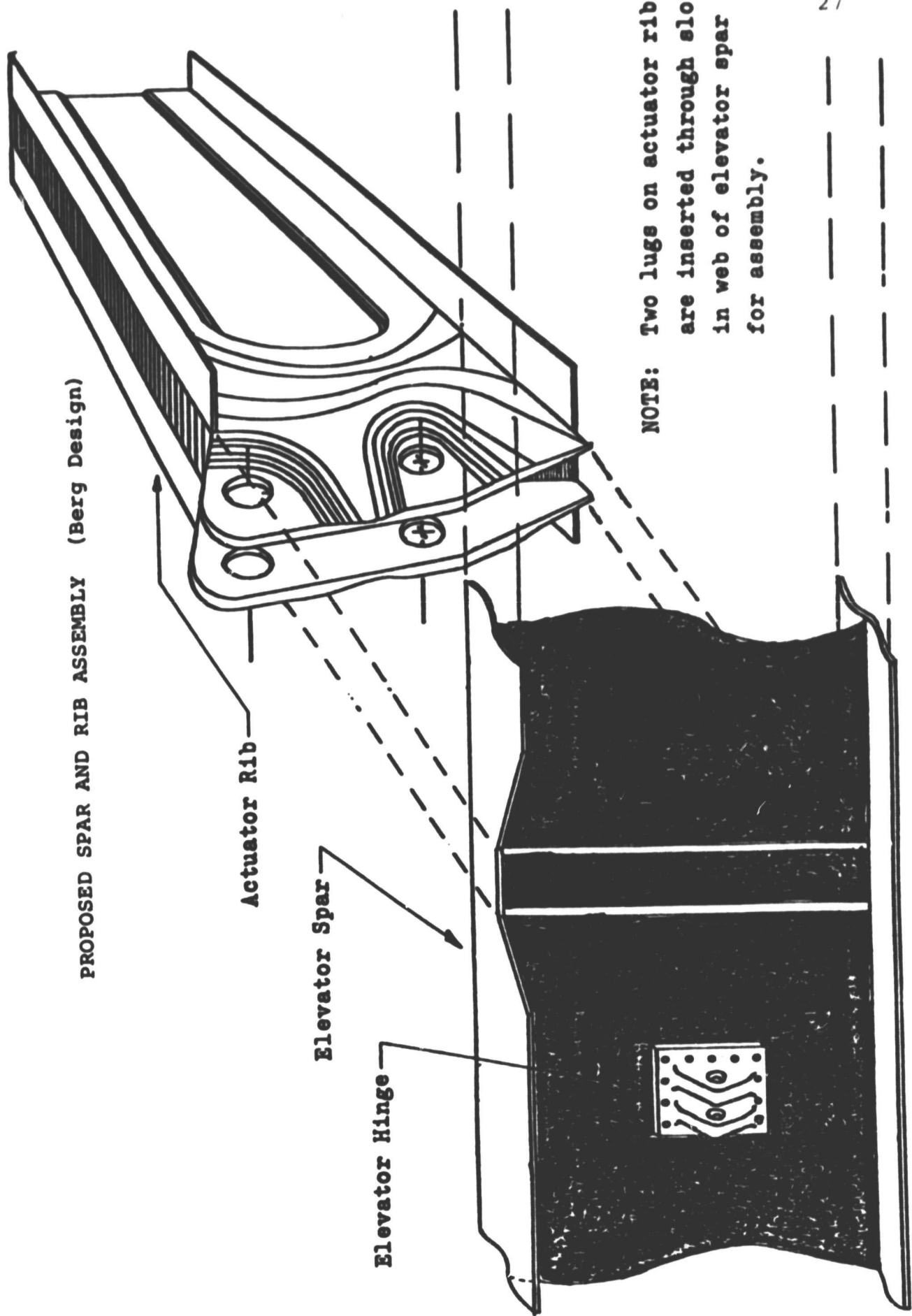
PROPOSED SPAR AND RIB ASSEMBLY (Berg Design)

Actuator Rib

Elevator Spar

Elevator Hinge

NOTE: Two lugs on actuator rib
are inserted through slots
in web of elevator spar
for assembly.

Figure I-5
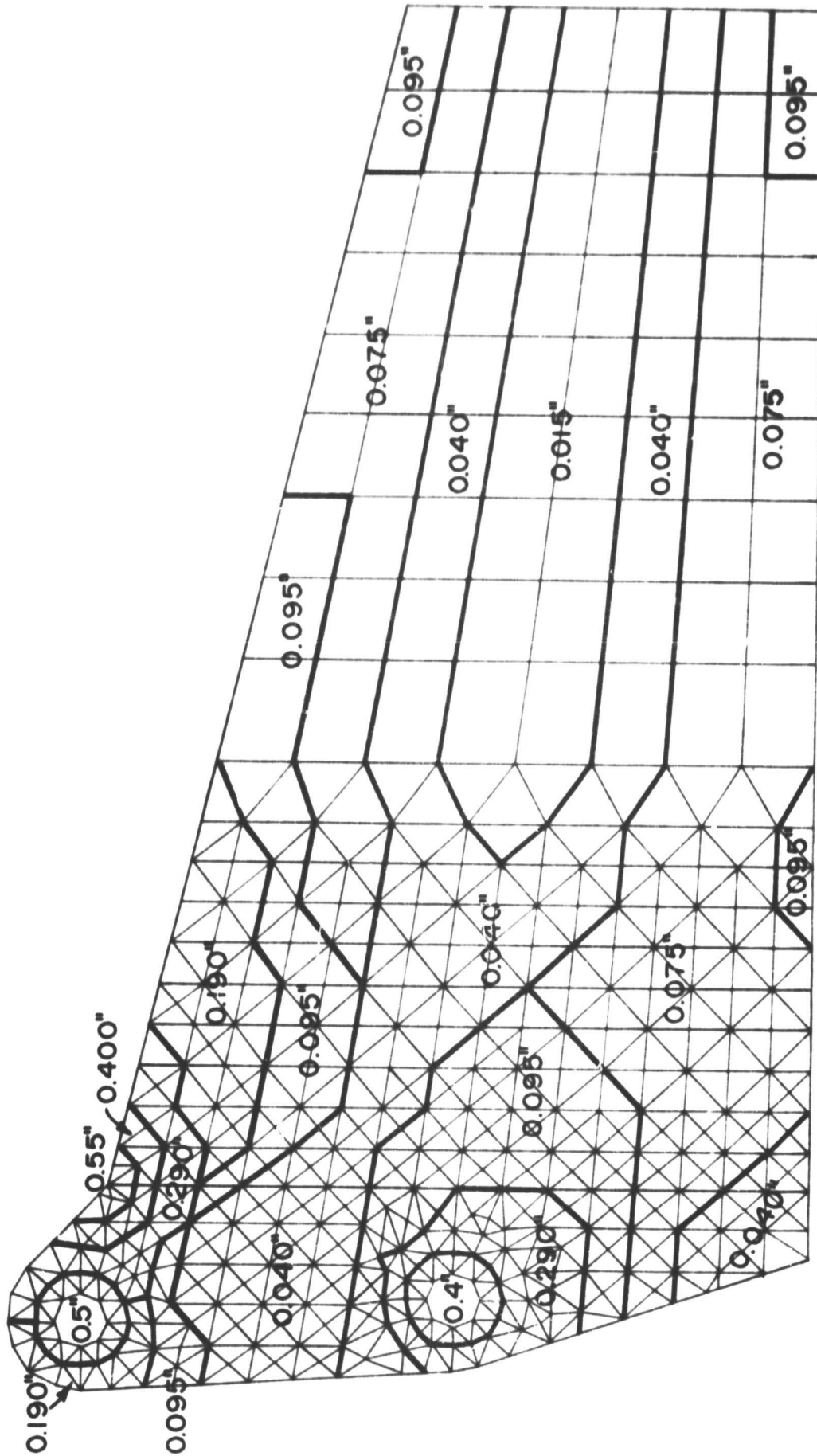
VARIABLE THICKNESS FINITE ELEMENT MESH

Figure I-6

Figure I-7a

Left-Hand Member Elevator Actuator Attachment Rib
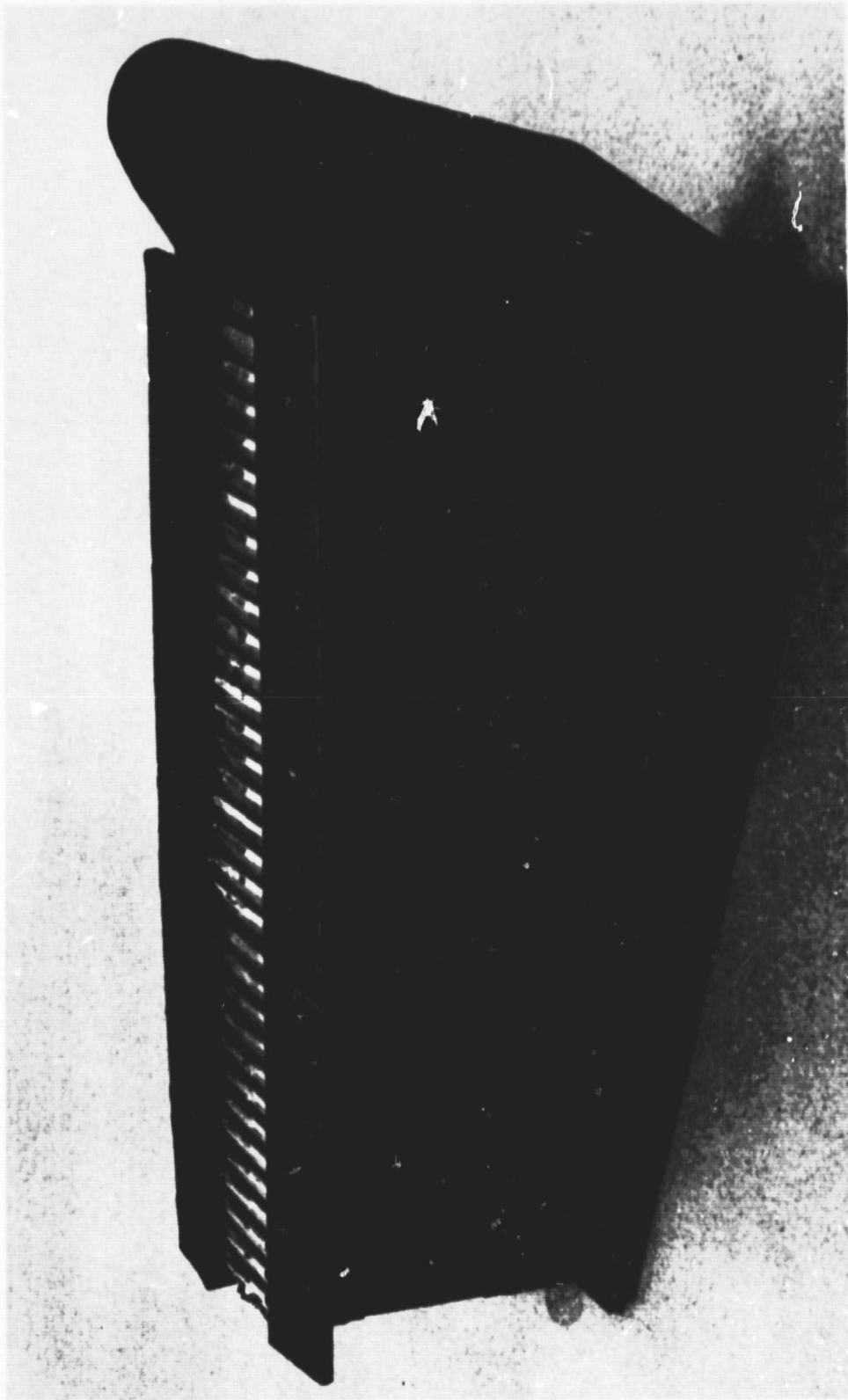
Figure I-7b

Elevator Attachment Rib Assembly
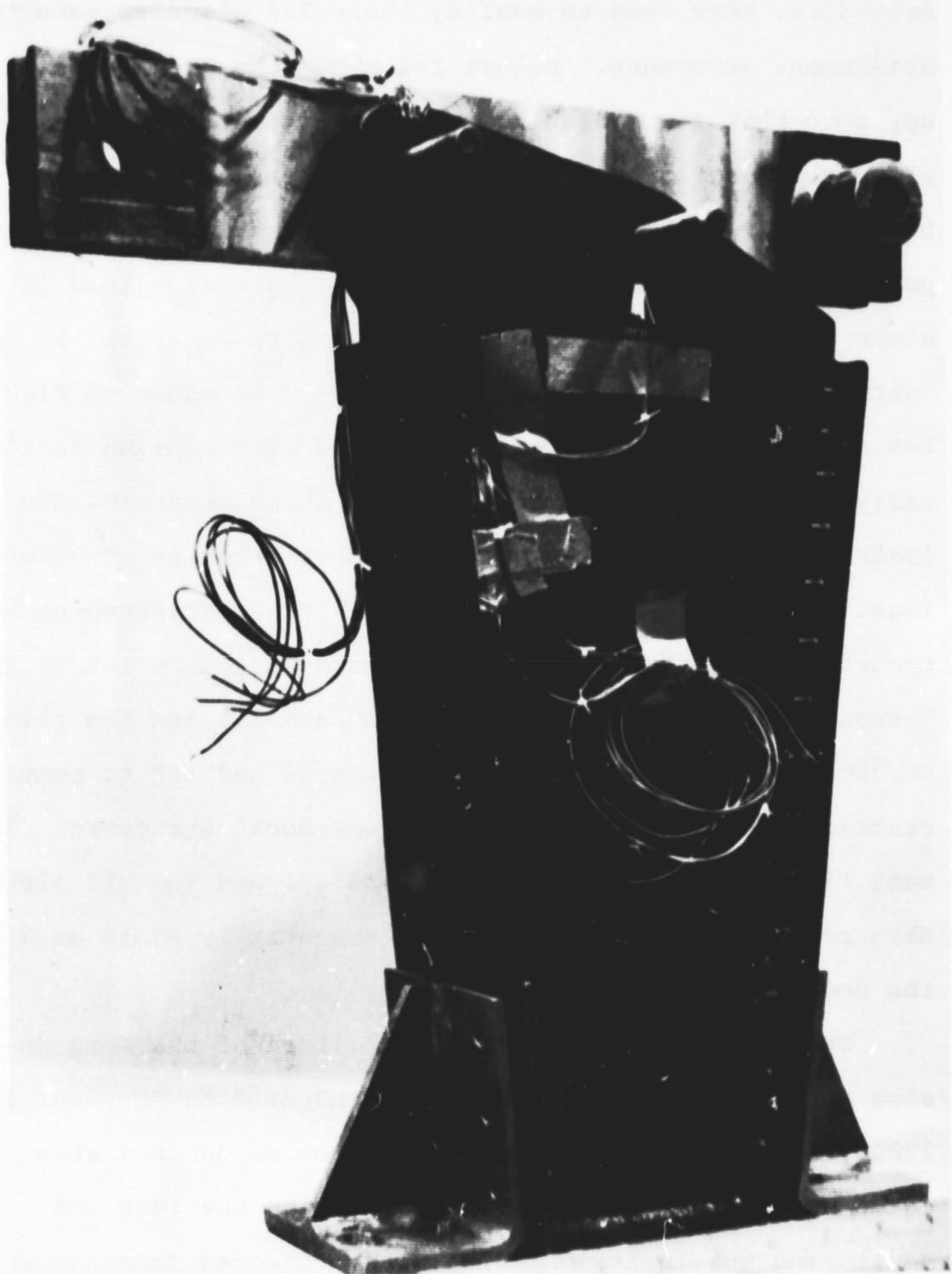
Figure I-7c

Elevator Attachment Rib Assembly Mounted and
Instrumented for Testing

Airplane Company provided a full description of the testing procedures they used to qualify their 727 elevator actuator attachment structure. Figure I-8 shows the Boeing test set-up; note that two hydraulic cylinders (mounted horizontally) provide the actuator load and reaction through a vertical bar which is bolted to the two elevator actuator attachment points. In the absence of such mobile hydraulic load generators at RPI, the equivalent loadings were generated in an Instron testing machine through linkages as shown in Figure I-9. In the campus test set-up, loads were applied vertically to a bar oriented horizontally which transmits the loads through two bolts to the elevator actuator attachment lugs. Equilibrium analysis of this linkage arrangement was reported in Reference [2]. Also shown in Figure I-9 is the "strong-back" structure (items 9, 10 and 11) and the reinforcements of the elevator rib (items 12 and 13) to ensure reaction-load transfer to the "strong-back" structure. These test fixtures (i.e., items 9, 12 and 13) and the aft elevator skin reinforcements (item 14) are essentially those used in the Boeing test.

The first proof load test to failure of the Berg design actuator attachment rib was conducted on December 12, 1980. Both strain gage and acoustic emission data were taken during this test. Those conducting the test and monitoring the instrumentation were protected from the possibility of failed parts, such as rivets, being propelled away from the structure by the strain energy stored in it
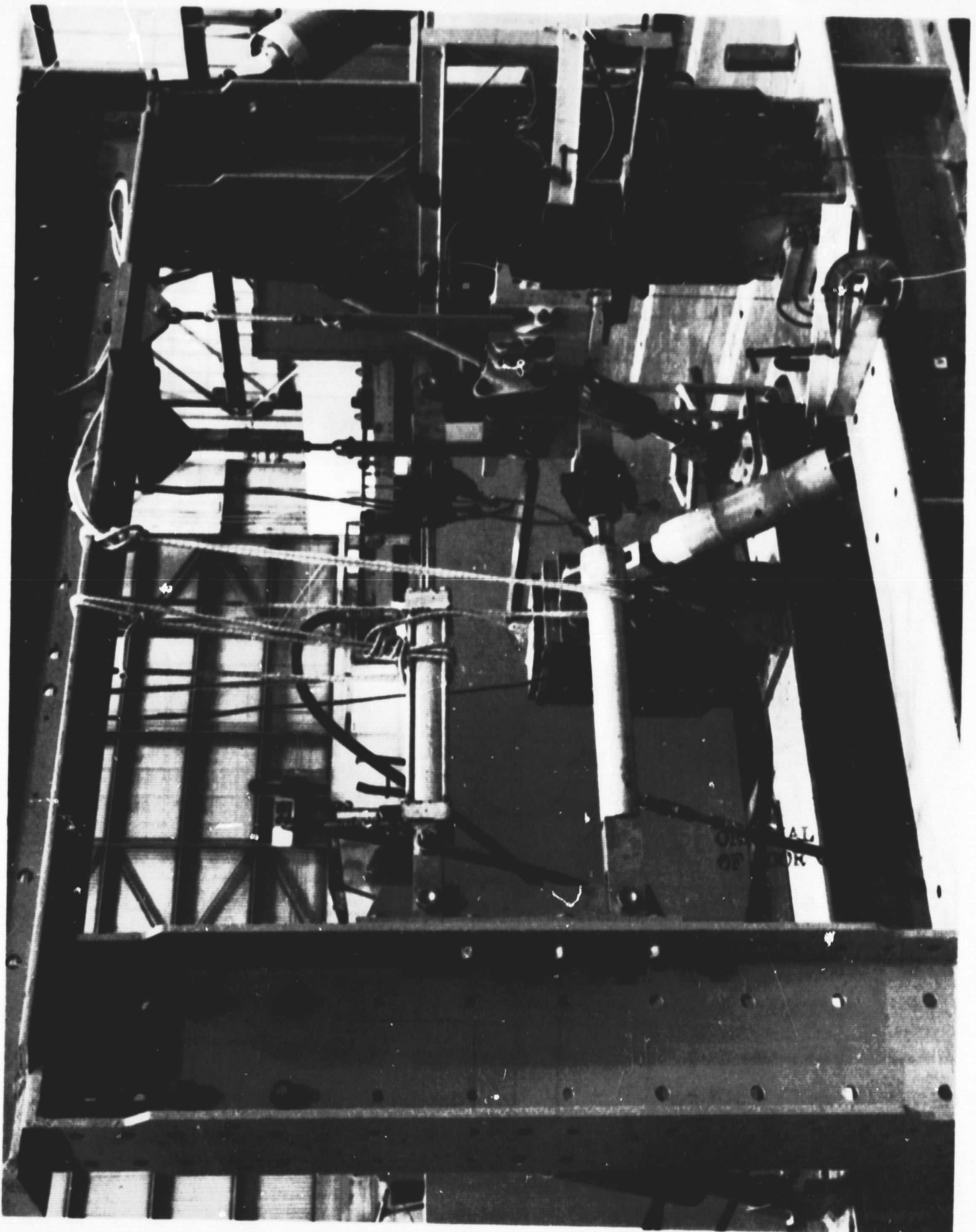
Figure I-8   Advanced Composite Elevator
Rib Test (BAC/NASA 727)

34
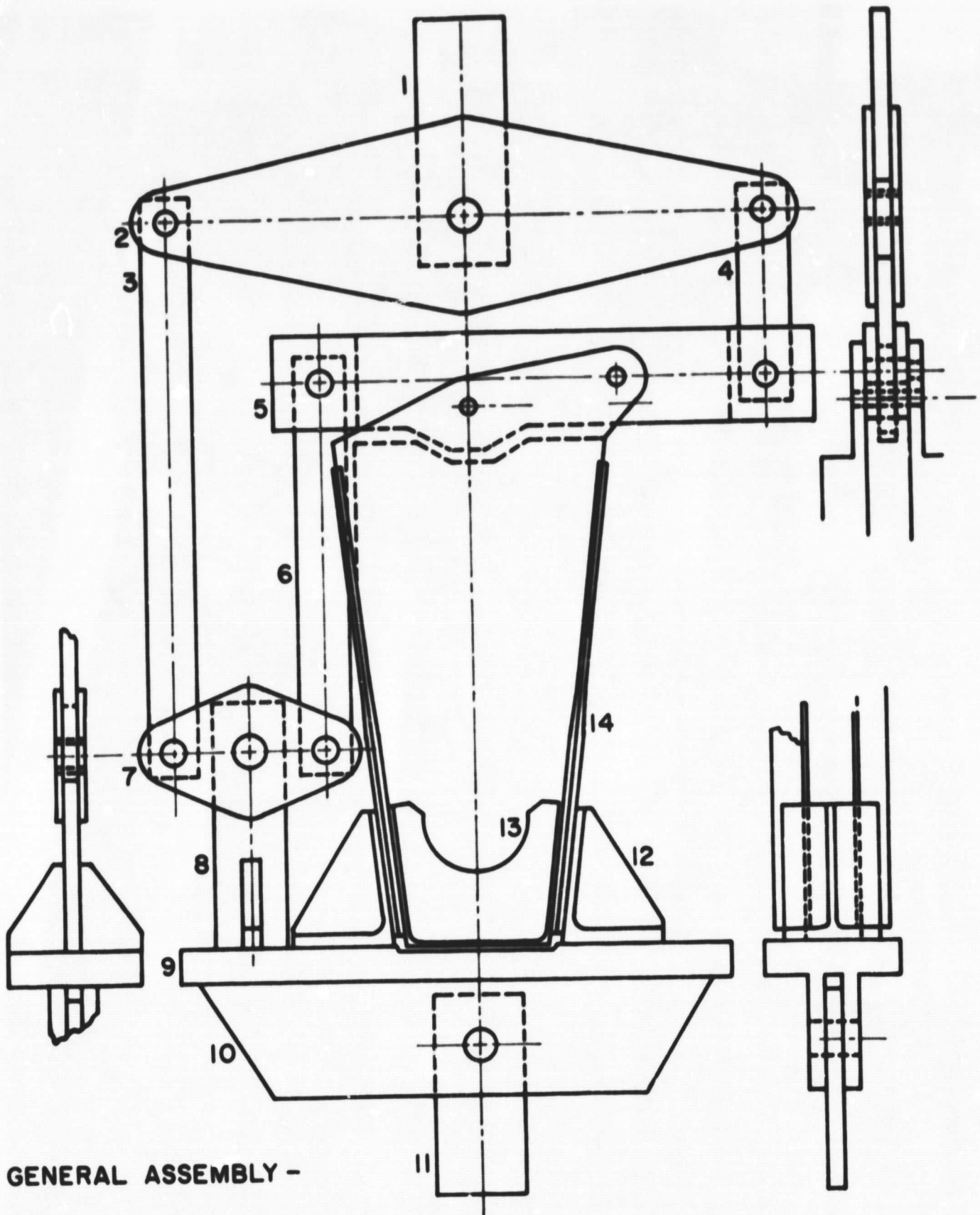
Figure I-9 Rib Test Fixture

near maximum load. This protection was provided by a transparent Plexiglas and wire-mesh barrier.

In virtually all respects this was a completely successful test. The design, which was intended to be conservative, failed at approximately 120 per cent of design ultimate load. Failures occurred close to where they were expected and were multiple in nature.

The instrumentation used to test our specimen is shown in Figure I-10 without the personnel protection barrier and in Figure I-11 with the barrier. A list of the instrumentation follows:

a) For strain gage analysis, we used six 45°
   strain rosettes wired into an FX Data Logger
   Strain Monitor[3].

b) For acoustic emission monitoring, three acoustic emission transducers were installed and
   used in conjunction with the AET 5000 Acoustic
   Emission System[4] provided for this test
   through the courtesy of the Acoustic Emission
   Technology Corp.; namely;

Sensor	Type	Resonance (kHz)	Preamp. Model No.	Gain (dB)	Bandwidth (kHz)
1	AC 175C	175	160	60	125-250
2	AC 175C	175	160	60	125-250
3	AC 375L	375	160	60	250-500

c) Load application was performed using an Instron
   1333 machine, with maximum capacity of 251.68 kN
   (56,500 lbs)[5].
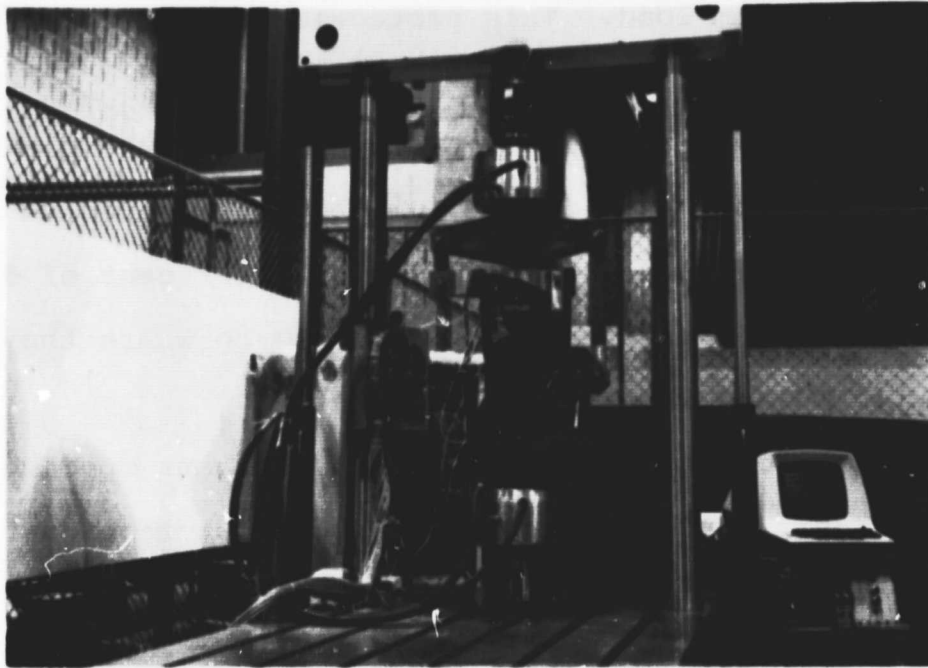
Figure I-10

Elevator Actuator Attachment Rib Test Fixture and
Instrumentation (without personnel protection barrier)
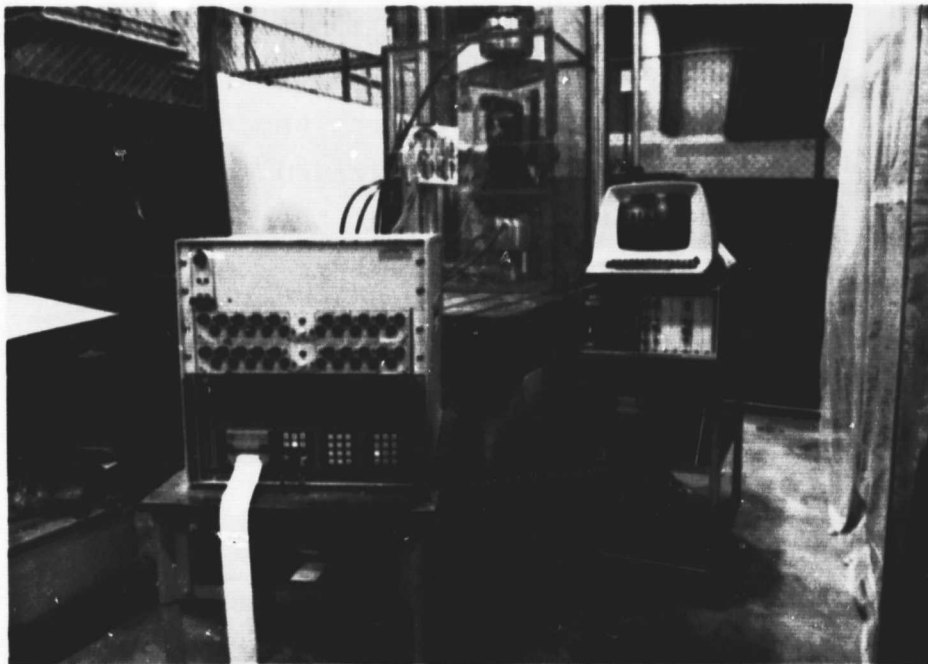
Figure I-11

Elevator Actuator Attachment Rib Test Fixture and
Instrumentation (with personnel protection barrier)

The conditions of loading (Figure I-12) can best be described as continuous loading with discontinuous slope. Initially, load was applied at a constant rate of approximately 0.19 kN/sec (43 lbs/sec). At each ten per cent increment of the full scale Instron load, 125.84 kN (28,250 lbs.), the loading condition was held constant for a period of about 45 seconds. This was done so that two acoustic emission amplitude distributions for sensors AE 1 and AE 2 could be obtained from the line printer. Visual inspection of the specimen also was accomplished during these periods.

Strain gage output and acoustic emissions were both monitored continually and cumulatively beginning with the initiation of load on our composite specimen. The functions monitored were:

a) Strain as a function of time for the six 45° rosettes.

b) Applied load as a function of time.

c) The number of acoustic events versus acoustic emission amplitude for sensors AE 1 and AE 2 .

d) The total number of acoustic emission events versus load for sensors AE 1 , AE 2 and AE 3 .

Locations for all strain gage and acoustic emission sensors were chosen by studying the principle stress contour map developed using finite element analysis[6,7] and shown in Figure I-13.

Strain gage analysis at the failure site C, by graduate student Chi-Min Chang, revealed a non-symmetric loading
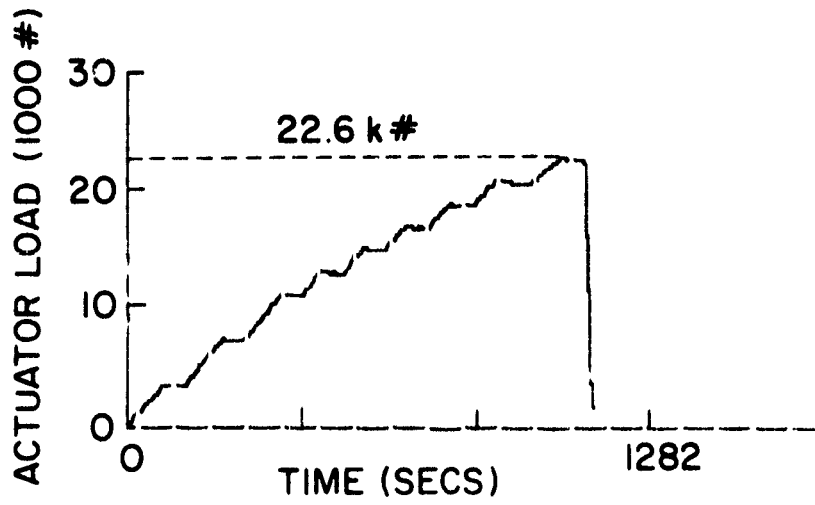
Figure   I-12

Elevator Actuator Attachment Rib
Test Load Time History

39
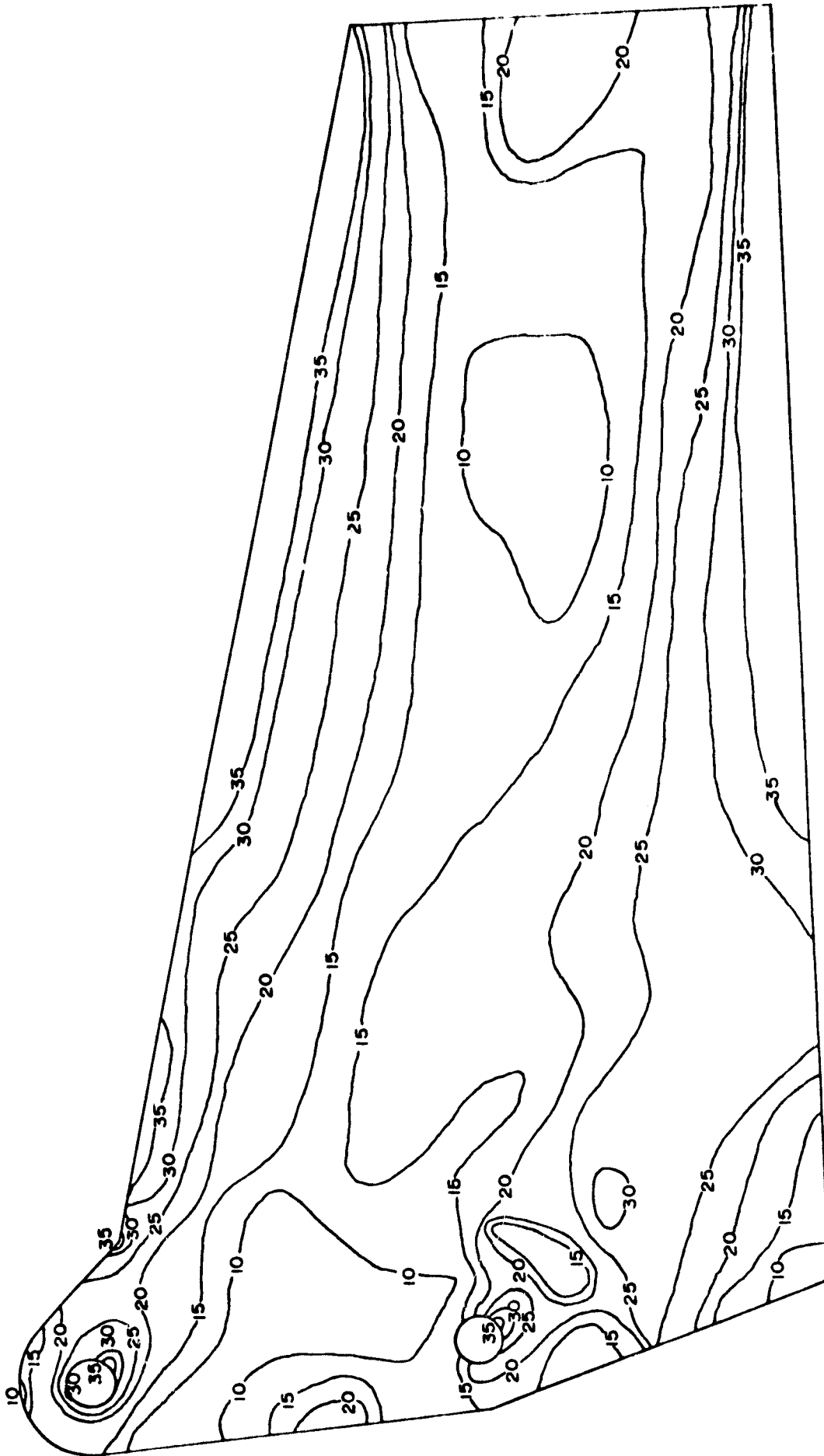
(VALUES IN KSI.)

Figure I-13

Principle Stress Contours for Variable Thickness Mesh for the
Boeing 727 Elevator Actuator Attachment Rib

condition. The strain in the y direction varied by 18.75% from one side of our composite specimen to the other (Figure I-14). Considering the source of this dissymmetry led to the following analysis. If the line of action of the applied load were off-center a distance ϵ, as shown in Figure I-15, equilibrium of moments requires

$$\frac{R_2}{P} = \frac{\frac{D}{2} + \epsilon}{D} = \frac{1}{2} + \frac{\epsilon}{D} .$$

Equilibrium of forces, however, states

$$P = R_1 + R_2 .$$

So that

$$\frac{1}{2} + \frac{\epsilon}{D} = \frac{R_2}{R_1 + R_2} .$$

From our tests

$$1 - \frac{R_1}{R_2} = 18.75\%, \text{ so that } R_1 = R_2(0.8125).$$

Hence

$$\frac{1}{2} + \frac{\epsilon}{D} = \frac{R_2}{1.8125R_2} \text{ and } \frac{\epsilon}{D} = .052 .$$

It is clear that positioning the line of action of the applied load is very important (D = 2") and considerable care will be taken with that aspect in future tests.

The strain analysis results also showed, as expected, that one of the regions of highest calculated principal stress (see Figure I-13) exhibited the highest measured principal strain (near strain rosette gage C; Figures I-16a

Figure   I-14

Strain Values in 2 Directions at C & C'
Solid-Line for Strain at C Point
Dash-Line for Strain at C' Point

Time at Failure
of Strain Gage
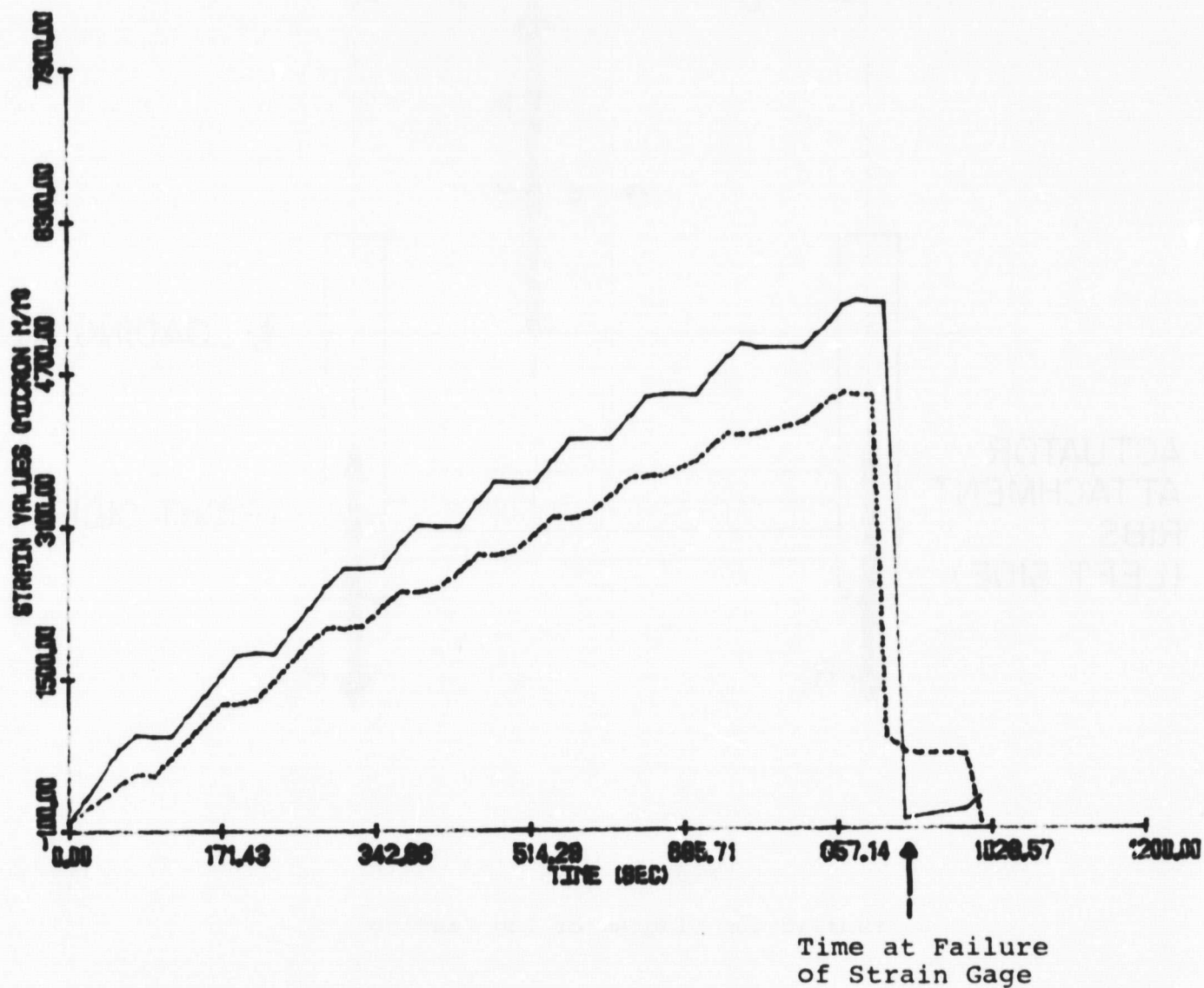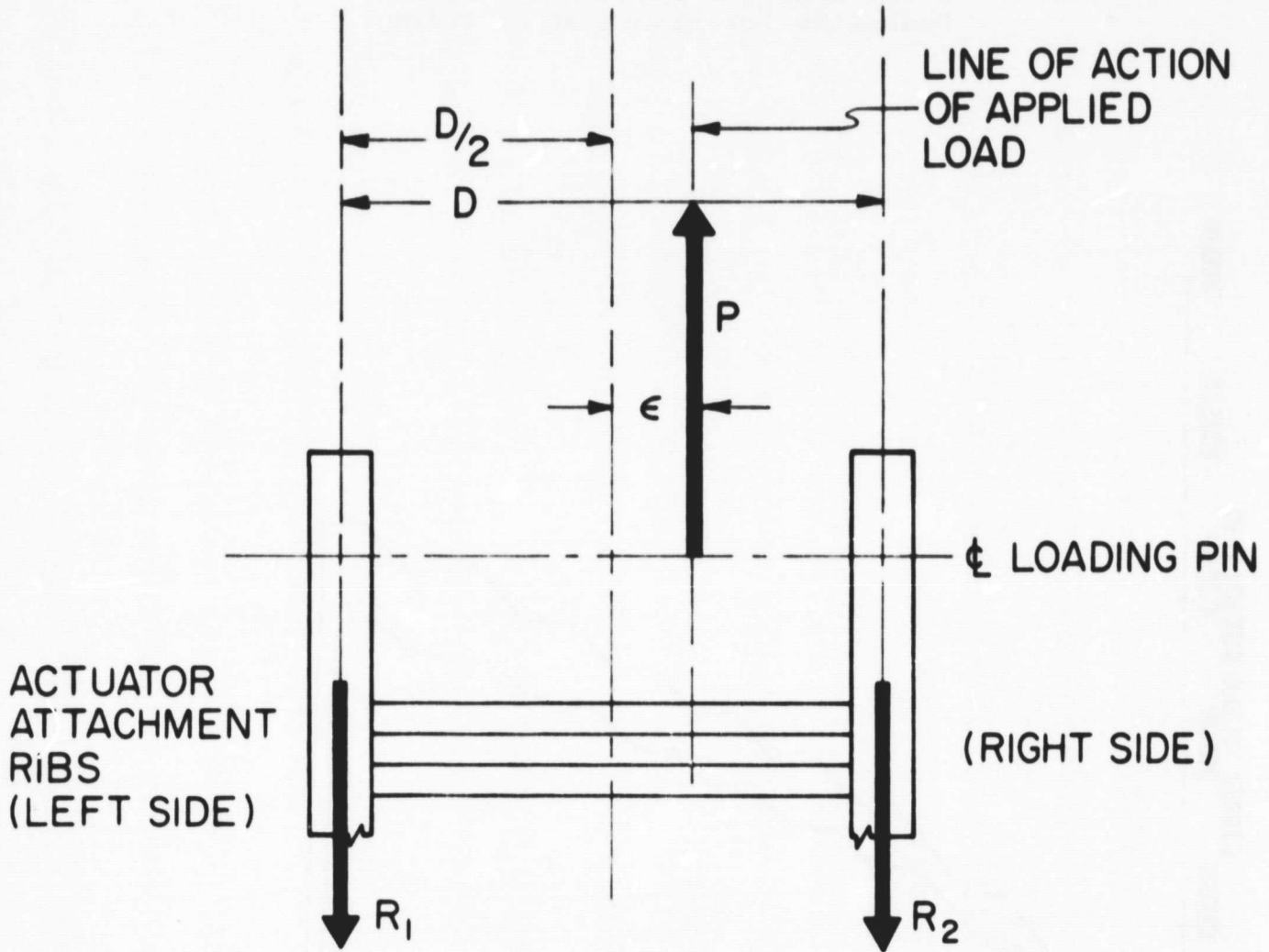
Figure I-15

Equilibrium Diagram of Lug Loading

and I-16b). It is a source of some satisfaction that strain gage C was destroyed nearly at the precise moment of failure; the crack went through the middle of it. The maximum principal strain at strain gage C reached a value of 5,405 μm/mm roughly 910 seconds into the test, as shown by the plot of strain versus time for strain gage C in Figure I-14. The maximum strain was in the y direction, as shown in Figure I-16b. Using the principle stress in gage C from Figure I-13 and the principle strain value of Figure I-14 and assuming the principle directions coincide, we are led to conclude that the equivalent Young's modulus of this structure's material is

$$35,000 \times \frac{22,600}{19,000} \times \frac{1}{5405 \times 10^{-6}} = 7.7 \times 10^{6} \text{ psi.}$$

This checks reasonably well with theoretical values of 8.3×10^{6} psi for the laminate used.

Acoustic emission data near the failure site was obtained from sensor AE 3. From the graph of Total Acoustic Emission Events versus Load for sensors AE 1, AE 2 and AE 3 (Figure I-17), we can estimate the point of critical activity; i.e., the point at which the slope of the curve of events increases sharply with increasing load. (ASTM specification E 569[8]). It occurs at an actuator pin load of 60.5 kN (13,600 lbs.) at 515 seconds, while ultimate failure occurred at an actuator load of approximately 100.5 kN (22,600 lbs.). The design load was 84.6 kN (19,000 lbs.) at 890 seconds (see Figure I-12). It is interesting to

Figure I-16a

Orientation of Rosettes and Location of Acoustic
Emission Transducers on Boeing 727 Elevator
Actuator Attachment Rib

STRAIN GAGE 45° ROSETTE
ACOUSTIC EMISSION SENSOR } LOCATIONS

END VIEW A-A
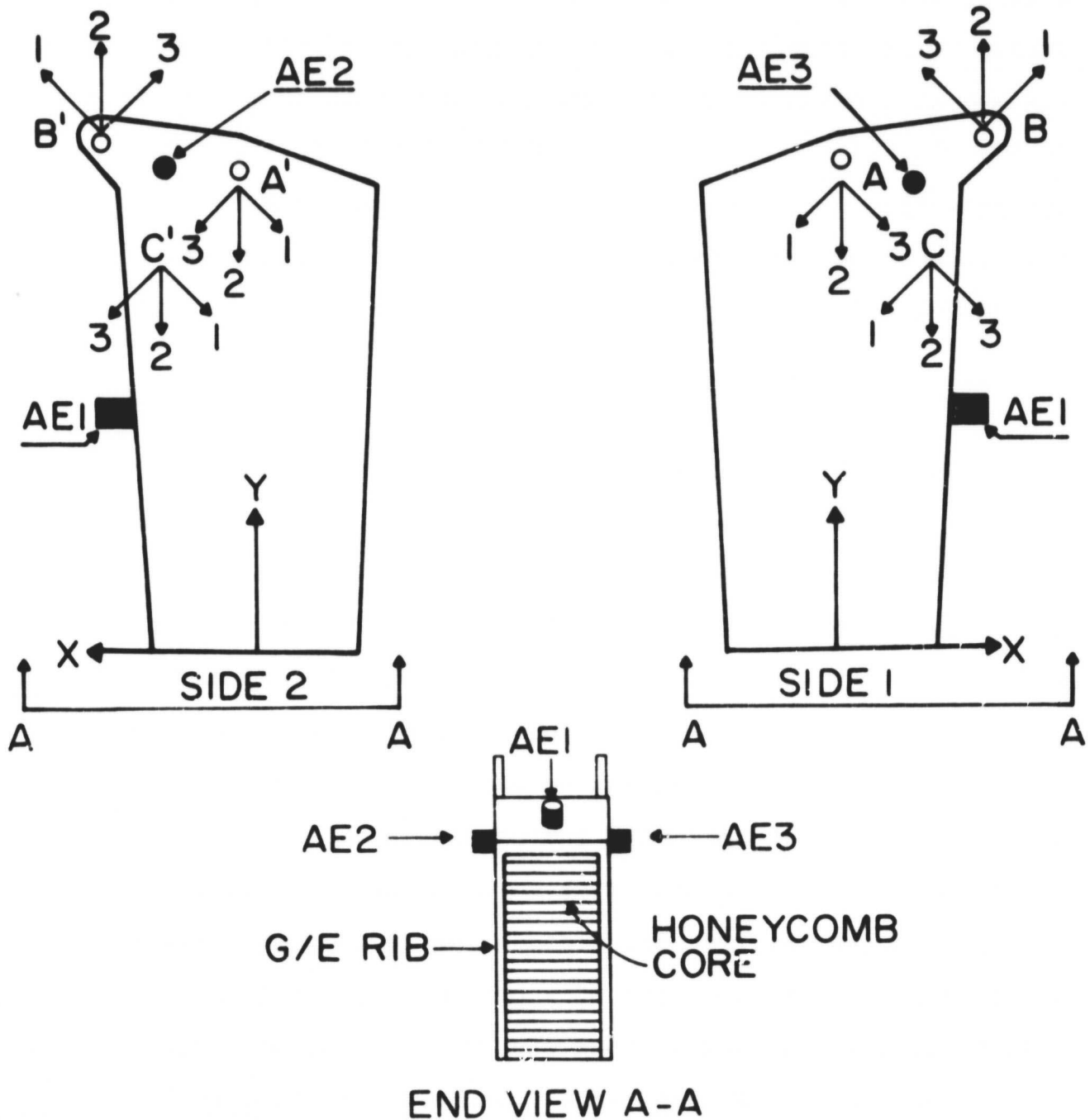
Figure I-16b

Directions of Maximum Strain and Acoustic Emission
Sensor Locations for Boeing 727 Elevator Actuator
Attachment Rib
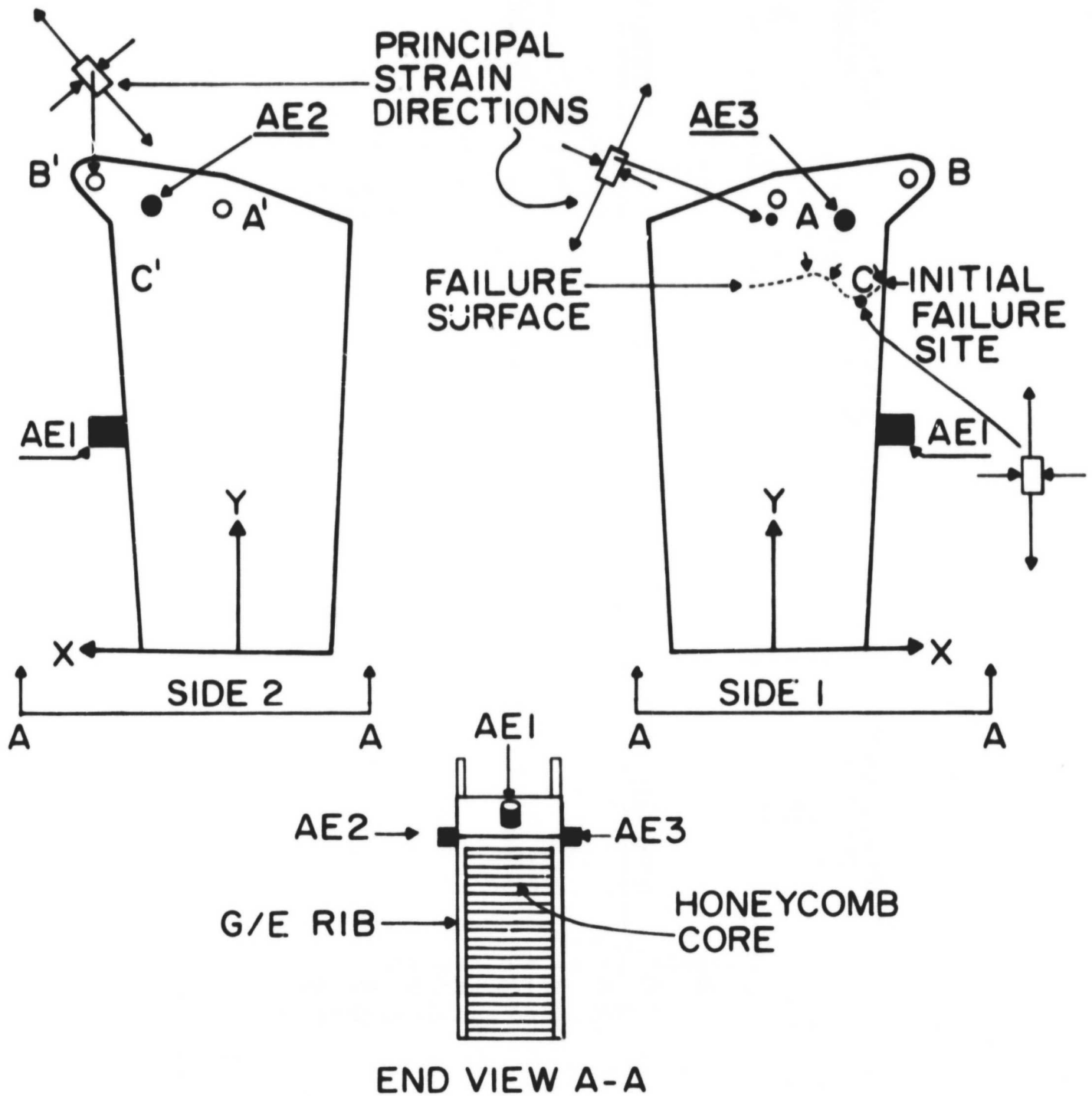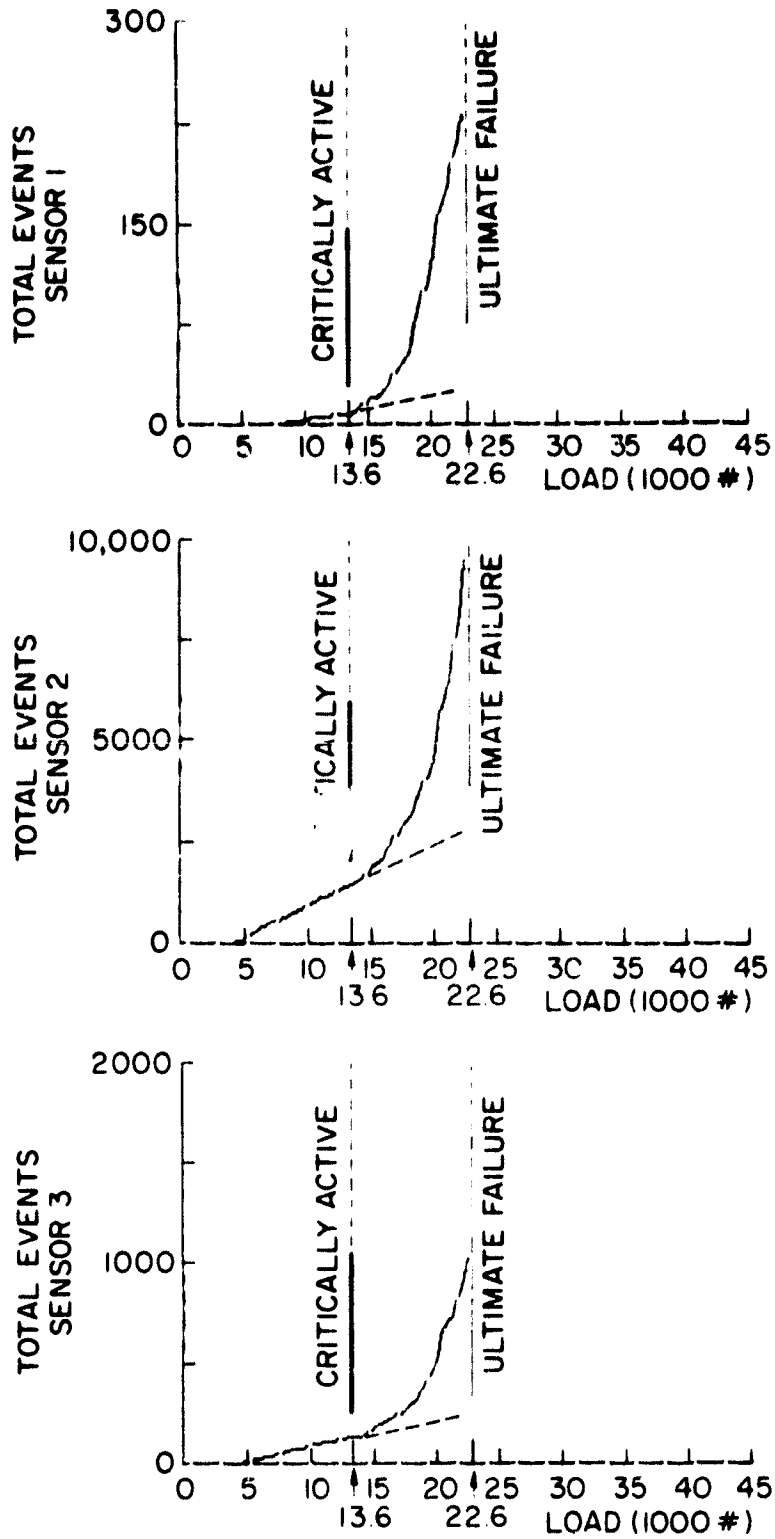
Figure I-17

Total Events Versus Load for Elevator Actuator
Attachment Rib Indicating Point of Critical Activity

compare these results with those obtained with an earlier Boeing design[9] that became critically active at 60.1 kN (13,500 lbs.) and ultimately failed at 114.9 kN (25,800 lbs.).

A comparison of the acoustic emission amplitude distribution data at sensor AE 2 early in the test (Figure I-18) with that at failure (Figure I-19), shows the tendency toward the anticipated multimodal amplitude distribution referred to in earlier AE work with composites[10,11,12]. The large number of low amplitude events occurring between 30 and 40 dB suggests matrix cracking. The higher amplitude acoustic activity at sensor AE 1 occurring above 55 dB is, at least retrospectively, a clear sign of fiber breakage occurring even at a pick-up point where lower amplitude events have been lost due to attenuation and transmission loss in the titanium Hi-Loc fastener joint. Note that the break in the sensor AE 2 curve (Figure I-19) was caused by the sudden failure of the specimen in the middle of an amplitude distribution updating in the 42 dB interval. It should also be noted that the collection of all events whose amplitudes were 64 dB and above and displaying them as though they occurred at 64 dB took place because we chose to use a 60 dB gain preamplifier. For example, a 40 dB preamplifier provides an 84 dB dynamic range. This might have been more appropriate for use with these high amplitude signals and allowed separation of the high amplitude events, rather than collecting and showing them in the 64 dB "bin"[11]. Finally, the data

DIST. 1 OF EVENTS BY PEAK AMPLITUDE FOR SENSOR 1
NUMBER OF INTERVALS = 64   INTERVAL SIZE = 1

DIST. 1 OF EVENTS BY PEAK AMPLITUDE FOR SENSOR 2
NUMBER OF INTERVALS = 64   INTERVAL SIZE = 1
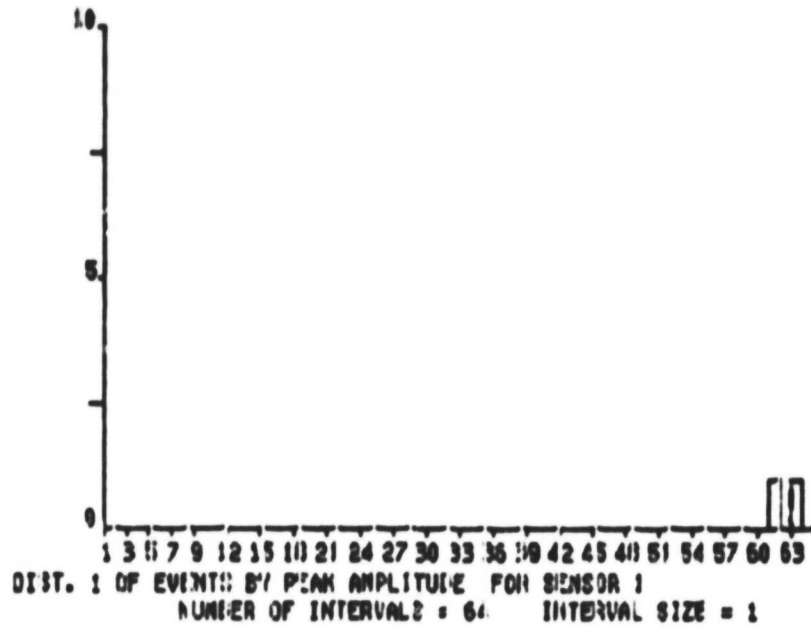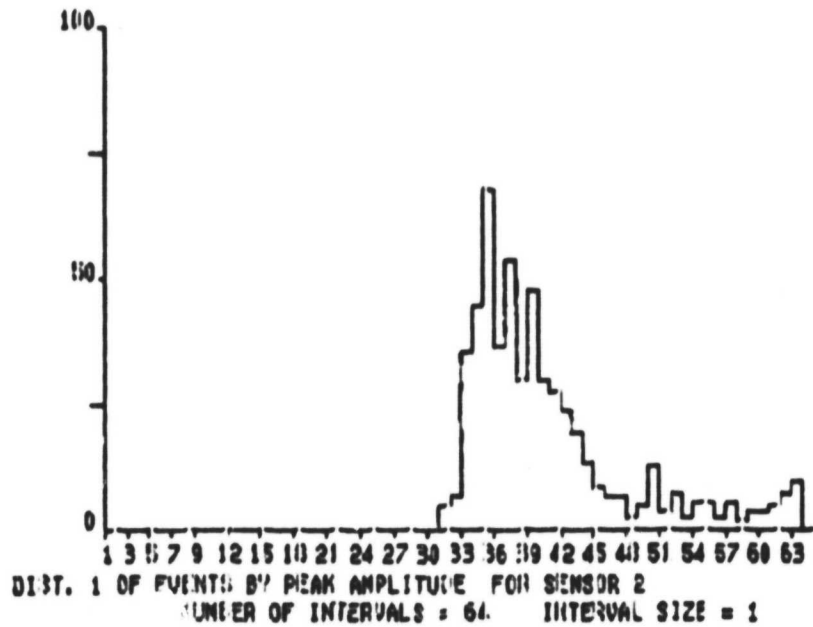
Figure   I-18

AE Amplitude Distributions Early in the Test
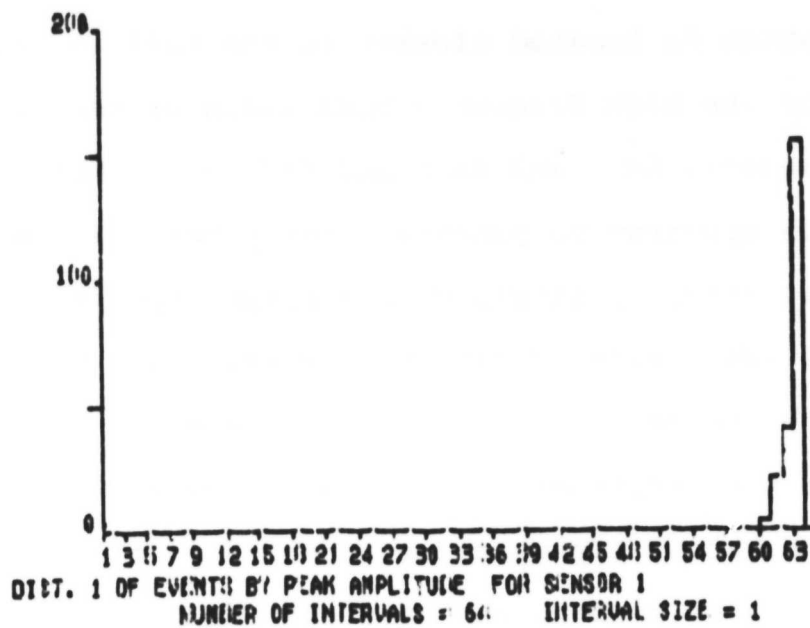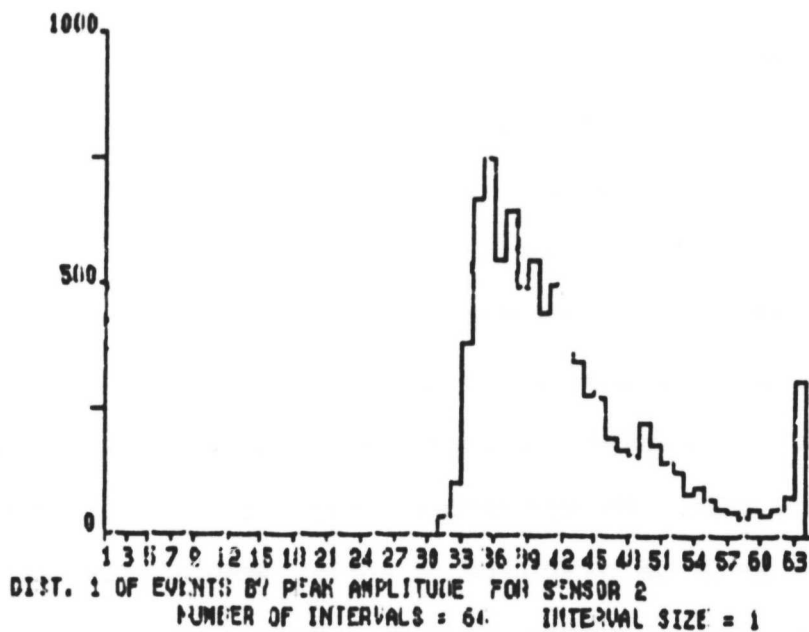
Figure I-19

AE Amplitude Distribution at Failure

from those collected at the lower number of AE events for sensor AE 3, which is located closest to the failure site, is a result of the high frequency band width of sensor AE 3 compared to sensors AE 1 and AE 2 and indicates that these AE events have spectrum components largely below 250 Hz.

Post-test visual analysis of the failed specimen (Figures I-20 and -21) in the vicinity of strain gage C clearly implicates the precise cause of local failure as tool marks around the Hi-Loc fastener. A slight unevenness in that region was induced by improper curing there. Attempts to level the flange by sanding may have weakened it. In addition, the bottom of the last fastener nut (Figure I-21) was filed off in an attempt to contour its bottom with the composite. This probably caused stress concentrations at the fastener-composite interface in the vicinity of the sharp transition between flats.

Figure I-22 shows that the composite surface layers have partially delaminated in the vicinity of many of the fasteners. It is noted that no washers were used beneath the fasteners on this test. In one sense, multiple failures of the structure are reassuring; a strong analytical effort was made to achieve a constant stress level throughout the actuator attachment rib. On the other hand, application of the results of the work of graduate student, Wonsub Kim (see the following sections), to this kind of fastening is clearly indicated.
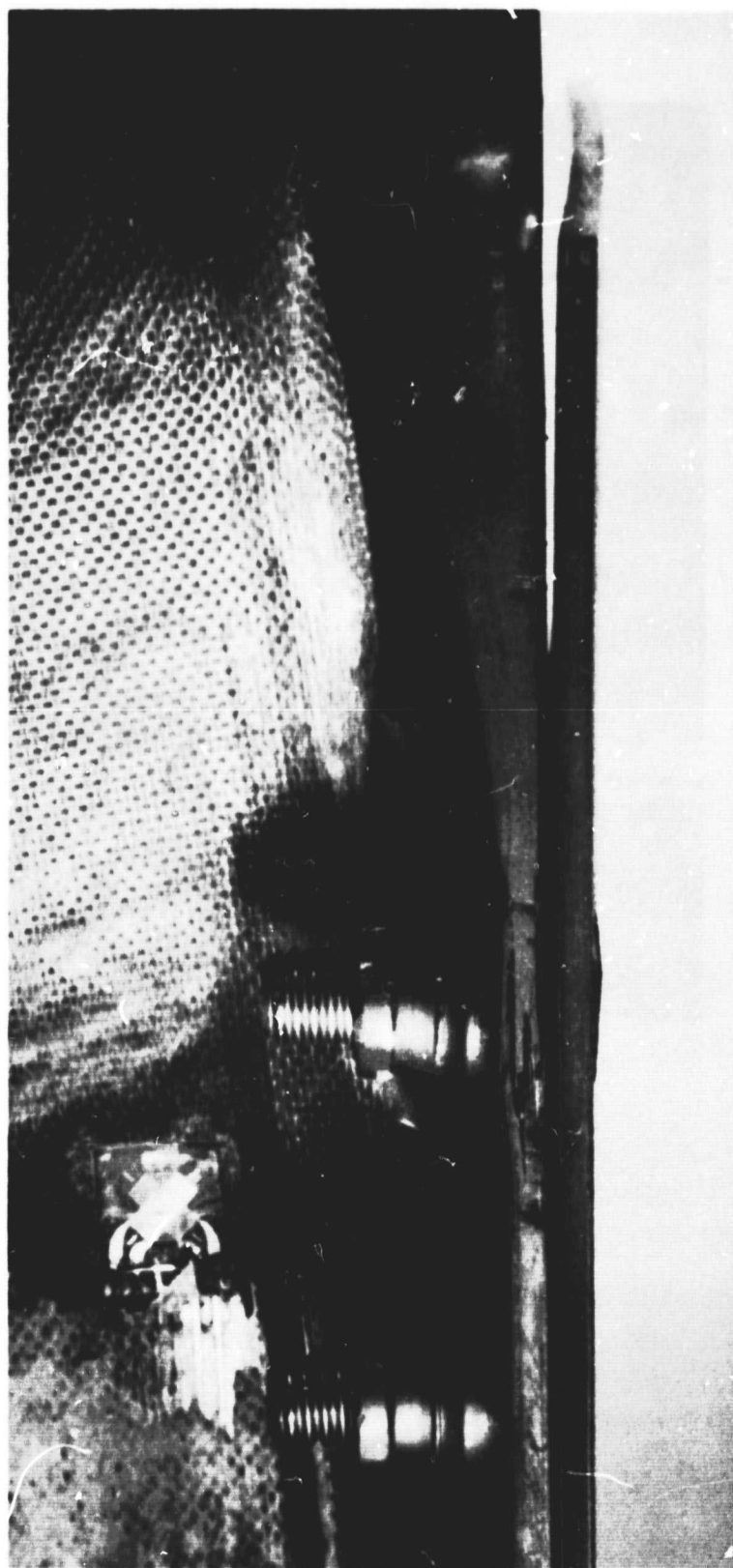
Figure I-20

Failed Section and Strain Gage
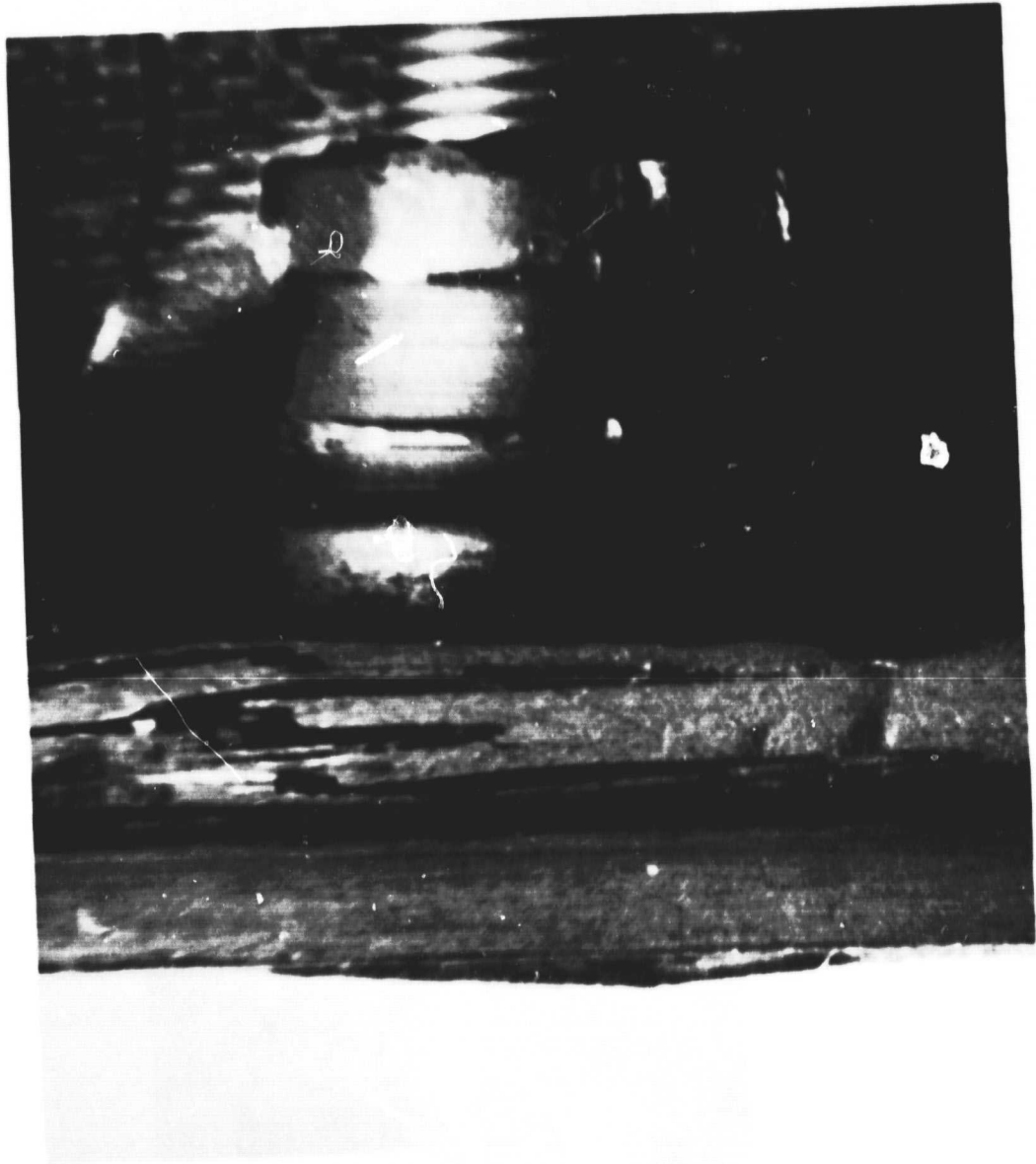
Figure I-21

Close Up of Failed Section
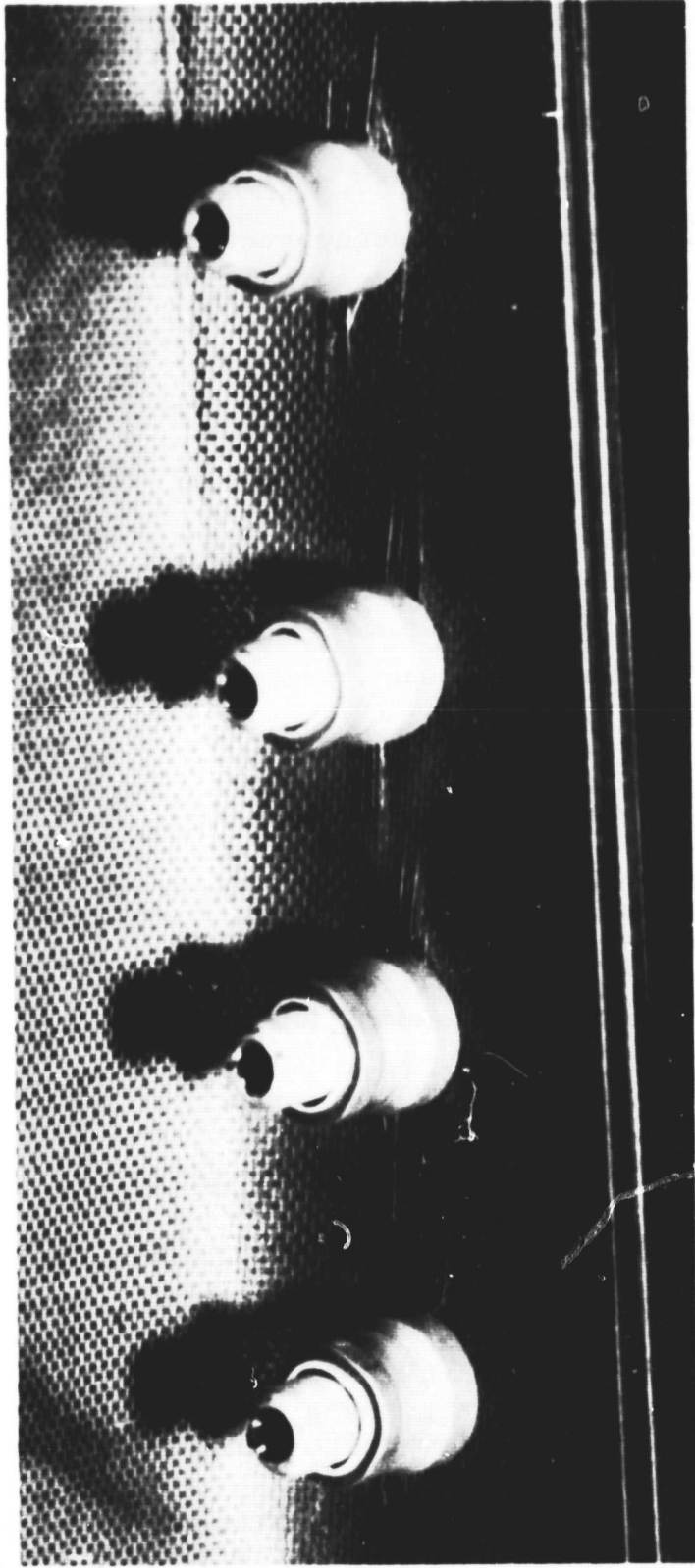
Figure I-22

Composite Partial Delamination in the Vicinity of Non-failed Rivets

In the period ahead, a second elevator actuator attachment rib will be fabricated. In this effort, attempts will be made to incorp·rate some of the lessons learned in this first test. Loadings to failure will be repeated, and strain gage and acoustic emission instrumentation will again be used.

ACKNOWLEDGEMENT:

A. References

1) Hoff, N. and R. Loewy, "CAPCOMP", NASA/AFOSR 38th Semi-- Annual Progress Report, Composite Structural Materials, June 1980, pg. 34.

2) Hoff, N. and R. Loewy, "CAPCOMP", NASA/AFOSR 39th Semi- Annual Progress Report, Composite Structural Materials, January 1981, pp. 19-58.

3) FX Systems Corp. (Data Acquisition and Control Systems), Dept. T. R., P. O. Box 1818, Kingston, NY   12401.

4) Acoustic Emission Technology Corp., 1812J Tribute Road, Sacramento, CA   95815.

5) Instron Corp., 100-A Royall Street, Canton, MA   02021.

6) Feeser, L. J. and M. S. Shephard, "COMPAD", NASA/AFOSR 38th Semi-Annual Progress Report, Composite Structural Materials, June 1980, pp. 86-96.

7) Hoff, N. and R. Loewy, "CAPCOMP", NASA/AFOSR 37th Semi- Annual Progress Report, Composite Structural Materials, December 1979, pp. 13-48.

8) "Acoustic Emission Monitoring of Structures During Controlled Stimulation", American Society for Testing and Materials, ANSI/ASTM E569-76, 1976, pp. 623-626.

9) Nichols, E. F., "Boeing/NASA 727 Advanced Composite Elevator Rib Verification Test", Test Report T6-6047, Informal Report No. 1, Structural Test Lab., The Boeing Company, June 21, 1978.

10) Otsuka, H. and H. A. Scarton, "Variation in Acoustic Emission between Graphite and Glass-Epoxy Composites", Journal of Composite Materials, Accepted for publication.

11) Otsuka, H. and H. A. Scarton, "Acoustic Emission Testing of Composite Tensile Specimens", NASA/AFOSR 38th Semi-Annual Progress Report, Composite Structural Materials, June 1980, pp. 133-139.

12) Otsuka, H. and H. A. Scarton, "Acoustic Emission of Composite Materials Undergoing Fatigue", NASA/AFOSR 39th Semi-Annual Progress Report, Composite Structural Materials, January 1981, pp. 167-178.

13) Green A. T., AET Corporation, Personal Communication, 1981.

3.   Lockheed L-1011 Engine Drag Strut (CAPCOMP II)
(D. Goetschel)

Following a visit by Dr. R. Loewy to the Lockheed California Company on November 12, 1980 and subsequent meetings and discussions in the NASA headquarters office of the Project Officer, we have jointly selected the drag strut of the wing-mounted, jet engine nacelles of the Lockheed L-1011 commercial transport aircraft for redesign in composites as the second CAPCOMP project. A drawing of the strut, currently a steel forging, is shown in Figure I-23. The manner of its installation is shown in Figure I-24. Both of these drawings, along with the first of the considerable information needed to perform this design, have graciously been provided by the Lockheed Company.

Material costs and test fixture costs may make it desirable to actually build a strut that is shorter than
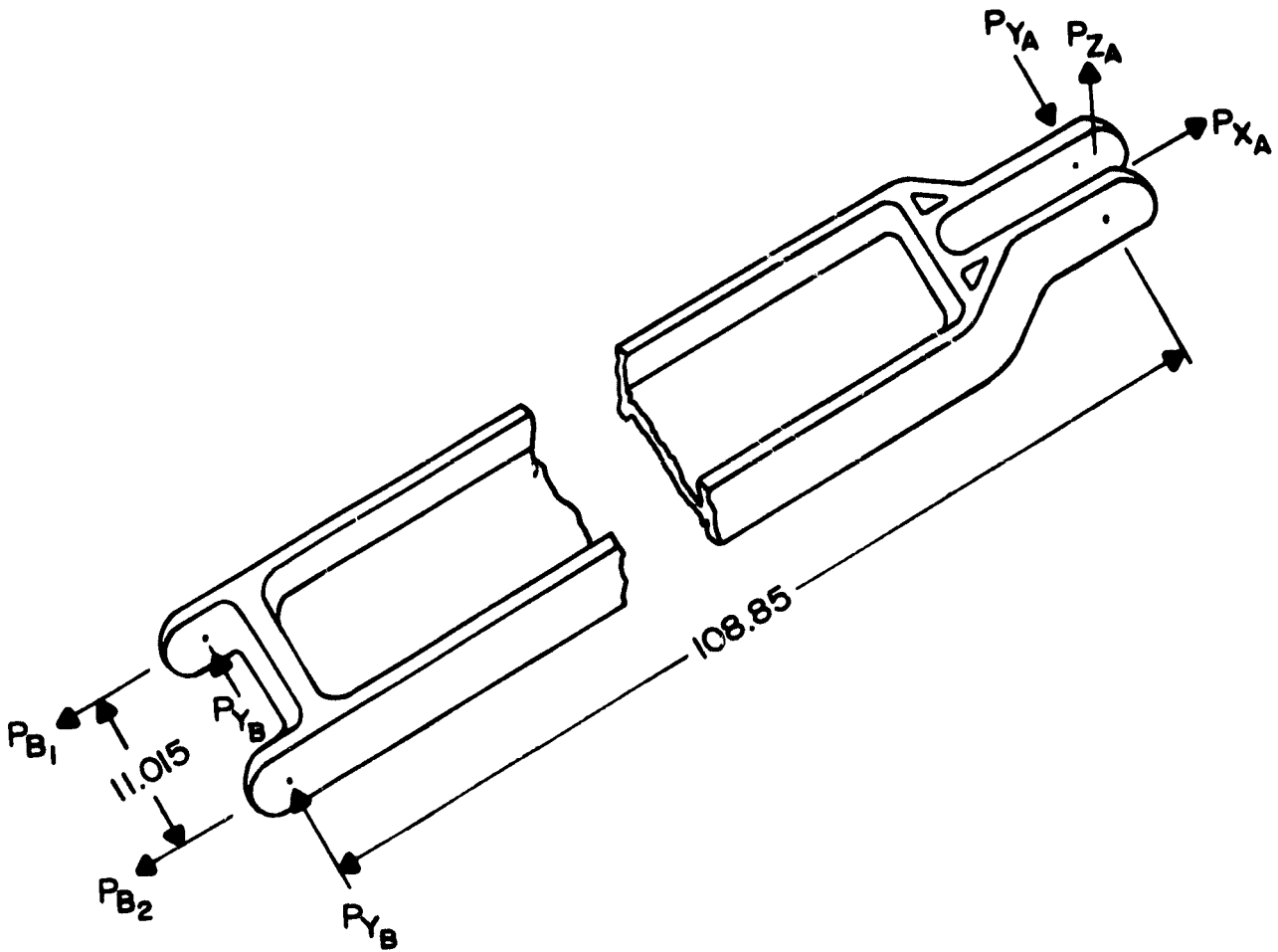
Figure I-23

Lockheed L-1011 Engine Drag Strut (Schematic)
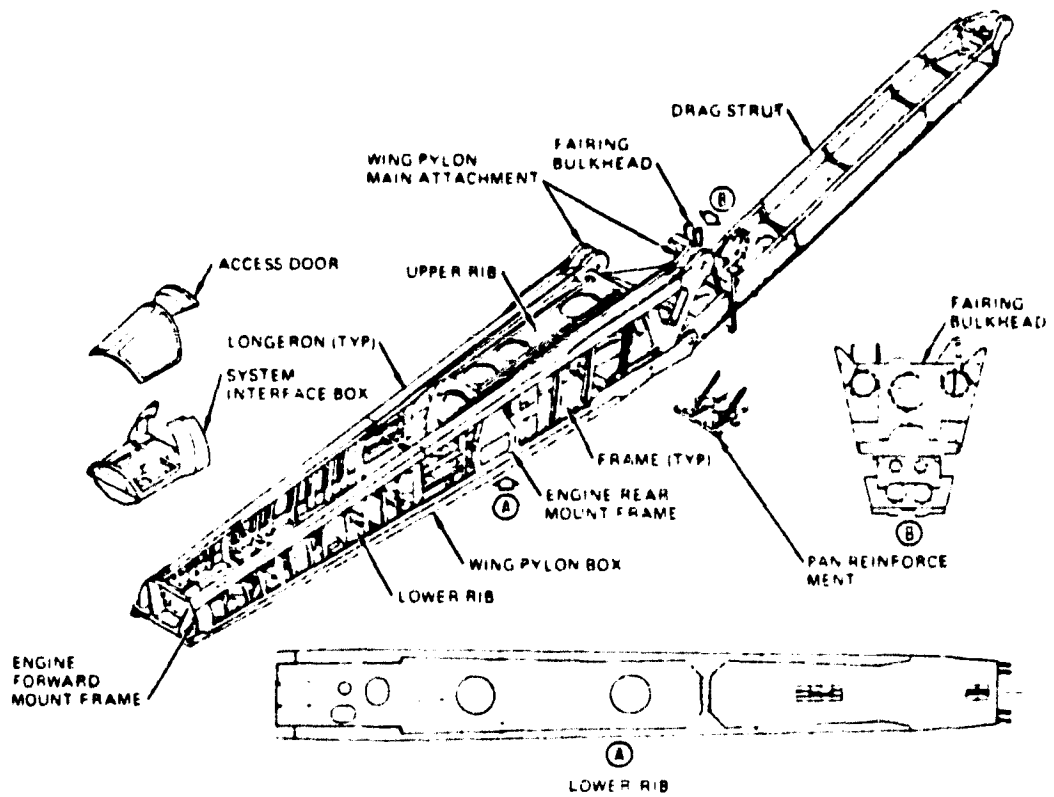
Figure I-24

Lockheed L-1011 Wing Pylon Structure Assembly

required on the aircraft. This should be possible without detracting from the substantial challenge of the project. If the strut is of uniform cross-section over most of its length, then St. Venant's principle would allow reduction of the length of the uniform cross-section portions without altering the stress distribution in the ends of the strut. To justify this it will be necessary to quantify the rate of decay of stress irregularities for the particular cross-sectional shape and anisotropic material properties employed. To this end, a computer program has been written and is currently being debugged. This program models the cross sectional shape with finite elements and assumes an exponential form for the decay rate for self equilibrating end loads. An eigenproblem analysis is then performed to determine the values of the decay rates (eigenvalues) and cross-sectional stress distributions (eigenvectors) for each mode.

Several preliminary design concepts have been explored for the redesigned drag strut structure considering composite materials. These preliminary designs suggest that a substantial weight savings can probably be made.

A preliminary design has also been made of a test fixture to be used in conjunction with RPI's electronically controlled, 56,500 lb. maximum load Instron machine. Hopefully this test fixture would allow both the static and fatigue testing of the strut to be performed on the Instron despite the fact that nominal ultimate load for the L-1011

drag strut is 500,000 lbs.

Plans for the upcoming period include completing the debugging of the prismatic St. Venant's computer program. We then intend to perform analyses to determine how short a candidate strut can be made without changing the essence of the design problem and its supporting analysis. It should also be possible to examine several candidate designs in detail and perform one iteration of detailed design and supporting analysis. A detailed design of the test fixture should also be possible.

4. Optimizing Fiber Orientations in the Vicinity of Heavily Loaded Joints
(N. J. Hoff)

A. Introduction

The purpose of this work is to find ways of arranging fibers in a composite structure that lead to high load-carrying capacity-to-weight ratios in the neighborhood of discontinuities such as mechanical joints and openings. The paucity of theoretical information of this kind and the scarcity of long-time practical experience with composite joints have compelled designers to use metals for fittings rather than composites in most highly-loaded cases. It is believed that composites offer the possibility of saving weight in such joints and, thus, merit a detailed investigation.

B. Status on September 30, 1980

A closed-form solution was found for the stress distribution in a circular plate with a central hole of radius r = 1 and an outer radius r = R under uniform tension σ in the x-direction when the material of the plate is cylindrically orthotropic and the four compliances $S_{rr}, S_{r\theta} = S_{\theta r}, S_{\theta\theta}$ and S_{66} are constant. This configuration and the associated notation are shown in Figure I-25. The maximum value of the circumferential stress $\sigma_{\theta\theta}$ at the edge of the hole (r = 1) was found and was expressed in terms of only two combined parameters. The first of these is the ratio $\bar{S}_{rr} = S_{rr}/S_{\theta\theta}$, and the second $\bar{S} = 2\bar{S}_{r\theta} + \bar{S}_{66} = 2(S_{r\theta}/S_{\theta\theta}) + (S_{66}/S_{\theta\theta})$.

The results of the calculations indicate that the stress distribution in the circular plate depends greatly on the values of the parameters $\bar{S}_{rr}$ and $\bar{S}$. In some ranges of the values the stresses are given by exponential functions of r with real argument, in others by products of trigonometric and exponential functions (all with real argument), and in still others by pure trigonometric functions (with real argument). In addition, it turned out that the behavior at infinity, that is in the limit as R was made to increase beyond all bounds, also differed greatly in different ranges of the parameters.

The numerical values of the stress concentration factor were calculated for a small number of combinations of values of the two compliance parameters. They were found reasonable
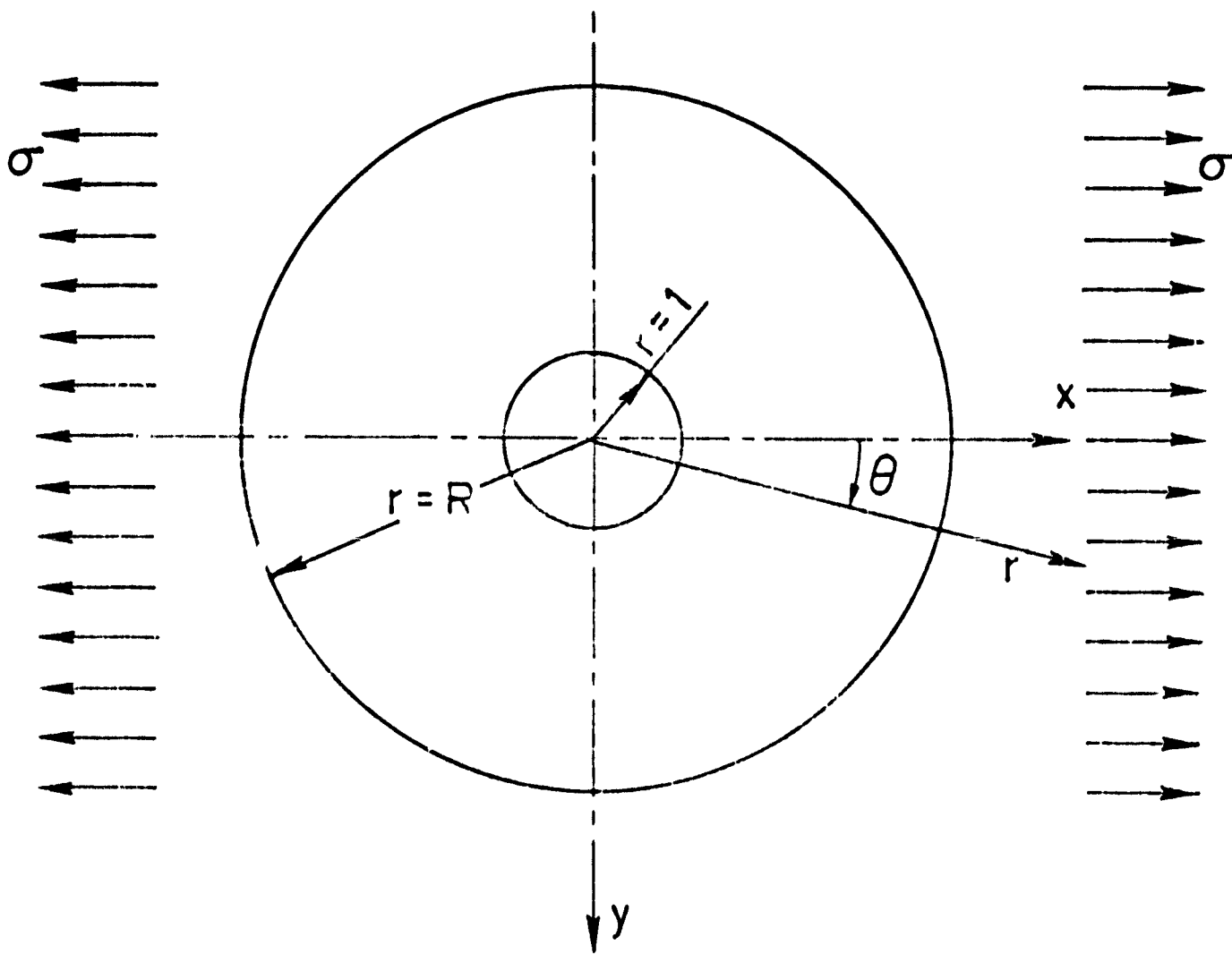
Figure I-25

"Notation"

in comparison with known stress concentration factors for isotropic and orthotropic (in a cartesian system of coordinates) plates.

In addition, much work was done as part of the research of graduate student C. Muser, to calculate the stress-concentration factor in plates whose compliances vary as functions of the radius r. In the constitutive equation, the constant compliance S_{pq}^{*} was augmented by a radius-dependent term $S_{pq}^{*} e_i r^{2h}$, where e_i and h are constants. As a first approximation to the solution of the new system of equations, the known solution of the system for which $e_i = 0$ was chosen. To correct for the error, an infinite series was added to the solution and the coefficients of the series were determined.

A few cases were worked out in full numerical detail. In these, h was chosen either as 2 or as -2, and the values of the constants e_i were so selected as to approximate roughly the values of the compliances of plates for which, at r = 1, all the fibers run at angles ·45°, and at R = 10, the fibers are arranged so as to yield a quasi-i··tropic material.

The variation in compliance values and the variation of the circumferential stress, both as functions of r, were presented diagramatically in the last semi-annual report. It can be seen from these diagrams that the stress distributions are quite different from those occurring in plates with constant quasi-isotropic compliance values.

C. Progress During Report Period

The expressions obtained earlier for the stress concentration factors were evaluated for a wide range of the values of the parameters $\bar{S}_{rr}$ and $\bar{S}$. The numerical work was carried out for R = 6 and R = 10. The results differ little in these two cases, and they appear to be satisfactory when used for test specimens of finite size even though the specimens are not circular. If very accurate results are needed for rectangular specimens, probably calculations by finite element methods are unavoidable. Finite element analyses, of course, give results only for the particular specimen treated and lack the generality of the present treatment of the problem.

In the present case, the formulas derived earlier can be re-written in the following modified form:

$$G = \alpha + \beta = \left[1 + \bar{S}_{rr} + h^2\bar{S} + 2(n^2 - 1)\sqrt{\bar{S}_{rr}}\right]^{\frac{1}{2}}$$

$$H = \alpha - \beta = \left[1 + \bar{S}_{rr} + n^2\bar{S} - 2(n^2 - 1)\sqrt{\bar{S}_{rr}}\right]^{\frac{1}{2}}$$

$$\alpha^2 - \beta^2 = GH \quad (\tfrac{1}{2})(G + H) = \alpha \quad (\tfrac{1}{2})(G - H) = \beta$$

$$\alpha\beta = (\tfrac{1}{4})(G^2 - H^2)$$

When the expressions in braces for both G and H are positive, both G and H are real. In such a case, the circumferential stress at the edge of the hole can be written as

$$\sigma_\theta \Big|_{r\,=\,1} = (\sigma R/4)(N/D) \cos 2\theta$$

with

$$N = GH\{G(R^{G/2} + R^{-G/2})(R^{H/2} - R^{-H/2})$$

$$- H(R^{G/2} - R^{-G/2})(R^{H/2} + R^{-H/2})$$

$$- (\tfrac{1}{2})(G^2 - H^2)(R^{G/2} - R^{-G/2})(R^{H/2} - R^{-H/2})\}$$

$$D = (2G^2 - H^2) + H^2(R^G + R^{-G}) - G^2(R^H + R^{-H})$$

Since both G and H are real, the following relations hold:

$$(\tfrac{1}{2})(R^G + R^{-G}) = (\tfrac{1}{2})(e^{G \log R} + e^{-G \log R}) = \cosh (G \log R)$$

$$(\tfrac{1}{2})(R^G - R^{-G}) = (\tfrac{1}{2})(e^{G \log R} - e^{-G \log R}) = \sinh (G \log R)$$

and similar expressions can be written for combinations of R^H. (Here log R stands for the natural logarithm of R.)

Similar formulas can be written for those regions of the parameters $\bar{S}_{rr}$ and $\bar{S}$ in which the roots of the characteristic equations are conjugate complex or pure imaginary.

Figure I-26 shows how the character of the roots varies in the $\bar{S}_{rr}$ - $\bar{S}$ plane. With the aid of this information, it was possible to calculate the stress-concentration factor for all possible cylindrically orthotropic plates provided the compliances were constant. The final results of the calculations for the case when R = 10 are presented in Figure I-27. The R = 10 case was shown by computations to be representative of the behavior of specimens of finite size.
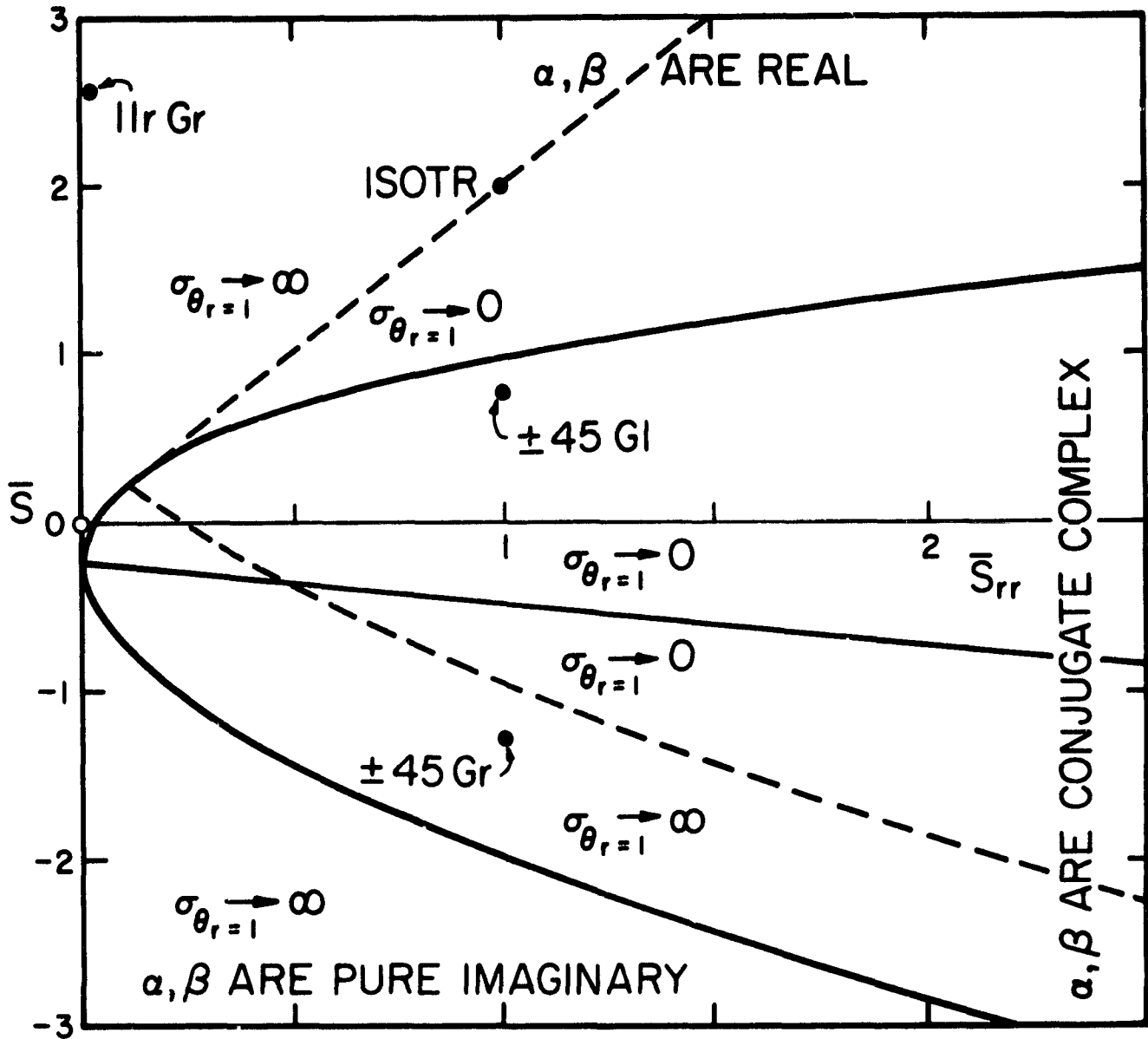
Figure I-26

Ranges of Solution of Equations

Gr - graphite-epoxy

Gl - glass-epoxy

LINES OF EQUAL STRESS CONCENTRATION
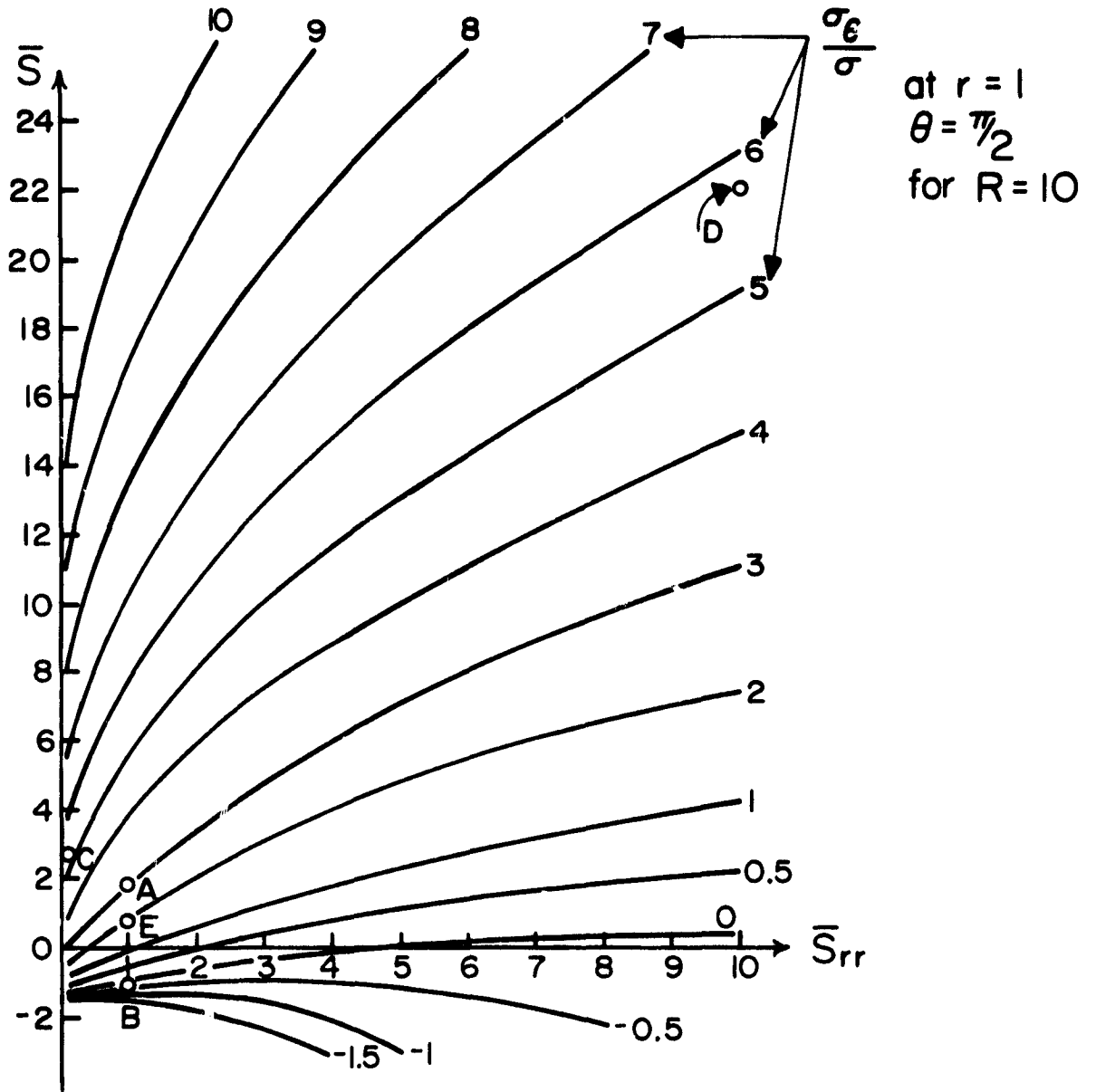
Figure I-27

One general observation can be made on the basis of Figure I-27; for any fixed value of $\bar{S}$, the stress concentration factor increases as $\bar{S}_{rr}$ decreases, and it becomes very high as $\bar{S}_{rr}$ approaches zero.

In the cases in which compliances vary with the radius, the variation was represented by the constitutive equation

$$\begin{Bmatrix} \varepsilon_r \\ \varepsilon_\theta \\ \gamma_{r\theta} \end{Bmatrix} = \begin{bmatrix} S'_{rr} + S^+_{rr}r^h & S^*_{r\theta} + S^+_{r\theta}r^h & 0 \\ S^*_{r\theta} + S^+_{r\theta}r^h & S^*_{\theta\theta} + S^+_{\theta\theta}r^h & 0 \\ 0 & 0 & S^*_{66} + S^+_{66}r^h \end{bmatrix} \begin{Bmatrix} \sigma_r \\ \sigma_\theta \\ \tau_{r\theta} \end{Bmatrix}$$

By selecting h properly (it can be either positive or negative), the actual variation of the compliances along the radius can be approximated satisfactorily in most cases by the powers of r shown. If higher accuracy of the representation is desired, terms with r^{2h}, r^{3h}, $\cdots$ can be added in the matrix, but, of course, the time needed for the solution increases considerably.

The solution is started by assuming the known solution for the case when all the S^+_{pq} are zero. (This is the case when the compliances are constant, i.e., independent of r.) When this is done, the compatibility condition is satisfied for all those terms in which the S^+_{pq} do not appear. There remains, however, a non-vanishing residue R_h which is multiplied by r^{h-2}. (In this residue the S^+_{pq} appear.) To get rid of this, one adds to the first solution a term multiplied

by r^{-h} and by a constant, K_h. Part of the residue in the compatibility equation due to this term, which can be denoted R_h^*, again contains a multiplier r^{h-2}. From the requirement that $R_h + R_h^* = 0$, $h = 0$, one can calculate the necessary value of K_h.

It should be evident that the second term in the solution will leave a residue R_{2h} which can be eliminated by adding a term with a factor r^{2h} to the solution, and the process can be continued ad infinitum. This process was carried out and expressions were derived for the constants K_h. The convergence of the process was investigated and the limits were stated within which convergence is found. Of course, the analysis had to be carried out both for terms multiplied by functions of θ and for those independent of θ. Also, a number of special cases had to be treated (for instance, when $\bar{S}_{rr} = 1$).

Numerical results were obtained for many cases and a report on the work is now in preparation.

D. Current Publications or Presentations by Professor Hoff on this Subject

"Stress Concentrations in Cylindrically Orthotropic Composite Plates with a Circular Hole"

Accepted for publication in the Journal of Applied Mechanics.

Presented at the Joint ASME/ASCE Mechanics Conference, Boulder, Colorado, June 23, 1981.

5. Supporting Research on Lightly Loaded Mechanical Joints
(R. Loewy)

A. Introduction

The work of graduate student Wonsub Kim continued to concentrate on stress distributions around pin-loaded holes in composite membranes and plates (with no special fiber arrangements around the hole) and the associated bearing strength and failure mechanisms.

The general stress analysis problem of composite plates joined mechanically in this way cannot be solved with any single known analysis method. The difficulties arise because of the variability of contact between the loading pin and hole. Any real joint usually has clearance between the pin and hole. (See Figure I-28 for parameter definition.) Exceptions include "shrink" or interference fits. When clearance exists, it reduces the initial contact region to less than half the perifery of the hole. Since the most critical area in the domain is the area close to the hole, and since the stress distribution depends highly on the contact area, a proper stress analysis should use boundary conditions based on the correct contact region. On the other hand, where there is clearance, the angle of contact cannot be known at the outset.

To overcome this frustrating situation, a semi-empirical stress analysis method was employed which we call a "mixed" method. The method is based on the fact that the isochromatic
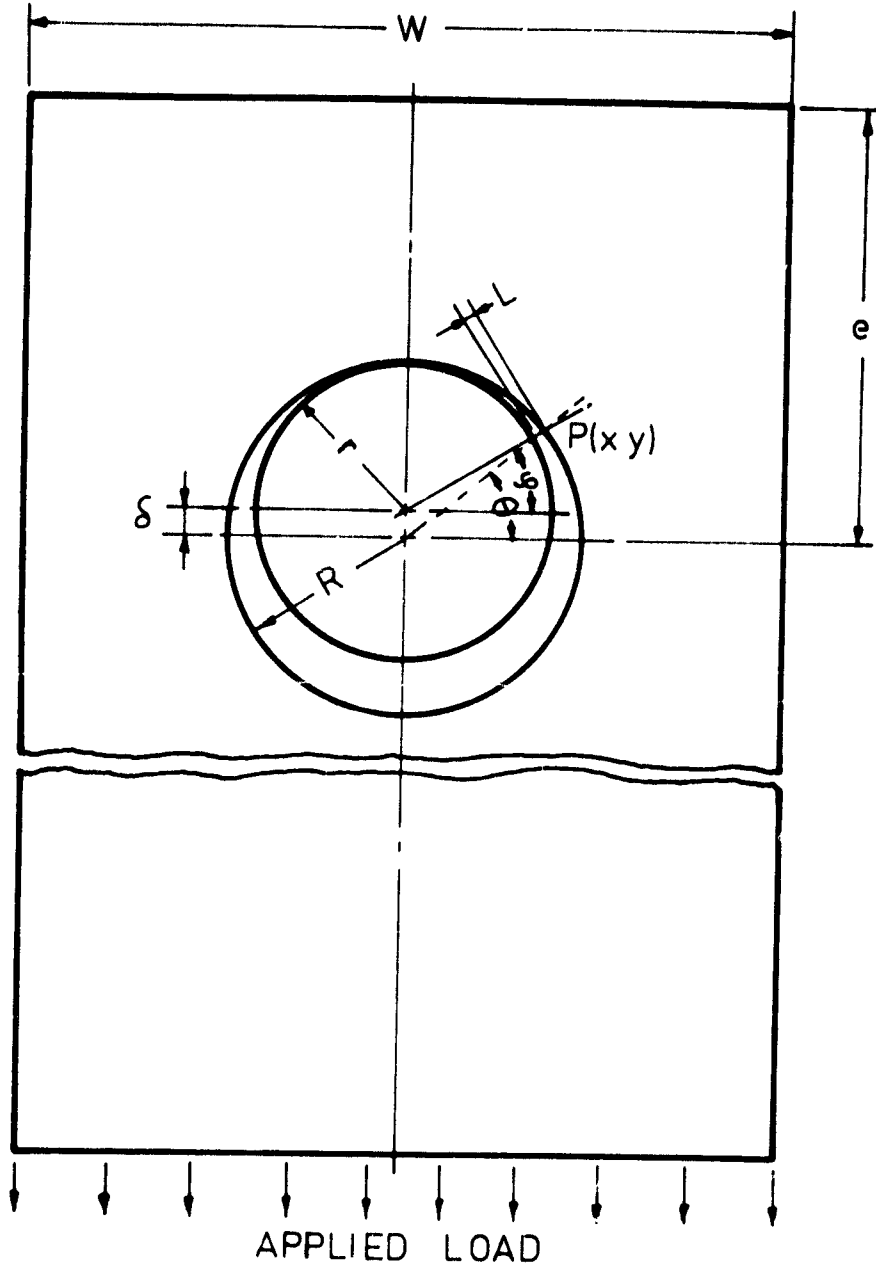
Figure   I-28

Clearance Fit Problem Definition

fringes in photoelasticity depict the maximum shear strain distributions. These same distributions can also be reproduced by a finite element analysis, if a contact region is assumed. If the contours produced by the finite element method match well with the isochromatics, then it is reasonable to believe that the assumed contact region is correct. All of the corresponding stress analysis results, in fact, can then be assumed to be correct within the limitations of finite element theory. This "mixed" analysis approach can be used to analyze a clearance-fit joint as well as tight-fit cases.

Considering the deformation of the part of the surface of the hole which is contacted by a pin under load, it seems clear that any attempt to predict the ultimate strength of a joint based on a stress analysis with the assumption of half circle contact - as is often done - is unlikely to yield useful results.

B. Status

In the previous progress report, the development of computer programs to implement the "mixed" method was reviewed in some detail. The first attempt to draw the maximum shear strain contours was also reported and discussed. It was pointed out that the values of the maximum shear strain contours were almost twice as high as the values indicated by the corresponding isochromatics. Subsequently, it was found out that an input error was responsible for that result. In

the finite element analysis, we took advantage of symmetry and analyzed a model that is half the width of the photoelastic specimen; we therefore should also have used one-half the applied load. As a result of using the total load applied to the photoelastic experiment, the analysis predicted stresses two times too high, since the material properties are linear.

C. Progress During Report Period

The work to check the adequacy of this method as applied to the joint problem has been continued. The sample examined was the plate with fiber arrangement $[+45/-45/90]_{6s}$, where the angles are measured from the direction of the applied load. The mesh used in the finite element analysis is shown in Figure I-29. Figure I-30 is a photograph of a photoelastic experiment showing the isochromatic fringes at 3,000 lbs. load. The diameter of the loading pin was measured as 0.5001 inch, while the maximum diameter of the drill bit used was 0.499 inch. To assemble, a very hard hand push was necessary to put the pin through the hole; i.e., clearance was quite small. In Figures I-31 through -33, maximum shear strain distributions are shown, as predicted by finite element analysis for contact angles (θ_c in Figure I-28) of 80, 50 and 40 degrees, respectively. The strain values per fringe are the same for both methods; finite element analysis (Figures I-31 through -33) and photoelasticity (Figure I-30). Comparing
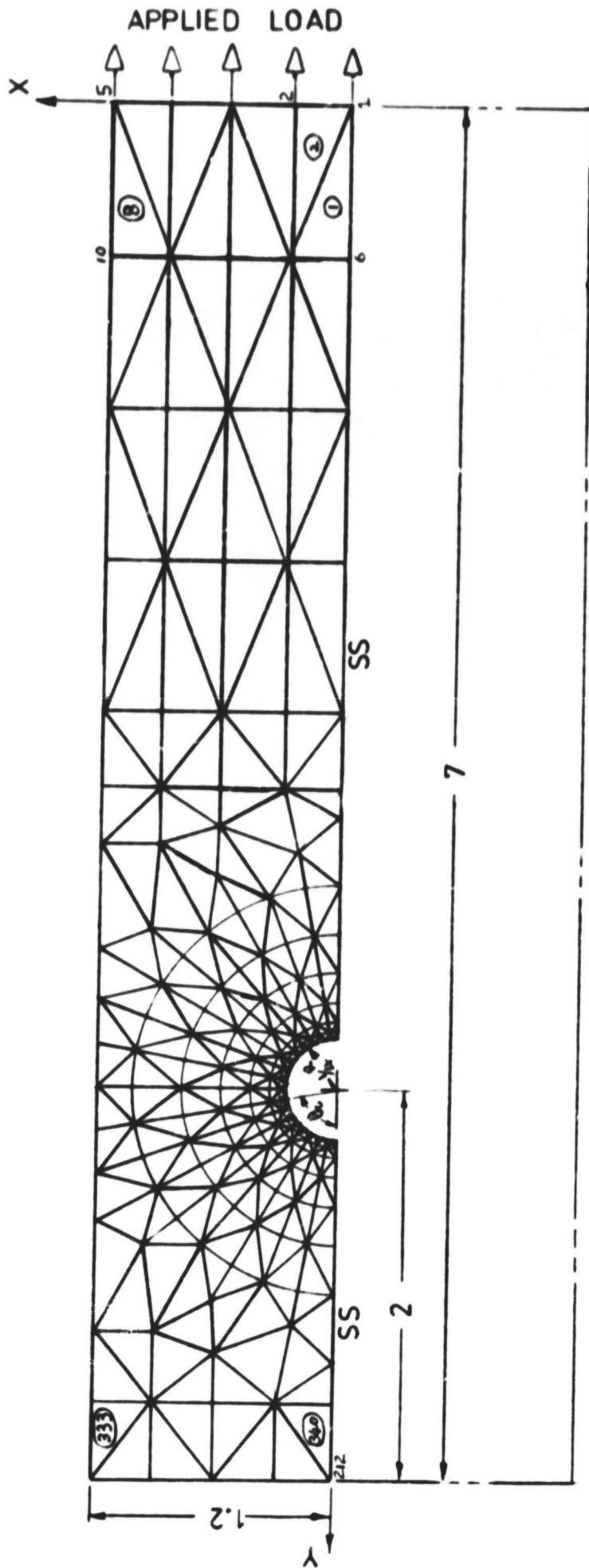
Figure I-29

Finite Element Idealization
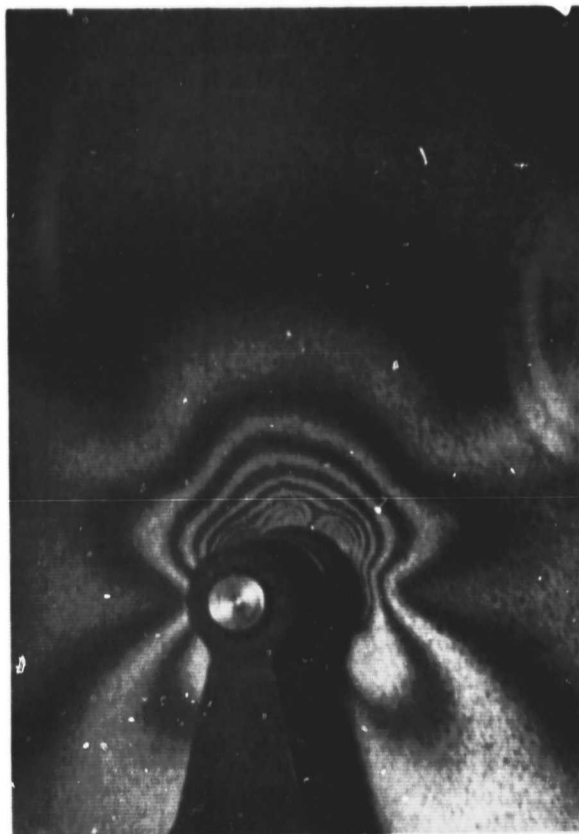
Figure   I-30

Photoelastic Fringes (Isochromatic)
(Applied Load 3,000 lb.)
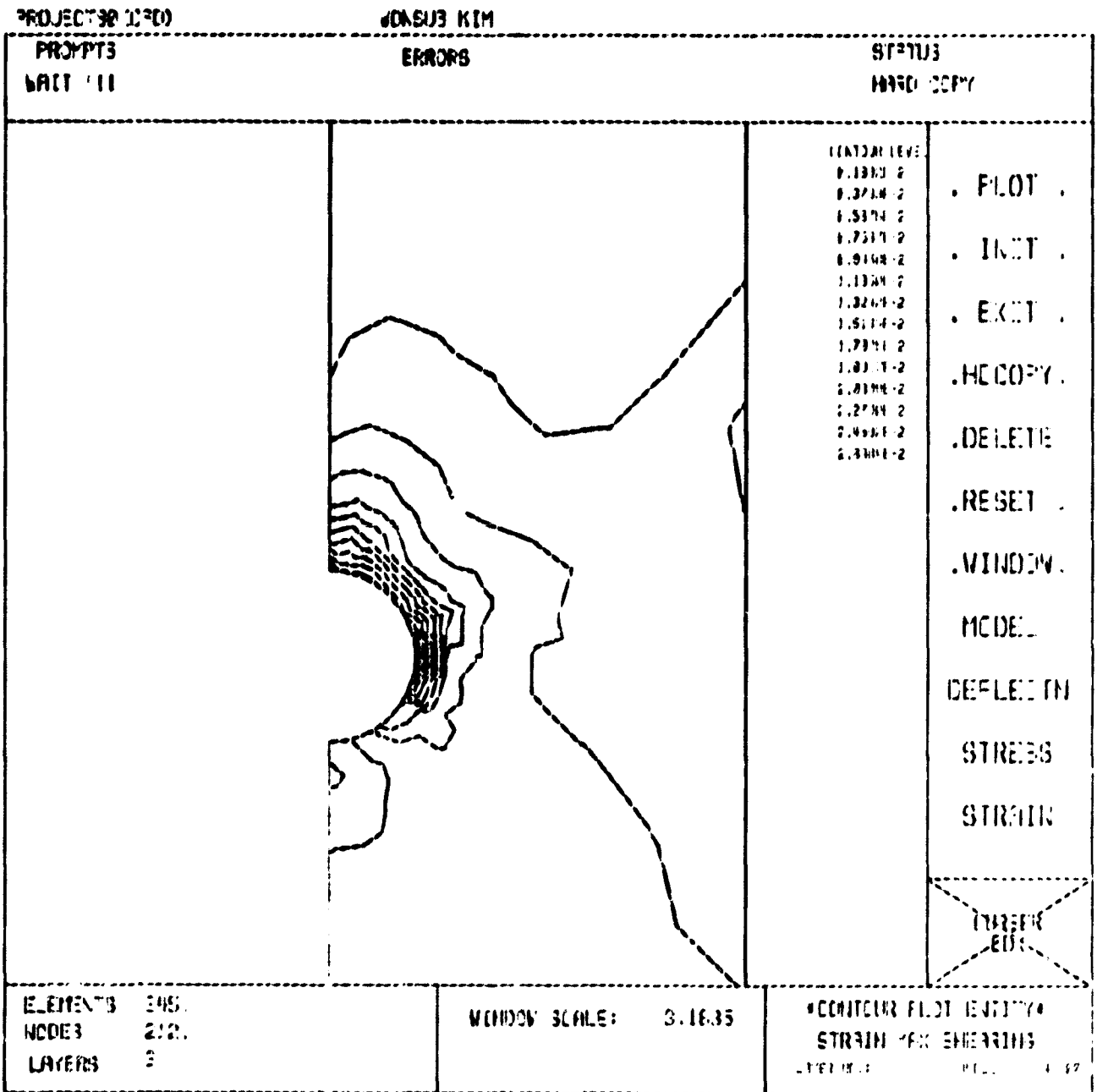
Figure I-31

Maximum Shear Strain Contour
(Contact Angle 80°, Applied Load 3,000 lb.)
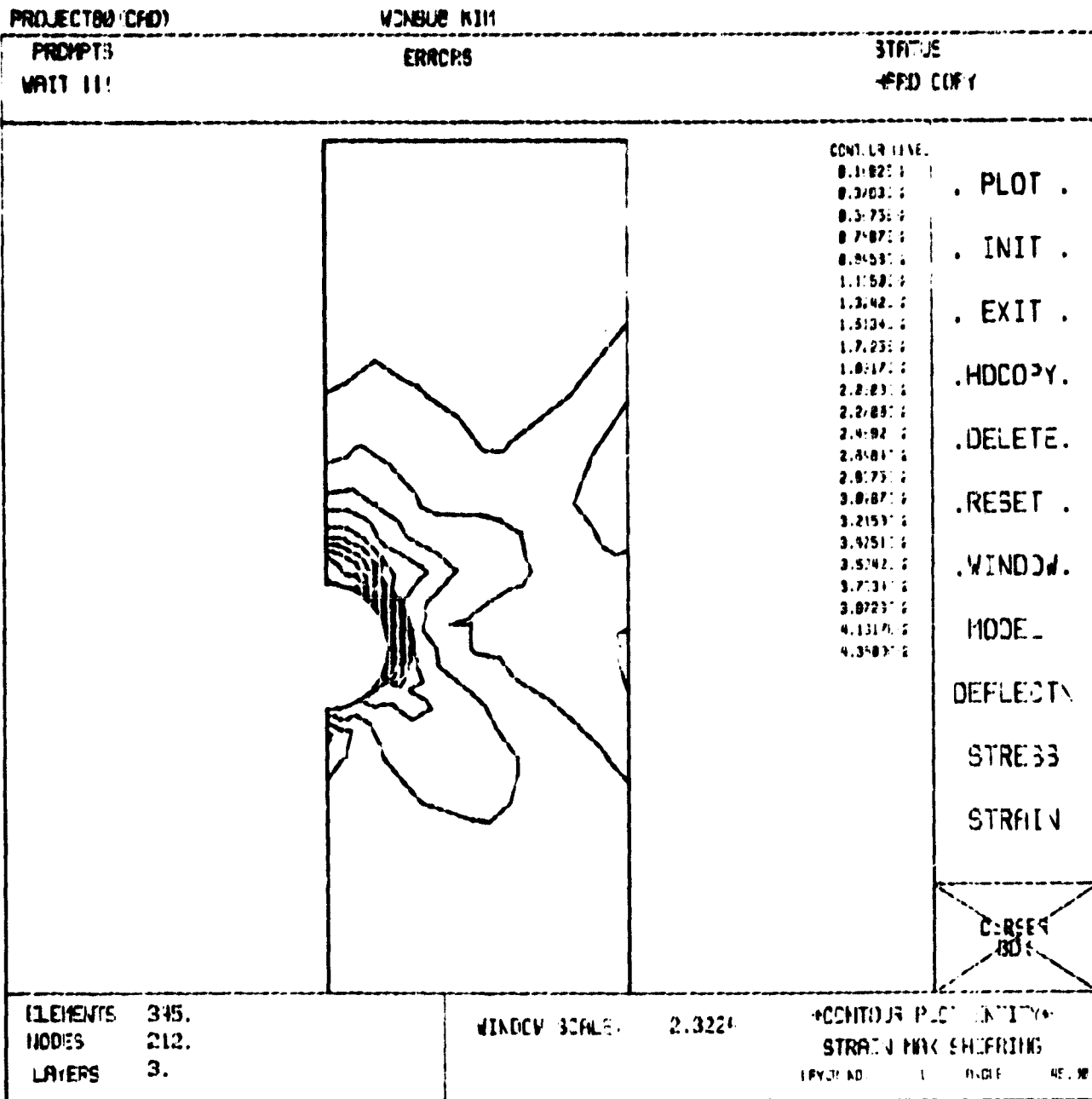
Figure I-32

Maximum Shear Strain Contour
(Contact Angle 50°, Applied Load 3,000 lb.,
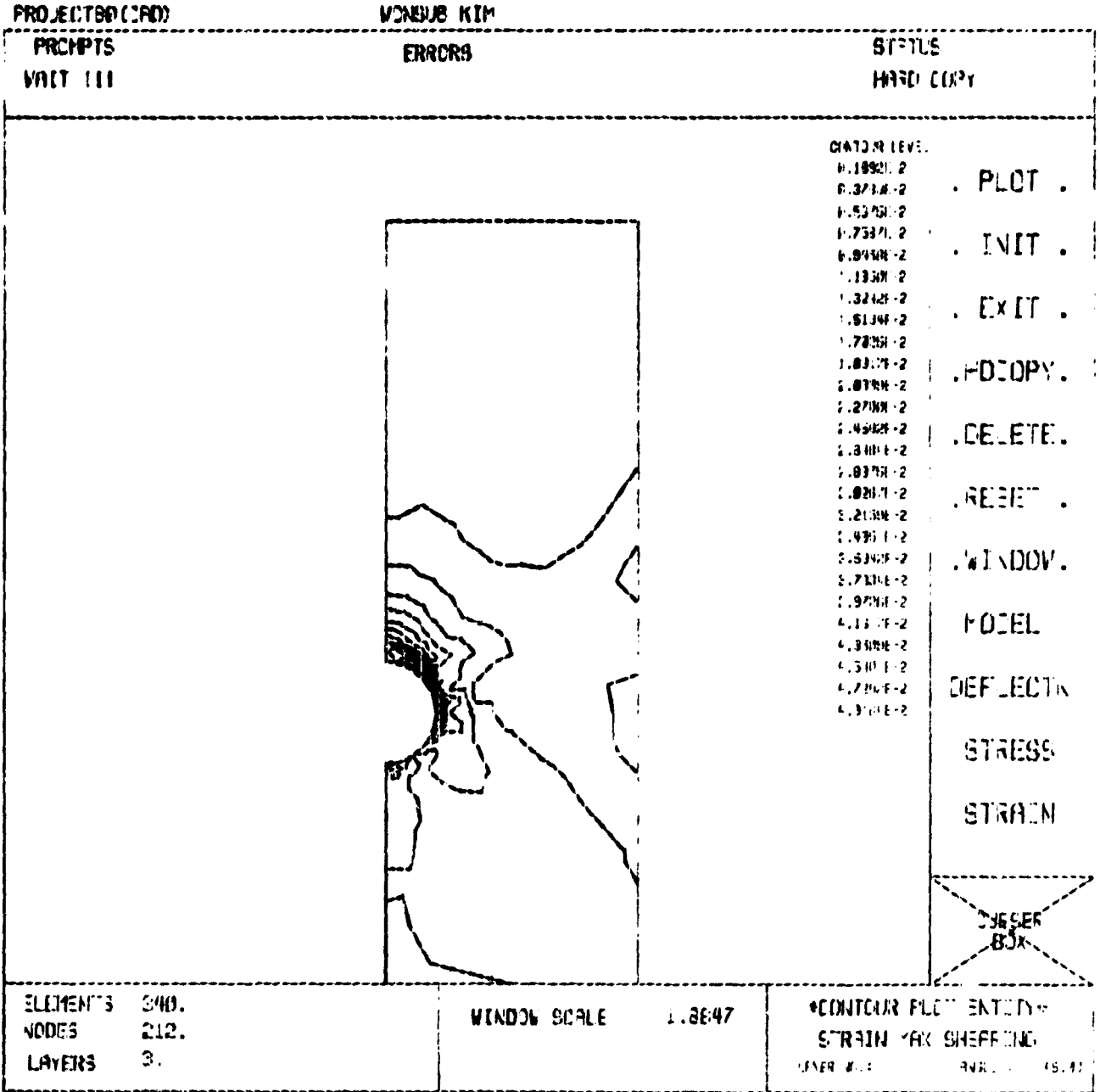
Figure I-33

Maximum Shear Strain Contour
(Contact Angle 40°, Applied Load 3,000 lb.)

these diagrams, it appears that the 50 degrees contact angle assumption is the best among the three. It should be noticed that even 10 degrees variation in contact angle resulted in substantial differences in stress distributions. (Compare Figures I-32 and -33)

Although fine adjustments to complete this sample problem remain to be done, even at this point it satisfactorily establishes the principles involved. It would appear that in this case of very small clearance, the actual contact angle is closer to 50 degrees than the 90 degrees of a half circle contact assumption.

The finite element model shown in Figure I-29 is changed slightly from that reported for the last period. The density of element population was increased near the hole and decreased in remote areas to improve accuracy while keeping costs at the same level.

A more significant change was in the constraint equations employed in the boundary conditions for the finite element analysis. The previous constraint equation set the radial displacement to zero at nodes on the loaded edge of the hole. This put points on the loaded part of the hole into contact with the pin regardless of the load state. The new constraint equation simulates more closely the actual behavior in that area. That is, a point within the contact region does not touch the pin initially, but its final location is on the surface of the loading pin at the equilibirum state.

Rather than setting radial displacements to zero, this simulation imposes precalculated values of radial displacement on individual nodal points to bring them into contact with the pin within this region. A description of the way this restriction was calculated from the geometry follows.

The schematic drawing of the clearance fit joint problem at zero load state is shown in Figure I-28. $P(x,y)$ is a representative point on the hole boundary within the soon-to-be-contacted region, and, x and y are the location of point P in a global cartesian coordinate system with origin at the intersection of the plate center line and the loaded edge. The allowed radial displacement of this point is L in a polar coordinate whose origin is located at the center of the loading pin. L can be expressed in terms of components of the displacement at P as,

$$-L = u \cos \phi + v \sin \phi \tag{1}$$

where, u and v are x and y displacements, respectively, in terms of global coordinates, and y is given by

$$\phi = \arctan \frac{(y - \delta - y_o)}{x} \tag{2}$$

where y_o is not shown in Figure I-28 but is the distance, in the loading direction, between the center of the hole and the loaded edge. From the geometry of Figure I-28,

$$L = c \cos \phi + (y - \delta - y_o) \sin \phi - r \tag{3}$$

where, r is the radius of the loading pin. Equation (1) is the new constraint equation.

When the clearance, δ, is zero, r = R, $\delta = \theta$ and equation (3) becomes,

$$L = x \cos \theta + v \sin \theta - R = 0 \qquad (4)$$

so that equation (1) becomes

$$0 = u \cos \theta + v \sin \theta \qquad (5)$$

This is the old constraint equation. Significantly, this new constraint equation enables the clearance-fit analysis of a mechanical joint as well as tight-fit analysis.

Now it appears that the semi-empirical "mixed" stress analysis method is completely established and ready for use.

D. Plans for Upcoming Period

To attack real joint problems, we will test several more photoelastic specimens. Grid meshes will be engraved on the photoelastic coating materials of all future specimens to improve accuracy. This technique has already been tested and the results were satisfactory. The pin/hole clearance of future specimens will also be carefully controlled in the fabrication process. (ASTM D1602-60, pp. 156-159, 1979)

Analyses will be performed for five to six loading steps for each specimen to determine the relations between the contact angle and applied load. After that, if time allows, we will try to link the results of our stress analyses to the fracture strength of the specimens.

PART II

CAPGLIDE (Composite Aircraft Program Glider)

CAPGLIDE (Composite Aircraft Program Glider)
(R. J. Dienfendorf, H. J. Hagerup, F. Bundy)

1. RP-2

The design work on the RP-2 all-composite, high performance, ultra-light sailplane has been completed, and construction of the aircraft is well advanced. The preliminary design configuration described in the last semi-annual report was not significantly altered in the final design phase. The aircraft will have a wing span of 13.5 m (44 feet), wing area 11.1 m^2 (120 square feet), aspect ratio 17, (L/D) max. of 30 and the total empty weight with the auxiliary (launching) engine installed is expected to be less than 82 kg (180 lbs.). Performance estimates on the final design are for a stall speed of 47 kph (26 knots), minimum sink rate of 0.5 m/s (1.7 fps) and best glide ratio of 30. It is expected, however, that some tailoring of the wing-fuselage intersection as well as some fine tuning in general will be necessary to achieve this glide ratio. The final wing design incorporates all-graphite split flaps for glide path control, and the aircraft is structurally designed for a maximum nominal load of 5.5 g's at a diving speed of 160 km/h (85 knots). Additional information on the aircraft is given in Table II-1. The glide polar for the entire range of airspeeds is shown in Figure II-1.

In addition to designing for maximum air loads, problems of aeroelastic instability were also investigated. Two such
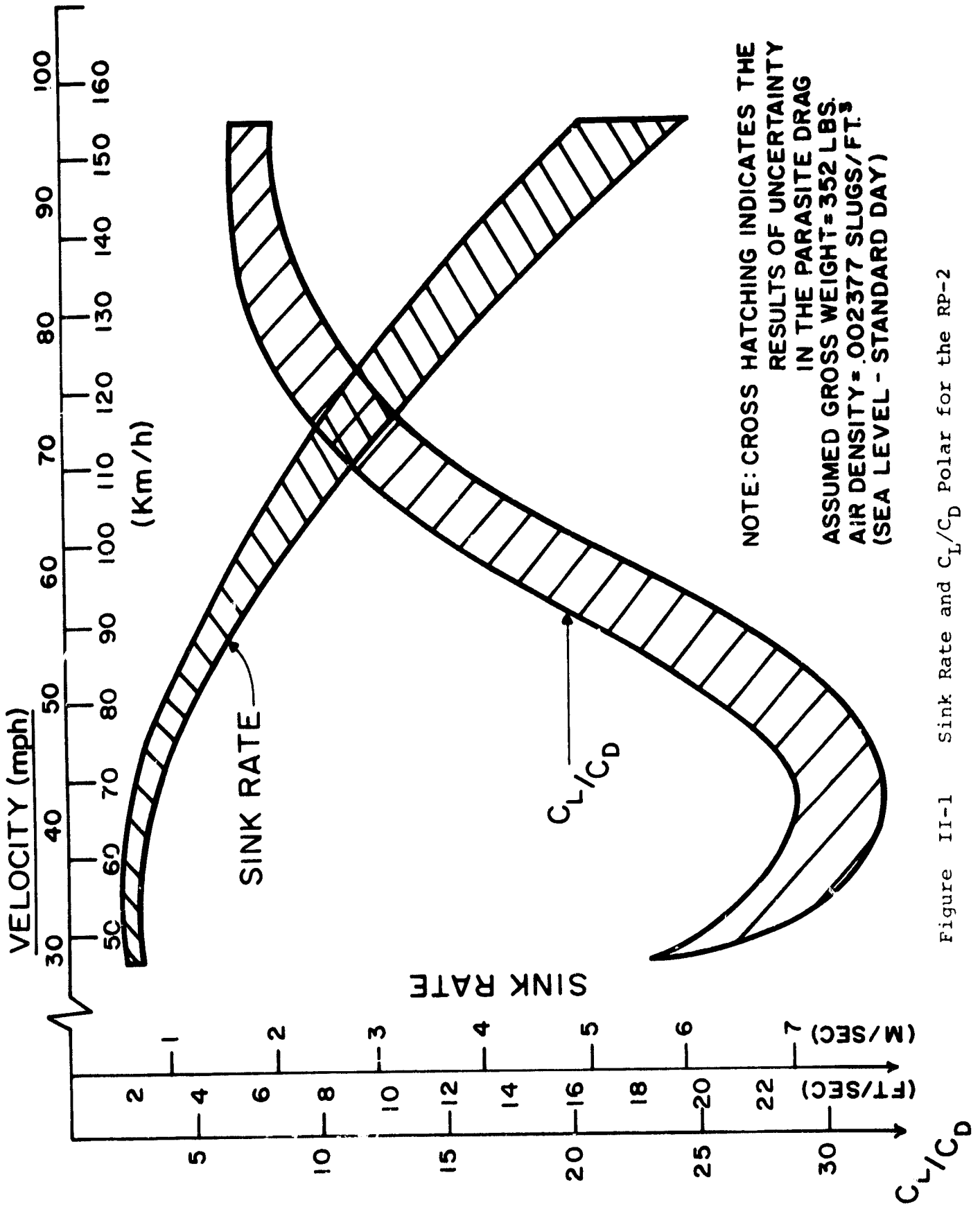
Figure II-1   Sink Rate and C_L/C_D Polar for the RP-2

NOTE: CROSS HATCHING INDICATES THE
RESULTS OF UNCERTAINTY
IN THE PARASITE DRAG

ASSUMED GROSS WEIGHT = 352 LBS.
AIR DENSITY = .002377 SLUGS/FT.^{3}
(SEA LEVEL - STANDARD DAY)

TABLE II-1
AIRCRAFT CHARACTERISTICS DATA FOR THE RP-2 SAILPLANE

Overall:

Span	m (ft)	13.5	(44.25)
Length	m (ft)	6.6	(21.65)
Height	m (ft)	1.25	(4.1)

Wing:

Area	m^2 (ft^2)	11.1	(120)
Aspect Ratio	--	17	
Section Profile	--	BOAF-63	

Vertical Stabilizer:

Span	m (ft)	1.25	(4.1)
Area	m^2 (ft^2)	0.5	(5.4)
Section Profile	--	FX-L-III-142	

Horizontal Stabilizer:

Span	m (ft)	2.50	(8.2)
Area	m^2 (ft^2)	1.00	(10.8)
Section Profile		FX-L-III-142	

Performance at a Gross Weight of 160 kg (353 lbs):

Stall Speed w/o Flaps kph (mph)	47	(29)
Minimum Sink Rate m/s (ft/s)	.53	(1.7)
Maximum Glide Ratio at V km/h (mph)	30/61	(30/38)

Empty Weight (estimated), kg (lb):   78   (172)

Tail Effectiveness:

V/V* Horizontal Surface	.42
V/V* Vertical Surface	.052

instabilities were examined; namely, torsional divergence of the wings and coupled torsion-bending flutter of the aft fuselage-tail assembly coupled with tail control surfaces rotation. The torsional divergence calculation was performed using a computer program package which applies matrix methods (for example, Reference 1[*]) to determine aerodynamic loading and deformations of composite wings. This program package was developed during the last reporting period and is general enough to account for double tapered planforms, two rates of linear built-in twist, dual skin thicknesses and arbitrary airfoil sections. It also accounts for the effects of finite span and load redistribution due to deformation. The theoretical torsional divergence speed was calculated using this method as 130 m/sec (290 mph).

The further analysis of the fuselage tail-boom assembly was done using the method of Reference 2. Natural vibration modes were used as generalized coordinates in the analysis. The structure was first modeled, therefore, as a discrete parameter, mass-spring system and a matrix Holzer procedure (Reference 3) was programmed for RPI's digital computer, the IBM 3033. By this means the natural mode shapes and frequencies of the fuselage aft of the wing were determined for both vertical bending and coupled side-bending-torsion cases.

---

[*] References in this section are listed on page 92.

Th3 information was then used in conjunction with the associated unsteady aerodynamics of the tail, to investigate the possibility of flutter with free control surface rotations. The assembly was shown to be flutter free within the flight envelope of the glider.

Status of construction at the close of the reporting period saw rib-stringer frameworks for empennage and both wings completed (Figures I-2 ana -3). In addition, skins have been prepared, and the bottom skins installed both on wings and horizontal tail. Kevlar-cloth/foam/Kevlar-cloth double-sandwich lay-ups are used for the center section wing skins, and Kevlar-cloth/foam open-sandwich construction is used for the skins of the tapered outboard wing sections. After inspection of the partially completed structure by the FAA, as required by Federal Air Regulations, the upper surface skins will be installed. Meanwhile, the tapered graphite tube which constitutes the aft two-thirds of the fuselage, the torque-box wing-fuselage connection and the main framework for the forward portion of the fuselage have been completed. The last of these consists of an "elephant tusk" type structure stabilized by cross beams at the pilot seat and cockpit flight control positions. Construction details can be seen in Figures II-4 and -5. The fuselage shell will be carved out of lightweight foam, reinforced with Kevlar/ epoxy for strength, and covered with glass/epoxy for surface finish.
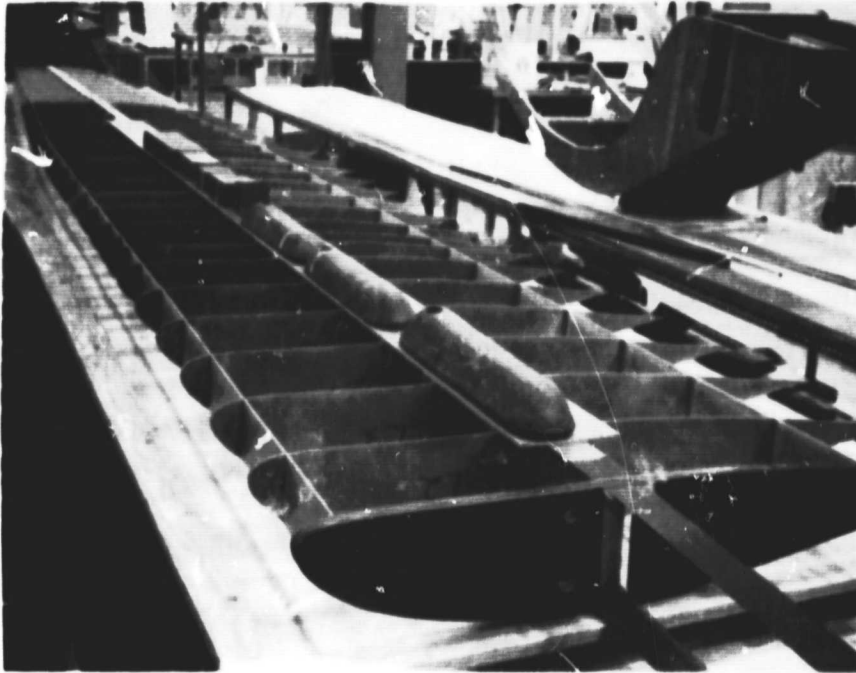
Figure   II-2

Wing-Spar-Rib Assembly in Construction
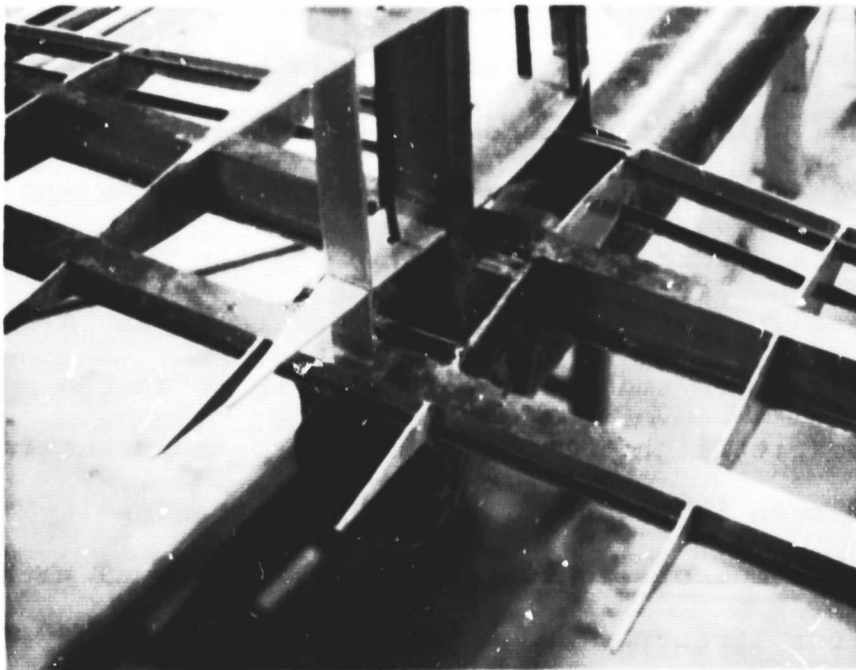
Figure   II-3

Empennage Rib-Spar-Stringer Assembly to Aft Fuselage

Figure   II-4

Rib-Stringer Frameworks for Empennage and Side Frame
("Elephant Tusk") of Fuselage Structure Before Assembly
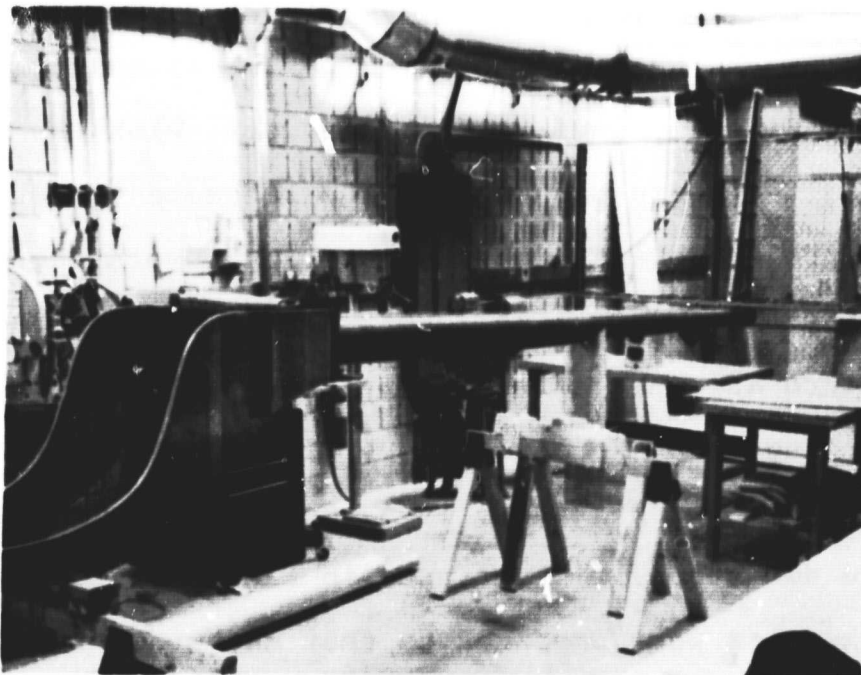
Figure   II-5

Fuselage and Empennage Structure In Assembly

The need for molds has been eliminated throughout, in the construction of the RP-2. It is expected that the main airframe will be completed and proof-tested structurally at the end of summer, with some detail work primarily on instrumentation and engine installation remaining for the fall.

RP-1, meanwhile, has been modified by the installation of a landing wheel to facilitate launch by winch-tow and operation from a hard-surface runway. It is expected that flight operations will resume in early to midsummer 1981, aimed at securing additional performance data for this aircraft.

Activity in the Composites Fabrication Laboratory during the present reporting period involved completion of individual student projects begun in the fall semester, and with the spring semester has been focused almost exclusively on fabrication of the RP-2. A total number of 45 undergraduate students are directly involved in this work, with the majority spending ten hours per week in the laboratory. Students new to the project started the semester by completing a series of basic lay-ups of the types typical of the RP-1 and RP-2 structure and were subsequently assigned to RP-2 working teams according to preference, e.g., wing group, fuselage group, etc. Each working team is headed by a student with one or more semesters of experience in the laboratory, and working schedules were prepared so that new students are always paired with sufficient numbers of experienced hands.

Large enrollment notwithstanding, the laboratory has continued to function smoothly under the management of Mr. Volker Paedelt, assisted by Mr. Steven Winckler who serves as chief designer of the RP-2. Individual student projects, following this procedure, will again be introduced in the fall. Two projects carried over from the previous reporting period are described below.

Project I - Tapered Graphite Tube. Using data obtained in the fall, an all-graphite fuselage boom was designed and built. The design is stiffness-limited, due to the requirement that the natural frequency in the bending-torsion mode be high enough to avoid flutter. The boom was constructed in two pieces because of autoclave limitations, and the two pieces are joined by a graphite inner sleeve. The lay-up consisted of twelve plies of prepreg at the root, tapering to eight plies at the tail, with four plies $\pm45°$, and the remainder lined up with the tube axis.

Project 2 - Graphite-Kevlar Leading Edge. This project was not developed to the point where it could be used on the RP-2. A successful prototype was fabricated, however, for a small typical wing section. The main problem in scaling this up for the full-size aircraft is the need for sheet metal leading edge molds of very high precision.

2. References

1) Bisplinghoff, R. L., Ashley, H. and Halfman, R. L., "Aero-Elasticity', Addison-Wesley Publishing Co., 1955.

2) Smilg and Wasserman, "Application of Three-Dimensional Flutter Theory to Aircraft Structures", USAF TR 4798, July 1942.

3) Targoff, W. P., "The Associated Matrices of Bending and Coupled Bending-Torsion Vibrations", October 1947.

C-2

PART III

COMPAD (Computer Aided Design)

COMPAD (Computer Aided Design)
(M. S. Shephard)

The objective of the computer aided design portion of the composites project is to provide computer "tools" for the analysis and design of composites structures. COMPAD's major thrust has been in the finite element area with effort directed at implementing finite element analysis capabilities and developing interactive graphics preprocessing and postprocessing capabilities. Recent efforts have been directed at completing the interactive graphics programs in the POFES[*] system making up a complete two-dimensional system that can be used effectively to solve a wide range of structural analysis problems. In addition, efforts have begun to develop the additional analysis capabilities required to employ finite element techniques in the investigation of both the moisture effects on carbon-epoxy composites and the micromechanical failure of composites.

The next three sections describe the progress made toward the completion of the two-dimensional portion of POFES and development of analyses capabilities for the two applications area. The last section discusses plans for the upcoming period.

---

[*] POFES (People Oriented Finite Element Software) is RPI's finite element software system.

1. Two-Dimensional POFES Progress

Effort during the current reporting period has concentrated on the addition or improvement of the following features:

a) Development of a link between the attribute editor and FEPROQ*.

b) Addition of a general triangulation algorithm to the preprocessor.

c) Generalization and improvement of the point load and boundary condition segment of the attribute editor.

d) Restructure of the material property segment of the attribute editor.

The link from the attribute editor to our in-house analysis program FEPROQ is a simple set of Fortran routines that takes the geometric information generated by the preprocessor along with the load, material property and boundary condition information specified with the attribute editor and formats it as required for the analysis program. This process is performed as the last step before the user exits the attribute editor. It is important to note that the preprocessor and attribute editor information is stored in general form, so it is a straightforward task to format it for any analysis program.

_____

*FEPROQ is one of RPI's in-house finite element analysis programs.

Although a simple task, creating the link between the attribute editor and an analysis was an important step because it completed the integration of all the two-dimensional portions of the POFES software. It is now possible to interactively generate, analyze and view the results for finite element models in minutes, using a software system that is easy to learn to operate.

The basic mesh generators in the preprocessor are based on linear blending functions[1]* and afford the user a powerful means of generating a wide variety of element meshes. However, they do require that opposite sides of the mesh patch have the same number of nodes. Since this does not allow for convenient mesh grading, some form of general triangulation technique is desirable. Therefore, in addition to the one element deep transition generator discussed in a previous report, a general triangulation generator[2] has been added. Although this type of mesh generator is not satisfactory as the basis for an entire preprocessor, it is useful in performing more complex transitions where each side of a mesh patch can have a different number of element edges. Figure III-1 shows how this capability can be used to fill a three-sided patch that has a different number of element edges on each side.

---

*Bracketed numbers in this section refer to the references listed on page 106.

98
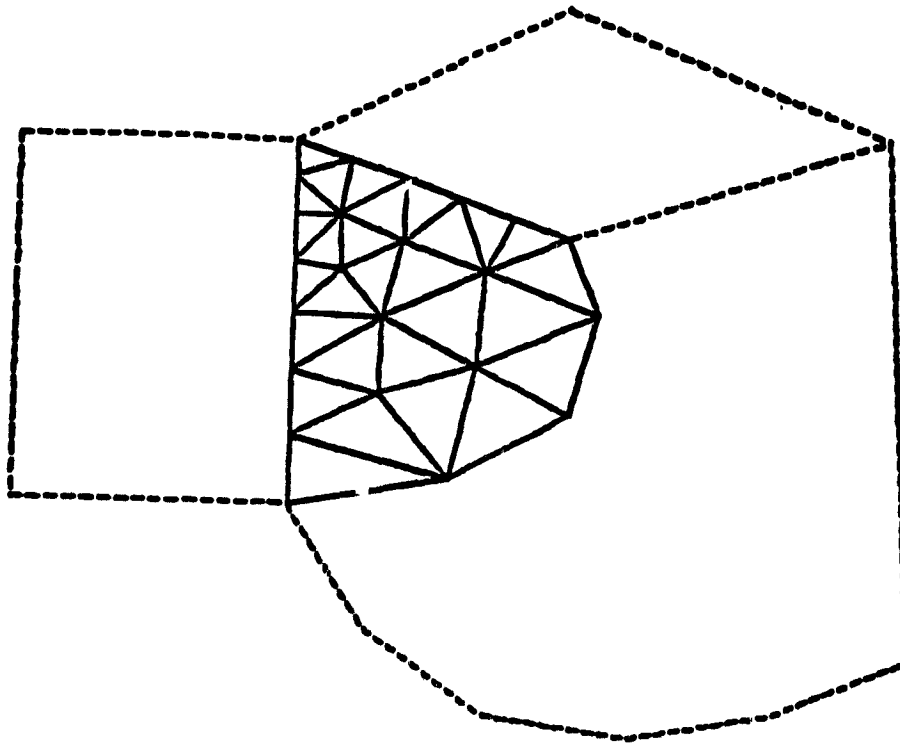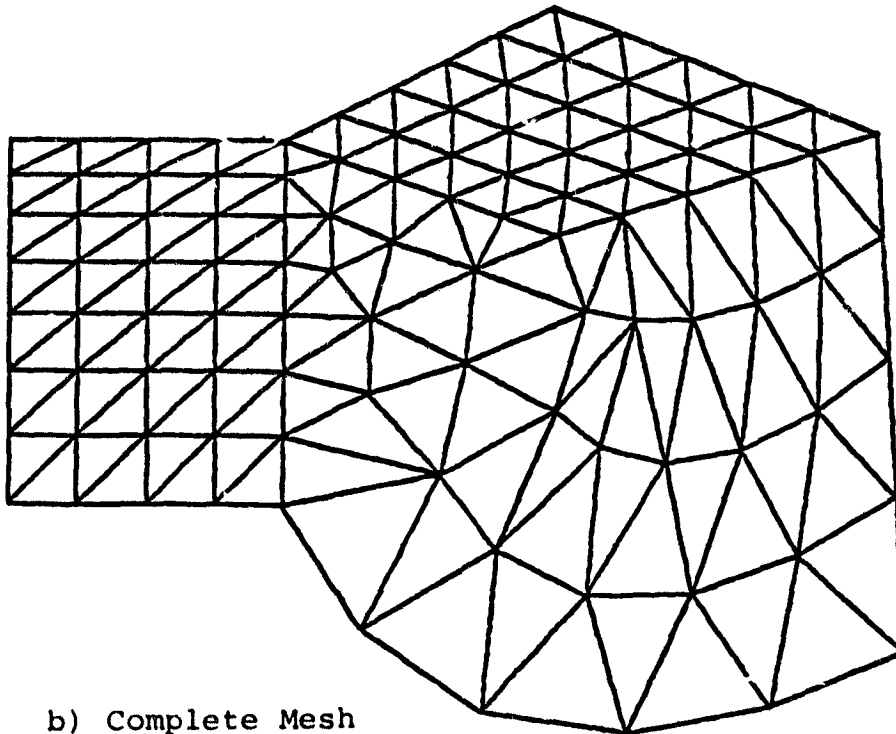
a) Transition Mesh

b) Complete Mesh

Figure III-1

Use of General Triangulation Capability to
Generate a Transition Mesh

Minor changes have been made to both the point load and
boundary condition segments of the attribute editor. Modifi-
cations were made to improve the features that allow the
user to check the conditions he has specified. In addition,
a feature has been added so that the user can specify the
number and type of nodal unknowns used. This enhances the
generality of the program by allowing for the use of non-
standard nodal unknowns.

After a short period of operation it was determined
that the mode of operation of the material property editor
described in the previous report could be improved by chang-
ing the way the material properties are displayed. Instead
of attempting to generate and display material properties on
the structure, a special display page is used to construct
a table of material properties which are then applied to the
structure. This allows the user to see much more material
information presented in a clear tubular form at one time.
In addition, it makes the operation of property duplication
and modification features much easier for the user.

2. Numerical Investigation of Moisture Effects

Efforts toward the numerical analysis of moisture ef-
fects on carbon-epoxy composites has led to the development
of a nonlinear finite element code by graduate student
Frida Lumban-Tobing. The moisture effects are introduced
into the problem through the nonlinear constitutive rela-
tion[3]

$$\sigma_{ij} = \alpha\delta_{ij} + \beta\epsilon_{ij} + \gamma\epsilon_{ik}\epsilon_{kj} \tag{1}$$

where

σ_{ij} is the stress tensor,

ϵ_{ij} is the strain tensor, and

α, β, γ are the multipliers that are, in general, a function of the strain invarients.

In the present problem, the multipliers are functions of the volume fraction of the liquid in the mixture and can be written as:

$$\alpha = \alpha_1 + \alpha_2 v_2$$
$$\beta = \beta_1 + \beta_2 v_2 \tag{2}$$
$$\gamma = \gamma_1 + \gamma_2 v_2$$

where the terms α_1, α_2, β_1, β_2, γ_1 and γ_2 are temperature dependent material constants and

$$v_2 = \frac{1}{\sqrt{I_3}}$$

where the strain invarient (I_3) is

$$I_3 = 1 + 2(\epsilon_{11} + \epsilon_{22} + \epsilon_{33}) + 4(\epsilon_{11}\epsilon_{22} + \epsilon_{22}\epsilon_{33}$$
$$+ \epsilon_{33}\epsilon_{11} - \epsilon_{12}^2 - \epsilon_{23}^2 - \epsilon_{13}^2) + 8(\epsilon_{11}\epsilon_{22}\epsilon_{33}$$
$$+ 2\epsilon_{12}\epsilon_{23}\epsilon_{13} - \epsilon_{11}\epsilon_{23}^2 - \epsilon_{22}\epsilon_{13}^2 - \epsilon_{33}\epsilon_{12}^2) \tag{3}$$

Starting from this point, there are two possible ways to proceed in the formulation of the set of nonlinear algebraic equations to be solved on the computer. One approach involves the use of the principle of virtual work, and the other is a weighted residual approach. The first method tried was a weighted residual approach employing Galerkin criterion operating on the equation of equilibrium[4]. This method involved a substantial amount of manipulation and required the use of several approximations in order to carry out the required integration by parts.

The virtual work principle[5], which equates the variation in the internal work to the variation in the external work, is more straightforward to apply. Its application, in the form of virtual displacements, operates on an assumed displacement field and the final set of algebraic equations[6].

$$([K^{\ell}] + [K_1^{n\ell}] + [K_2^{n\ell}])\{\Delta\} = \{F^b\} + \{F^d\} + \{F^{init}\} + \{F^{n\ell}\}$$

$$(4)$$

where the various terms are;

$[K^{\ell}]$ is the linear stiffness matrix,

$[K_1^{n\ell}]$ is the first nonlinear stiffness matrix,

$[K_2^{n\ell}]$ is the second nonlinear stiffness matrix,

$\{\Delta\}$ is the vector of unknown nodal displacements,

$\{F^b\}$ is the body force vector,

$\{F^d\}$ is the distributed load vector,

$\{F^{init}\}$ is an initial stress vector, and

$\{F^{n\ell}\}$ is a nonlinear load vector.

A complete definition of each of the terms is given in Reference [6]. Equation (4) is written as a linear function of the unknown displacements; two of the stiffness matrices and one of the load vectors, however, are functions of the displacements, thus making the entire system nonlinear. Therefore, it must be solved iteratively.

The nonlinear solution approach selected is a modified Newton method classified as a quasi-Newton method[7]. The advantages of this approach are:

a) it avoids the reformation and solution of new sets of stiffness equations,

b) it tends to converge quickly and

c) it appears to be quite stable.

At the conclusion of the current reporting period, both the virtual work and Galerkin approaches had been formulated and implemented, for plane strain, into a nonlinear, finite element analysis code. Currently, the program's element library consists only of the constant strain triangle. However, the general design will allow for the addition of other element types including three-dimensional elements. The formulation and quasi-Newton solution approaches have been tested by several simple sample problems. The program is now ready for testing using some realistic test problems.

3. Numerical Investigation of
Micromechanical Fracture of Composites

In order to better understand the mechanisms of failure
in composites it is necessary to understand the interaction
of the matrix and fiber as the load increases from zero to
total failure. The finite element method provides a means
whereby this process can be simulated on the computer. Sev-
eral investigators[8-10] have employed such an approach;
however, the modeling procedures that have been used can be
greatly improved.

Background work on this investigation has been carried
out by graduate student Nabil Yehia. He has also carried
out some desired modifications to the postprocessor. The
postprocessor modifications allow for the generation of
stress contours that can be discontinuous at the material
interfaces, in contrast to the usual procedure which smooths
stress distribution everywhere. This feature is important,
since much of the understanding to be gained from this work
will be based on visual displays such as contour plots of
stresses, and stresses are, in general, discontinuous at
material interfaces. As an example, Figure III-2 shows a
maximum principal stress and maximum shear stress plot for a
simple plate made up of two different materials. The plate
is fixed at the left end and loaded with a uniform load
parallel to the interfaces at the right edge. Since the
plate is made up of a soft material at the top and bottom
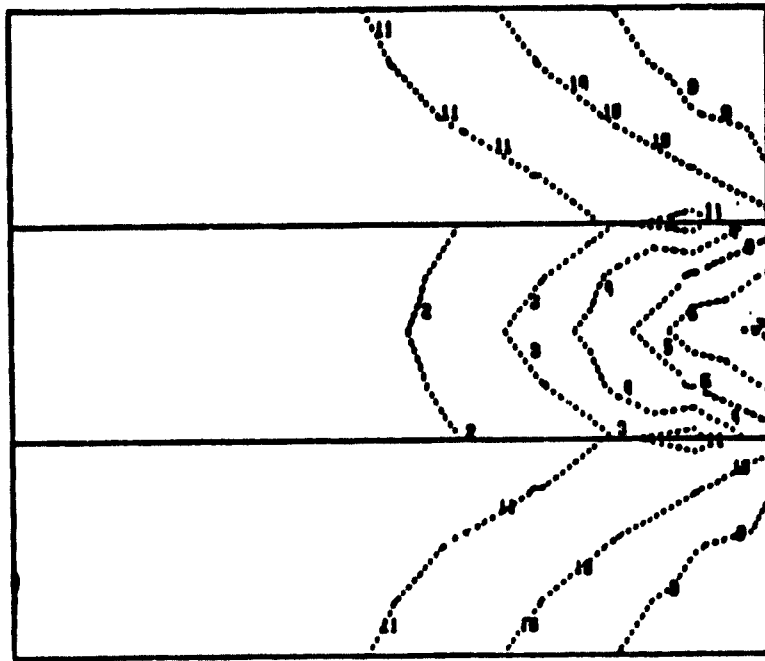
a) Maximum Normal Stresses
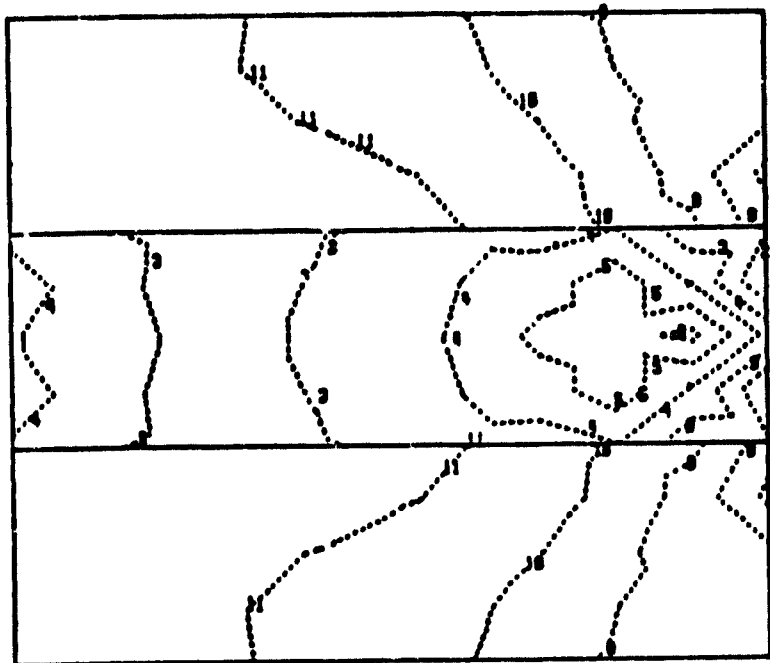
b) Maximum Shear Stresses

Figure III-2

Generation of Stress Contours in a Three-Layer,
End-Loaded Composite Laminate

and a stiff material in the middle, the majority of load transfers to the stiffer middle fiber as indicated by the contour plots. Stress discontinuities at the material interfaces are apparent. To exploit fully this new view of conditions at the interface is likely to require some proper representation of fracture mechanics for material interfaces. These matters are still under consideration.

4. Plans for the Upcoming Period

Work on the general finite element software during the next reporting period will concentrate on completing the attribute editor, making minor improvements to other parts of the software system and adding more extensive user documentation.

Continued efforts on the nonlinear finite element program for moisture effects in composites will concentrate on testing and debugging the program further, followed by a series of two-dimensional plane strain analysis studies examining the effects of moisture on carbon-epoxy composites. These analysis studies will investigate various conditions including fiber spacing, epoxy properties, moisture contents and loading conditions.

The majority of the effort on the micromechanical analysis of composite fracture during the next period will be on the design and initial development of a nonlinear finite element analysis code that is able to track the failure process. This program will require the use of nonlinear

constitutive relationships and must possess ability to define and propagate cracks through the element mesh. Although some of the features of the moisture effects program and other available programs can be used, this program will require a more complicated data base and several sophisticated checking capabilities. Based on the tentative timetable that has been worked out, approximately half of the next year will be spent on tracking down most of the basic components required for the program and designing its data base.

5. References

1) Haber, R. B., M. S. Shephard, J. F. Abel, R. H. Gallagher and D. P. Greenberg, "A General Two-Dimensional Finite Element Preprocessor Utilizing Discrete Transfinite Mapping", Int. J. Num. Meth. Engng., 1981.

2) Tracy, F. T., "Graphical Pre- and Post-Processor for Two-Dimensional Finite Element Programs", SIGGRAPH '77, ACM Vol 11, No. 2, 1977, pp. 8-12.

3) Sternstein, S. S., "Inhomogeneous Swelling in Filled Elastomers", J. Macromal Sci.-Physics, B6 (1), 1972, pp. 243-262.

4) Szabo, B. A. and G. C. Lee, "Derivation of Stiffness Matrices for Problems in Plane Elasticity by Galerkin Method", Int. J. Num. Meth. Engng., Vol. 1, 1969.

5) Koites, W. T., "General Theorems for Elastic-Plastic Solids", Progress in Solid Mechanics, I. D. Sneddon and R. Hill, Eds., North Holland Publ. Co., Amsterdam, 1960.

6) Lumban-Tobing, F., Research progress report presented to graduate committee, Rensselaer Polytechnic Institute, April 1981.

7) Geradin, M., S. Idelshon and M. Hogge, "Computational Strategies for Solution of Large Nonlinear Problems Via Quasi-Newton Methods", Computers and Structure, Vol. 13, 1981.

8) Ireneonger, M. J. and W. G. Wood, "Plastic Flow and Failure of Discontinuous Fiber Composite Materials", J. Strain Analysis, Vol. 5, No. 3, 1980.

9) Ko, W. L., "Finite Element Microscopic Stress Analysis of Cracked Composite Systems", J. Composite Materials, Vol. January 1978, p. 97.

10) Braum, H., A. Fleck and K. Herrman, "Finite Element Analysis of a Quasistatic Crack Extension in a Unit Cell of a Fiber Reinforced Material", Int. J. of Fracture, Vol. 14, 1978.

6. Current Publications or Presentations by Professor Shephard on this Subject

1) "The Synthesis of Near-Optimum Finite Element Meshes with Interactive Computer Graphics", (with R. H. Gallagher and J. F. Abel).

>Published in Int. J. Num. Meth. Engng., Vol 15, 1980, pp. 1021-1039.

2) "Finite Element Grid Optimization - An Overview"

>Presented at General Motors Research Labs, Warren, Michigan, March 2, 1981.

3) "Computer Graphics in Structural Engineering"

>Presented at 26th Annual Structural Engineering Conference, University of Kansas, March 27,1981.

4) "Computing at RPI - A Case Study", (with L. J. Feeser).

>Presented at 1981 Southeastern Section Meeting of ASEE, Chattanooga, Tennessee, April 6, 1981.

PART IV

INSURE (Innovative and Supporting Research)

A. Advanced Structural Analysis Methods for Composites, E. J. Brunelle

B. Ultrasonic Non-Destructive Testing of Composite Structures, P. Das and H. F. Tiersten

C. Transverse Properties of Composites with Anisotropic Constituents, R. J. Diefendorf

D. Fatigue in Composite Materials, E. Krempl

E. Acoustic Emission of Composite Materials, H. A. Scarton

F. Viscoelastic Characteristics of In Situ Resins and Neat Resins, S. S. Sternstein

IV-A ADVANCED STRUCTURAL ANALYSIS METHODS FOR COMPOSITES

Senior Investigator: E. J. Brunelle[*]

The effort to understand the behavior of an individual orthotropic lamina in as concise a fashion as possible continues. When this understanding is substantially completed, a rational investigation of laminate assemblages is possible. The present methods of analyzing a particular composite structure (by laborious, though straightforward means) yield numerical results, but are poorly posed to do meaningful parametric studies and are even less helpful in trying to obtain a stated optimum result with modest constraint conditions. A primary difficulty is that of too many variables in any particular problem. Besides the geometry and mass variables, and the stacking sequence of N laminae, there are 6N elastic constants for the laminate assemblage (This number is reduced by symmetry, anti-symmetry, multiple plies with the same orientation; however, the number is rarely small.). Thus, methods that allow solutions in terms of significantly fewer combinations of constants should be very valuable. These methods, which are being pursued for the individual lamina, will eventually be applied to the laminate assemblage.

1. Status

The principal results of the last period culminated in a generalized solution of the moisture diffusion problem

---

[*]RPI graduate student G. Oyibo and undergraduate student D. Kunstmann

associated with a three dimensional rectangular slab, a solution for the buckling of a simply supported plate with a core, a solution for the frequency spectrum of a simply supported plate with uniaxial compression, and a large series of generalized curves for the buckling coefficients $k_o = k_o(m, a_o/b_o, D^*)$ of (all except one) rectangular plates with various boundary conditions and various applied loads (shear, compression and bending).

2. Progress During Report Period

Effort in four areas has produced the major results as discussed in the following.

Result (i). On the basis of roughly thirty actual materials the range of D^* seems to be $0 \leq D^* \leq 1$, where $D^* = 1$ is the quasi-isotropic case (if in addition $a_o/b_o = a/b$ then it is the isotropic case). Appealing to the simplest micromechanics description of $D^* = D^*(V_f, E_f/E_m, \nu_f, \nu_m)$ it is seen, referring to Figure IV-A-1, that $D^* = 1$ when $V_f = 0$ and when $V_f = 1$ (these are the limits of an all-matrix isotropic material and an all-fiber isotropic[*] material), and that for all other values of V_f in the open interval 0 to 1, D^* is indeed less than unity. The minimum values of D^* are seen to occur at roughly $V_f = .55$. For given values of E_f/E_m, ν_f and ν_m, say $E_f/E_m = 50$, $\nu_f = .2$ and $\nu_m = .35$, Figure IV-A-1 shows

---

[*] Assuming, of course, that the fibers are themselves isotropic, which in practice is not always the case.

Figure IV-A-1

D^* VS. V_f FOR $\nu_f = .2$ AND $\nu_m = .35$

$E_f/E_m =$

2

5

10

50

100

D^*

1.0

.8

.6

.4

.2

0

$\nu_f = .3, \nu_m = .3$

$\nu_f = .1, \nu_m = .4$

0   .2   .4   .6   .8   1.0

V_f

$V_{f_1} = .145$

$V_{f_2} = .885$

ρ_f

$W_1 \sim \rho_m + .145(\rho_f - \rho_m)$

$W_2 \sim \rho_m + .885(\rho_f - \rho_m)$

ρ_m

$\underline{\Delta W} = W_2 - W_1 \sim .740(\rho_f - \rho_m)$

WEIGHT SAVINGS

0
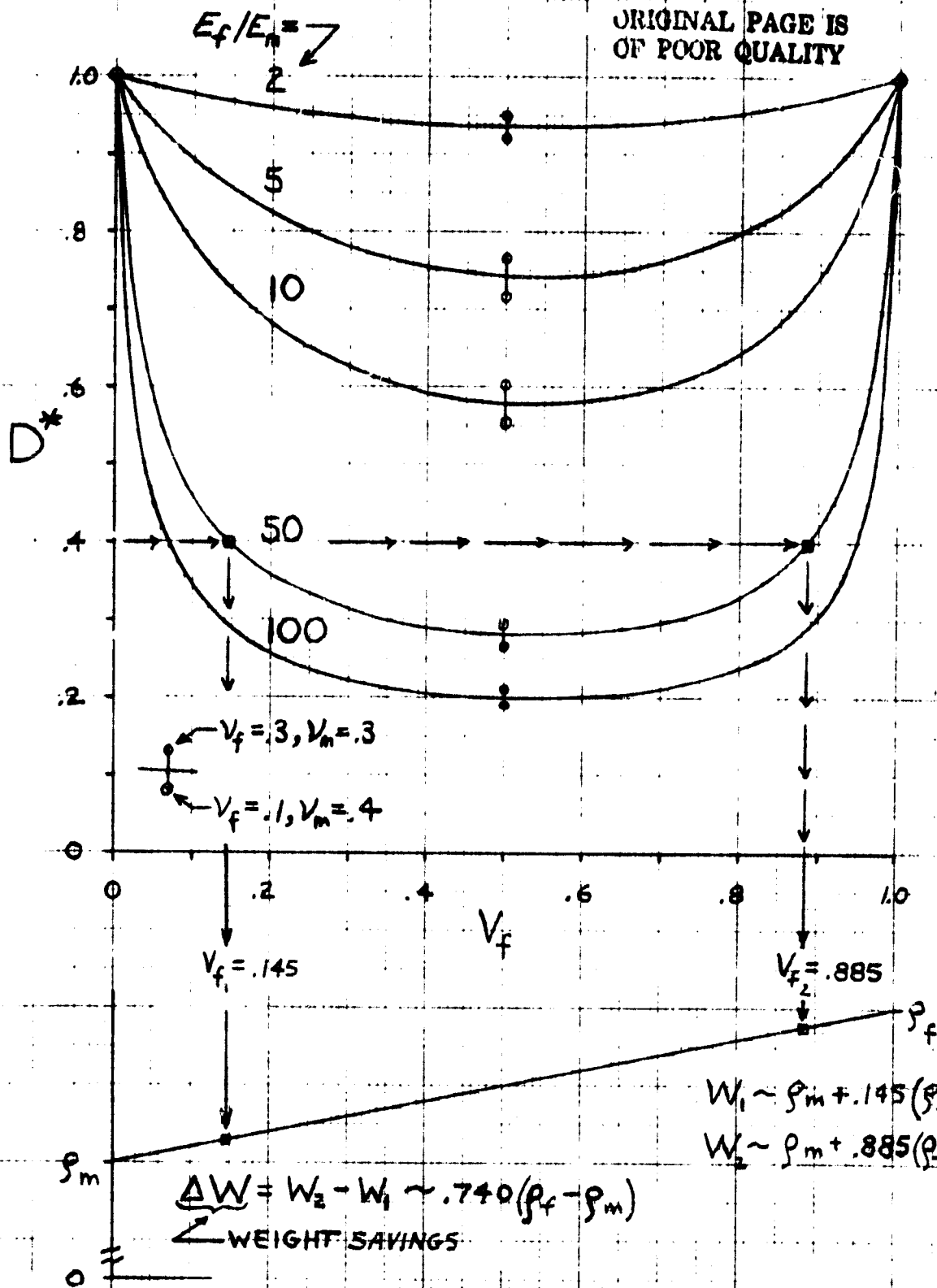
the minimum value to be 0.28. If one wishes to increase D*
to .4, it is seen that V_f = .885 and V_f = .145 will accom-
plish the task. Since $\rho_f > \rho_m$, a lighter plate (V_f = .145)
will have the same buckling parameter (k_o), the same non-
dimensional static deflections and higher frequencies than
the heavier plate (V_f = .885). Since buckling criteria pro-
duce (in general) a thicker plate than needed for tensile
criteria, it appears that very low fiber volume composites
may be very attractive new materials. The dimensional as-
pects are being investigated. If this confirms the non-
dimensional indicators, it seems that appropriate experi-
ments should be conducted to see if the theoretical advan-
tages of very low fiber volume composites are confirmed and
to see if there are any kinds of practical manufacturing or
fabrication difficulties.

Result (ii). The generally orthotropic plate equation

$$D_{11}\frac{\partial^4 w}{\partial x^4} + 4D_{16}\frac{\partial^4 w}{\partial x^3 \partial y} + 2(D_{12} + 2D_{66})\frac{\partial^4 w}{\partial x^2 \partial y^2} + 4D_{26}\frac{\partial^4 w}{\partial x \partial y^3}$$

$$+ D_{22}\frac{\partial^4 w}{\partial y^4} + \cdots = p(x,y)$$

has been transformed into the rotated (thru an angle θ) and
affinely stretched coordinates to yield

$$\frac{\partial^4 w}{\partial \bar{x}_o^4} + \bar{L}\frac{\partial^4 w}{\partial \bar{x}_o^3 \partial \bar{y}_o} + 2\bar{D}\frac{\partial^4 w}{\partial \bar{x}_o^2 \partial \bar{y}_o^2} + \bar{R}\frac{\partial^4 w}{\partial \bar{x}_o \bar{y}_o^3} + \frac{\partial^4 w}{\partial \bar{y}_o^4} + \cdots$$

$$= p(\bar{x}_o, \bar{y}_o)$$

where

$$\bar{L} = \bar{L}(D^*, D_{11}/D_{22}, \theta) = -\bar{R}(D^*, D_{11}/D_{22}, \theta \pm \frac{\pi}{2})$$

$$\bar{D} = \bar{D}(D^*, D_{11}/D_{22}, \theta)$$

$$\bar{R} = \bar{R}(D^*, D_{11}/D_{22}, \theta).$$

The values of $\bar{L}$, $\bar{D}$, $\bar{R}$ are easily found with modest amounts of computation and, as a separate operation, a Ritz-Galerkin solution (or any other weighted-residual method) may be obtained in which a_0/b_0, $\bar{L}$, $\bar{D}$ and $\bar{R}$ appear as generic constants. Short of finding an exact, closed form solution for the above partial differential equation (efforts will be made towards such a possibility), this is a very attractive scheme for performing parametric studies on any given type of problem (static, dynamic, instability).

It is interesting to note that $B = \dfrac{U_2}{4U_3} = B(D_{11}/D_{22}, D^*)$; where it is remembered that B governs the rotational behavior of all $\bar{Q}_{ij}(\theta) - \bar{Q}_{ij}(0)$ terms. Values of β for various combinations of D^* and the ratio E_1/E_2 are shown in Figs. IV-A-2 and -3. This relation will be examined for possible descriptional advantages.

Result (iii). The von Kármán plate equations for a specially orthotropic plate, due to Rostovstev,

$$\frac{1}{E_2}\frac{\partial^4 F}{\partial x^4} + \left(\frac{1}{G} - \frac{2\nu_1}{E_1}\right)\frac{\partial^4 F}{\partial x^2 \partial y^2} + \frac{1}{E_1}\frac{\partial^4 F}{\partial y^4} = \left(\frac{\partial^2 w}{\partial x \partial y}\right)^2 - \frac{\partial^2 w}{\partial x^2}\frac{\partial^2 w}{\partial y^2}$$

$$D_{11}\frac{\partial^4 w}{\partial x^4} + 2(D_{12} + 2D_{66})\frac{\partial^4 w}{\partial x^2 \partial y^2} + D_{22}\frac{\partial^4 w}{\partial y^4} = p(x,y) + h\left(\frac{\partial^2 F}{\partial y^2}\frac{\partial^2 w}{\partial x^2}\right.$$

$$\left. -2\frac{\partial^2 F}{\partial x \partial y}\frac{\partial^2 w}{\partial x \partial y} + \frac{\partial^2 F}{\partial x^2}\frac{\partial^2 w}{\partial y^2}\right)$$

Figure IV-A-2

B vs E_1/E_2 for various values of D*

116
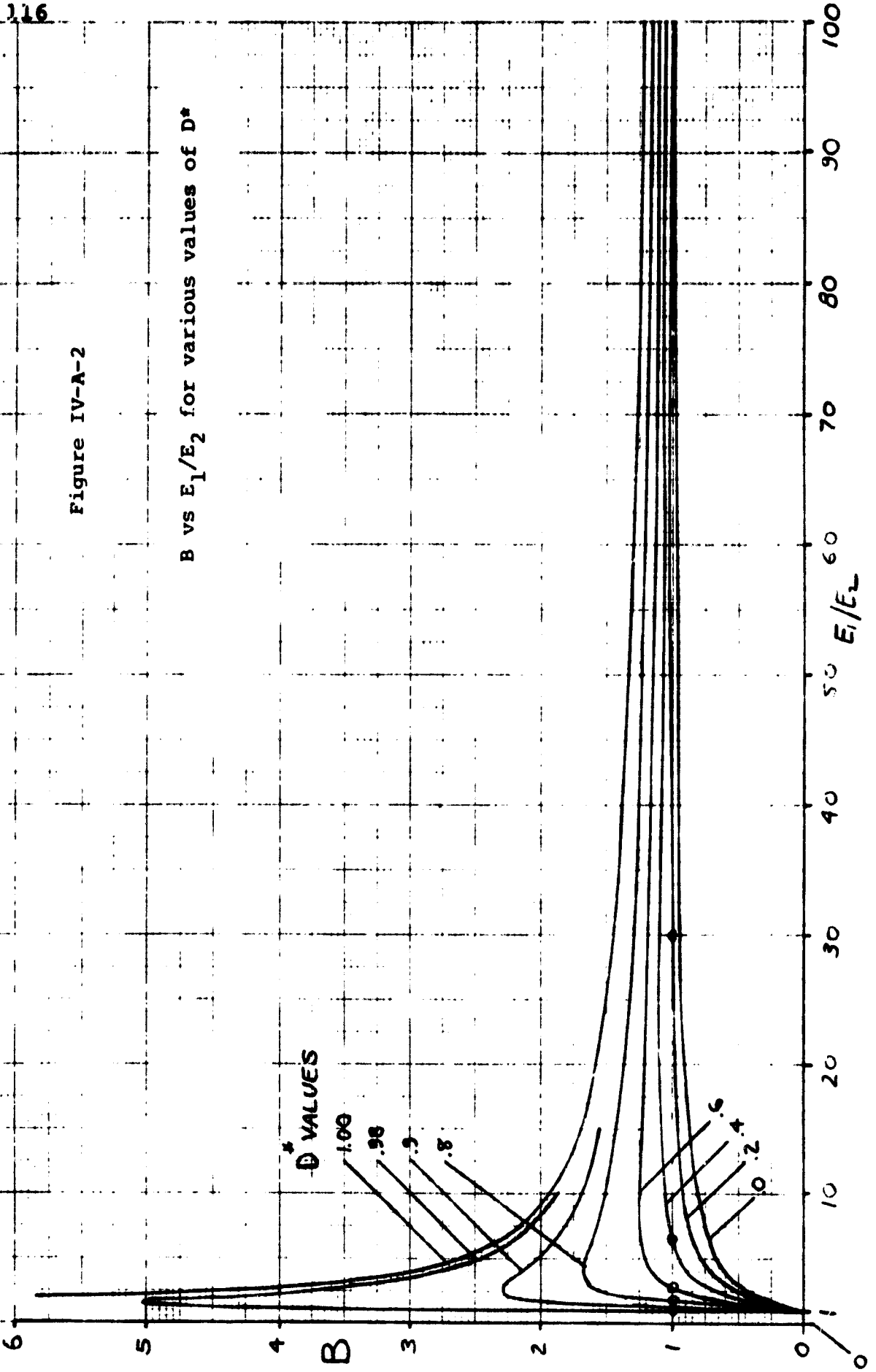
Figure IV-A-3

B vs D* for Various Values Over E_1/E_2
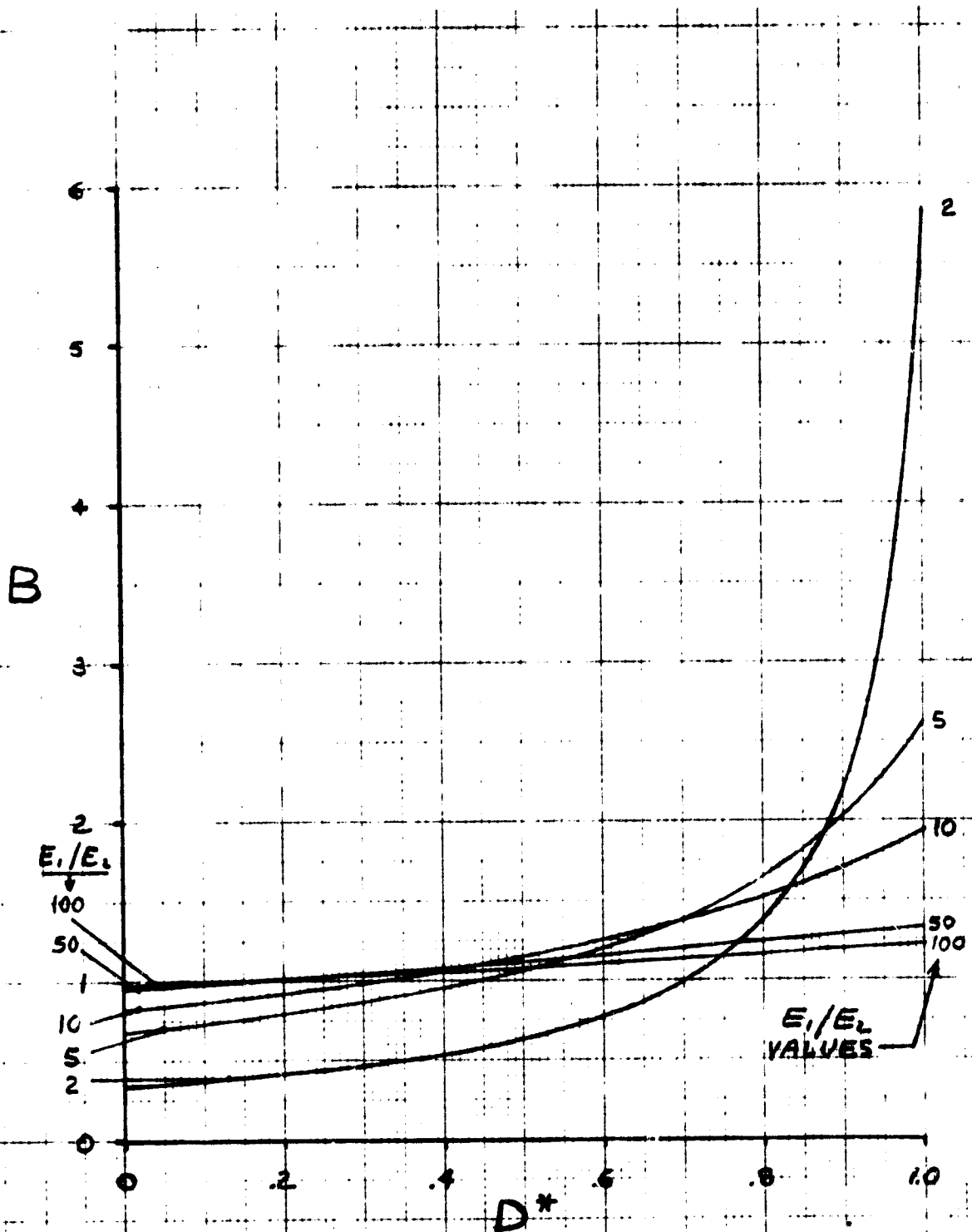
have been affinely transformed by the relations

$$w = h^{\frac{1}{2}}\sqrt{\frac{D_{22}}{E_{22}}}\,w_O$$

$$F = h^{-1}D_{22}\sqrt{\frac{E_{11}}{E_{22}}}\,F_O$$

$$\left.\begin{aligned} x^{\frac{1}{4}} &= h^{-1}D_{11}\sqrt{\frac{D_{22}}{E_{22}}}\,x_O^{\frac{1}{4}} \\[2em] y^{\frac{1}{4}} &= h^{-1}D_{22}\sqrt{\frac{D_{11}}{E_{11}}}\,y_O^{\frac{1}{4}} \end{aligned}\right\} \qquad \text{note:} \quad \frac{a_O}{b_O} = \left(\frac{D_{22}}{D_{11}}\right)^{\frac{1}{4}}\frac{a}{b}$$

to yield:

$$\frac{\partial^4 F_O}{\partial x_O^4} + 2H^*\frac{\partial^4 F_O}{\partial x_O^2 \partial y_O^2} + \frac{\partial^4 F_O}{\partial y_O^4} = \left(\frac{\partial^2 w_O}{\partial x_O \partial y_O}\right)^2 - \frac{\partial^2 w_O}{\partial x_O^2}\frac{\partial^2 w_O}{\partial y_O^2}$$

$$\frac{\partial^2 w_O}{\partial x_O^4} + 2D^*\frac{\partial^4 w_O}{\partial x_O^2 \partial y_O^2} + \frac{\partial^4 w_O}{\partial y_O^4}$$

$$= h^{-\frac{1}{2}}p(x_O,y_O) + \frac{\partial^2 F_O}{\partial y_O^2}\frac{\partial^2 w_O}{\partial x_O^2}$$

$$- 2\frac{\partial^2 F_O}{\partial x_O \partial y_O}\frac{\partial^2 w_O}{\partial x_O \partial y_O} + \frac{\partial^2 F_O}{\partial x_O^2}\frac{\partial^2 w_O}{\partial y_O^2}$$

Thus only D* and H* appear as constants (the thickness h modifies the loading only) and it has been noticed that H* = H*(D*,ε) where ε is the generalized Poisson parameter. These relations are shown in Figure IV-A-4. Hence any solution technique available in the isotropic

Figure IV-A-4

H* vs D* for Various Values of ε

ε = .2

ε = .3

ε = .4
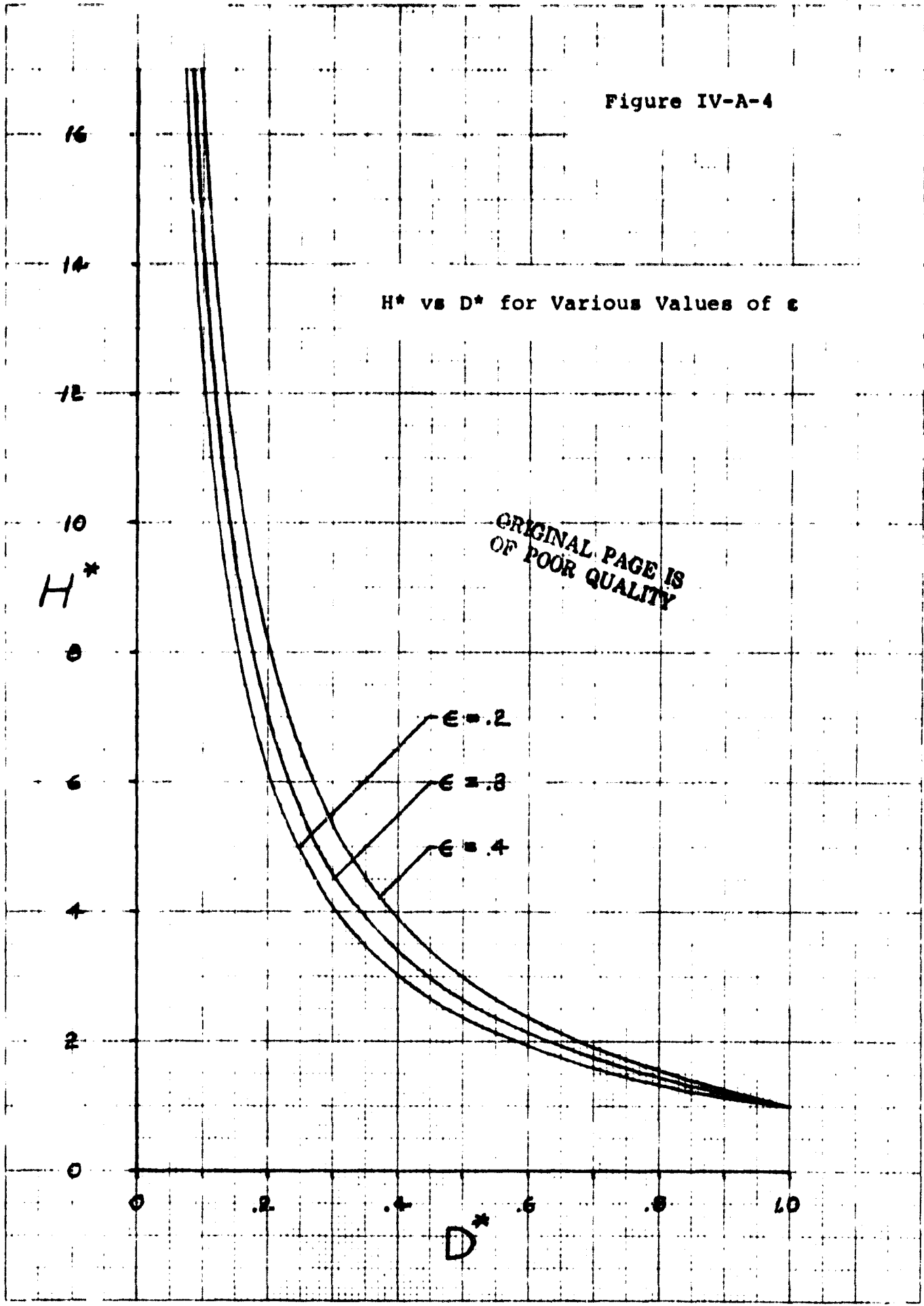
literature may be used to solve these equations. This positive attitude towards solution possibilities is in sharp contrast to Lekhnitski[1]* who states (referring to the original untransformed equations), "Their integration is accompanied by great difficulties ...; their exact solution is unknown for even one simple case of bending.".

Result (iv). The similarity laws for the orthotropic plate (with the two compressed sides simply supported)** buckling problem have been found, and related rules for the corresponding deflection and vibration problems are being cast in their final form for presentation to the academic community. The similarity laws are stated by demanding that the number pair

$$\frac{mb_o}{a_o}\sqrt{D^*} \quad \text{and} \quad B_o$$

be constants associated with any one k_o versus a_o/b_o curve for any one value of m (the number of half-waves in the x_o direction) and any one value of D^*. A more concrete (but more restrictive statement is that "given a buckling curve k_o versus a_o/b_o for $m = 1$ and $D^* = 1$, any other*** buckling

---

*The bracketed number in this text refers to the reference found on page 123.

**The case of two parallel sides simply supported and the perpendicular sides being compressed has also been investigated.

***For the same $y_o = o, b_o$ boundary conditions as the original curve. Note, however, that the form of the similarity laws are independent of the $y_o = o, b_o$ boundary conditions.

curve K_O versus a_O/b_O may be found for any desired values of m and $D^{*"}$. The second similarity parameter B_O is given by

$$B_O = \left[\left(\frac{a_O}{b_O m}\right)^2 k_O - 1\right] \cdot (D^*)^{-2}$$

and thus by defining $\theta_i = \left(\frac{a_O}{m b_O}\right)_i$ for states 1 and 2 we write,

$$\frac{D_1^*}{(\theta_1)^2} = \frac{D_2^*}{(\theta_2)^2} \quad \text{and} \quad \frac{-1 + (\theta_1)^2 (k_O)_1}{(D_1^*)^2} = \frac{-1 + (\theta_2)^2 (k_O)_2}{(D_2^*)^2}$$

The $D^* = 0$ case is excluded from the similarity sets since the similarity rules were obtained after a division by D^* (which is a valid operation only if it is not zero). However, once a single point is known on (say) the k_O versus a_O/b_O curve for m = 1, the entire m = 1 buckling curve may be constructed, as well as the complete curves for m = 2, 3,.... . Therefore, for $D^* = 0$ we may write a single degenerate similarity statement,

$$(k_O)_1 = \frac{1}{(\theta_1)^2} + (\theta_1)^2 \left[\frac{(\theta_2)^2 (k_O)_2 - 1}{(\theta_2)^4}\right]$$

These concepts are put into perspective by writing the highly non-linear buckling determinant in implicit form for various levels of sophistication.

(1) Basic P.D.E.[*]: $f(k, D_{11}, D_{22}, D_{12} + 2D_{66}, a/b, m) = 0$;
6 parameters.

(2) Divide P.D.E. by D_{11}: $g(k, \dfrac{D_{22}}{D_{11}}, \dfrac{D_{12} + 2D_{66}}{D_{11}}, a/b, m) = 0$;
5 parameters.

(3) Affinely Transformed P.D.E.: $j(k_o, D*, a_o/b_o, m) = 0$;
4 parameters.

(4) The Similarity Laws: $\theta\sqrt{D*}$ and B_o are a constant number pair; 2 parameters.

Form (3) reduces all possible calculations to a small finite set with D* as a parameter, $0 \leq D* \leq 1$. Form (4) provides another nearly infinite compression of calculations and provides the necessary insight into the fundamental mathematical structure of the solutions. Form (3) was developed by the principal investigator in June of 1979 and Form (4) was developed by the principal investigator in April of 1981, both while working under the present NASA/AFOSR grant.

3.   Plans for Upcoming Period

The principal thrust for the next few months is expected to be computational. The numerous theoretical advances described in Section 2 of this text need to be examined in terms of the solutions they produce, and the various equation parameters (such as $\bar{L}$, $\bar{D}$, $\bar{R}$, etc.) need to

---

[*]P.D.E.: "partial differential equation"

be calculated and carefully studied. Many specific problems are currently underway; they also will be completed and the numerical results presented. The material pertaining to uniaxial plate buckling (loaded sides simply supported, other sides with arbitrary support) will be written up and submitted for publication; a tentative title is "Stability of Specially Orthotropic Plates Using an Affine Transformation and Similarity Laws".

After the above matters are substantially completed it may be finally the right time to begin a systematic study of symmetric (and/or anti-symmetric) laminates.

4. References

1. Lekhnitski, S. G., "Anisotropic Plates", Gordon and Breach, 1968.

5. Current Presentations by E. J. Brunelle on this Subject

"The Use of Affine Transformations in the Solution of Composite Structures Problems"

Presented at the 17th Annual Meeting of the Society of of Engineering Science, Inc., December 15-17, 1980, Georgia Institute of Technology, Atlanta, Georgia.

IV-B   ULTRASONIC NON-DESTRUCTIVE TESTING OF COMPOSITE STRUCTURES

Senior Investigator: H. F. Tiersten[*]
P. Das

Ultrasonic waves are being exploited both in research and, increasingly, in routine non-destructive testing as a promising means of discovering and assessing manufacturing flaws and load-induced damage in composites. Our efforts in ultrasonic NDE are three fold: improving image quality through data processing and display techniques, transducer development and material flaw image identification.

1.   Status

As of the beginning of the reporting period, the hardware and software components of the ultrasonic imaging system had been developed to the point that creating a pseudo-colored, high resolution ultrasonic image is now a well established and routine procedure. A variety of samples of different materials have been imaged to further develop and refine the imaging and computer processing systems.[1][**]

2.   Progress During Report Period

Imaging and studies of composite samples similar to those discussed in the previous report (39th Semi-Annual Report, January 1981) have continued. To aid in this process, a Conrac high resolution color video monitor is now

---

[*] RPI graduate student R. Werner
[**] Bracketed numbers in this section refer to the references listed on page 129.

in the lab, providing the capability to immediately display and, if necessary, modify the ultrasonic image data. Software has been written to made the pseudocoloring and scroll and zoom capabilities of the Deanza image processor available for use with the monitor.

A sample of the images obtained during the reporting p.riod is presented in Figures IV-B-1 through 3. These were chosen since they show the effects of repeated loading. Table IV-B-1 describes the construction and loading of the samples.

TABLE IV-B-1

ULTRASONIC TEST SAMPLE CONSTRUCTION AND LOADING

Figure Number	Construction	Loading
IV-B-1	$[0/30/60/90/120/150]_s$	0-95 kg, 1 cycle (first failure)
IV-B-2	$[0/30/60/90/120/150]_s$	0-95 kg, 50 cycles
IV-B-3	$[0/30/60/90/120/150]_s$	0-55 kg, 50 cycles

Figure IV-B-1 shows a well-defined damage area centered around the loading point at the center of the sample. Contrasting this with Figure IV-B-2 shows that the repeated loading has caused the damage to spread out from the center. Figure IV-B-3 shows a sample loaded to a maximum of 55 kg for 50 cycles, as opposed to 95 kg for Figures IV-B-1 and -2. Although an image is not presented here, it is of interest to note that a sample loaded 0-55 kg for one cycle showed no damage[2].
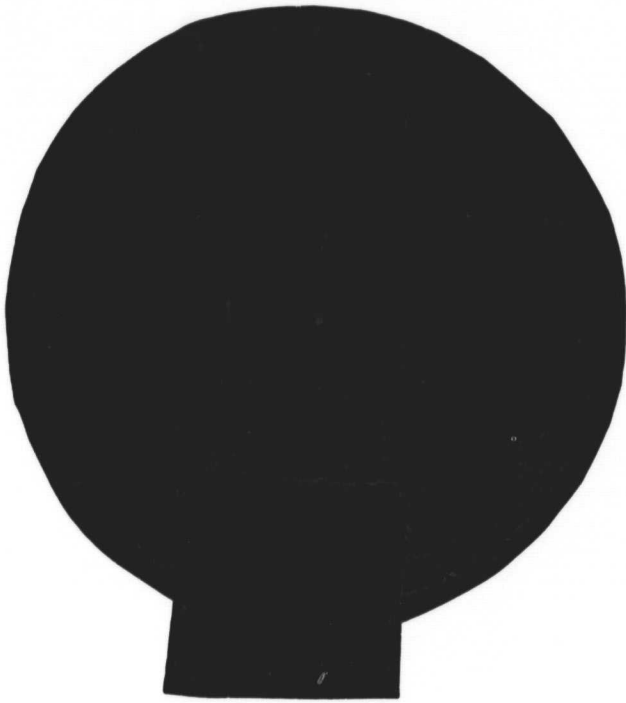
Figure IV-B-1

Figure IV-B-2
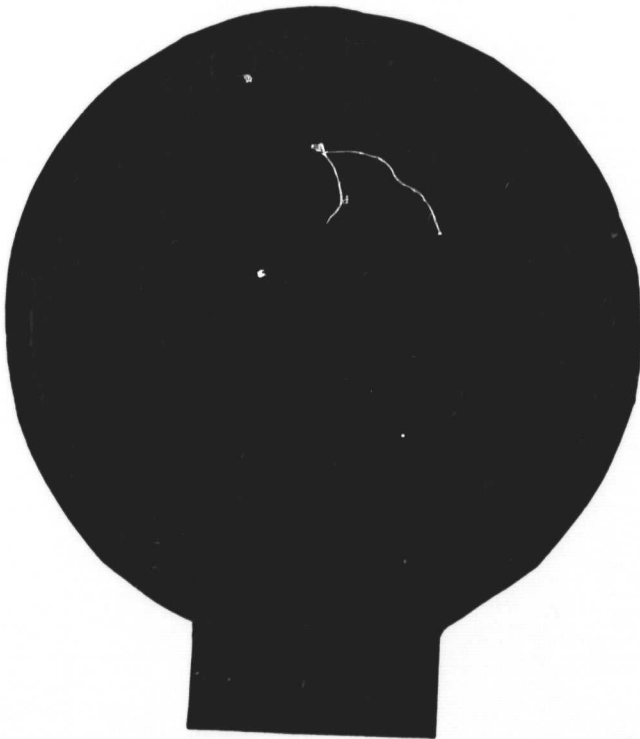
Figure IV-B-3

(See Table IV-B-1)

PRECEDING PAGE BLANK NOT FILMED

Work to implement further digital image processing of the data using the Image Processing Laboratory Prime 750 is now in progress. The mathematical process involved is deconvolution, and a theoretical discussion follows.

The spot size of the ultrasonic beam at the focal point is given approximately by:

$$d = \frac{f_1}{D} \lambda = \frac{f_1 c}{D \nu}$$

where d is the diameter of the spot, f_1 is the focal length of the transducer, D is the diameter of the transducer and λ, ν, and c are the wavelength , frequency and speed of sound in water, respectively. Substituting the characteristics of the transducers currently in use yields:

$$d = \frac{1.0 \text{ in.}}{1.5 \text{ in.}} \frac{1500 \text{ m/sec.}}{5 \times 10^6 \text{ Hz.}} = 450\nu$$

The distance between each sample point is currently 160ν. It is readily apparent that the spot size is larger than this, causing some overlap in the sampling of adjacent points. The maximum resolution of the stepping motors is 3.2ν, so by reducing the distance between sampled points, the overlap would be increased. Thus, deconvolution to account for the effects of the spot size becomes applicable.

The theoretical basis for the deconvolution is as follows:

The image data that is recorded by the system can be represented as:

$$g(x,y) = i(x,y) * f(x,y)^{\dagger}$$

where $i(x,y)$ is the true image data and $f(x,y)$ is the impulse response of the system. By taking the Fourier transform of the above equation, we get

$$G(i,j) = I(i,j) \times F(i,j)$$

and so the true image data can be recovered by dividing $G(i,j)$ by the Fourier transform of the impulse response of the system and then taking the inverse Fourier transform.

The impulse response of the system can be easily determined by imaging a sufficiently thick sheet of steel or other material with a very small hole drilled in the center, so that all but a negligible portion of the ultrasound signal will be attenuated except at the hole. The Fourier transform of this data will then be stored by the computer and used for deconvolution.

Since the actual impulse response of the system has not yet been determined, it has been assumed for testing of the computer programs to be a narrow Gaussian function; that is, of the form

$$f(x,y) = A \exp [-a(x^2 + y^2)]$$

and a Fortran program has been implemented to perform the deconvolution using the technique described above.

One problem that must be taken into account is that $f(x,y)$ may contain zeros. To account for this, a small,

---

† * is the symbol representing the mathematical process called convolution, that is $i(x,y) * f(x,y)$ is $i(x,y)$ convolved with $f(x,y)$.

positive offset is added to prevent errors caused by attempting to divide by zero.

3. Plans for the Upcomimg Period

Plans for the future include continuing improvement and application of the deconvolution algorithms to image data. In addition, phase data will be included with the amplitude data now being recorded in the imaging process. We intend to apply the refined computer aided image processing to a wide range of types of damage in composite materials. It is expected that this will provide additional information about the characteristics of the material and the damage being imaged.

A second objective will be to use linear and possibly two-dimentional arrays in place of the single transducer used to date to obtain ultrasonic images. In addition to application of conventional linear arrays, this will involve fabricating mosaic monolithic arrays using the energy trapping principle. Although we have fabricated some monolithic arrays before, in the coming year the emphasis will be to apply them to obtain ultrasonic images at a very fast rate compared to what is obtainable by the single transducer method.

4. References

1. Composite Structural Materials, 39th Semi-Annual Progress Report, January, 1981, pp. 116-123.

2. Das, P. and R. Werner, "Digital Enhancement of Ultrasonic Images and Its Application to Non-Destructive Testing of Composite Materials", Acoustical Imaging, Vol. II, to be published.

5. Current Publications or Presentations by Professors Das and/or Tiersten on this Subject

1) Das, P. and R. Werner, "Digital Enhancement of Ultrasonic Images and Its Application to Non-Destructive Testing of Composite Materials.

> To be presented at the 11th International Symposium on Acoustical Imaging, May 4-7, 1981, Monterey, California.

> To be published in Acoustical Imaging, Vol. 11.

2) Das, P., R. Werner, J. F. McDonald and H. F. Tiersten, "Mosaic Array Transducer Based on Energy Trapped Modes and Ultrasonic Imaging of Composite Materials".

> To be presented at the 6th International Symposium on Ultrasonic Imaging and Tissue Characterization, June 1-3, 1981, National Bureau of Standards, Gaithersburg, Maryland.

3) Das, P. and R. Werner, "Ultrasonic Imaging for Non-Destructive Evaluation of Composite Material".

> To be presented at Ultrasonics International 81, June 30-July 2, 1981, Brighton, UK.

> Proceedings to be published.

IV-C TRANSVERSE PROPERTIES OF COMPOSITES WITH ANISOTROPIC CONSTITUENTS

Senior Investigator: R. J. Diefendorf[*]

Composites are multiphase materials that often exhibit properties superior to the characteristics possessed by each constituent. However, in order to more efficiently utilize composites to their full potential and to accurately predict overall composite performance from its constituent properties, the effect of fiber anisotropy on the physical properties of the reinforcement must be considered.

In the case of the longitudinal direction (parallel to the fiber axis), the properties of fibers alone and in composites are both predictable from theory and are easily measured. The rule of mixtures predicts longitudinal modulus as represented in Equation (1) and shows good agreement with experimental results.

$$E_c = V_f E_f + (1 - V_f) E_f \tag{1}$$

Schapery[1][**] has formulated an expression for the longitudinal coefficient of thermal expansion (CTE), Equation (2).

$$= \frac{{}_m V_m E_m + {}_f V_f E_f}{E_m (1 - V_f) + E_f V_f} \tag{2}$$

The equation relates composite CTE to constituent properties

---

[*] RPI graduate students J. Helmer and C. Uzoh.

[**] Bracketed numbers in this section refer to the references listed on page 143.

such as modulus, CTE and fiber volume fraction. The theory
assumes that both fiber and matrix are isotropic and homo-
geneous. There is good agreement between the formulation
and experimental results, even for the case of anisotropic
fibers. This is due in part to the packing of the fibers in
the matrix. The axial properties of composites are not
strongly dependent on the type of packing of the fibers,
either square, hexagonal or random, as depicted in Figure
IV-C-1, thus accounting for the good agreement. The value
for α_{11} has been determined to be zero at room temperature,
which has been confirmed in the literature[2]. While there
exists a substantial amount of information on the properties
in the longitudinal direction of fibers and composites, the
information on the transverse direction is not similarly de-
veloped, particularly for anisotropic fibers. This was due
in the past to the difficulty in predicting transverse prop-
erties of anisotropic fibrous composites and also in the
direct measurement of these properties on the isolated fiber.

This information is essential in predicting the fatigue
and thermal cycling behavior of composite laminates. The
data on transverse coefficients is also indispensable for
predicting the thermal shock behavior of carbon/carbon com-
posites. Similarly, the transverse data may have a signifi-
cant impact in the area of carbon/aluminum composites. In
the case of carbon/aluminum matrix composites, poor trans-
verse properties impose a major limitation even after fifteen

FIBER PACKING
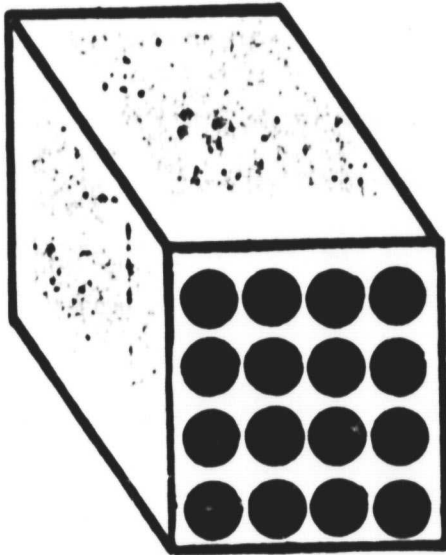
HEXAGONAL

SQUARE
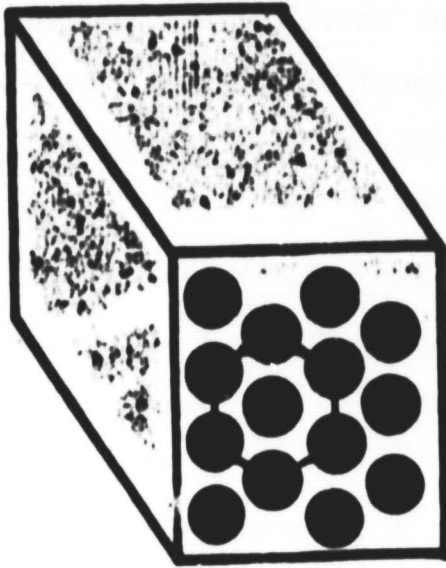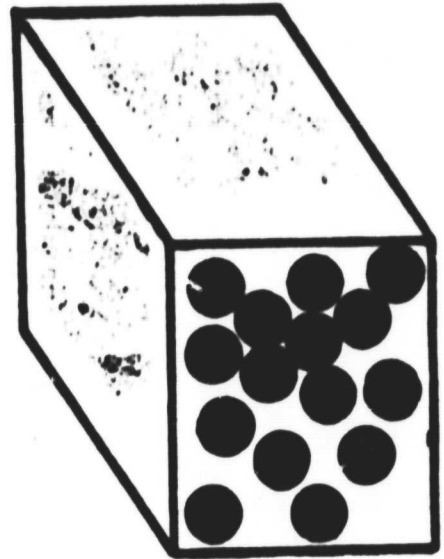
RANDOM

Figure IV-C-1

years of effort and may be inherent to the transverse properties of the constituents.

The transverse properties depend to a high degree on the geometry of fiber packing, and local variations produce significant property differences. This is one reason for the variations in properties predicted by existing theories. The problem is well suited for a finite element analysis technique (Khan et al.[3]), with results falling in between the rule of mixture's lower bound and an upper bound formulation proposed by Schapery[1].

A second reason for differing predictions among existing theories is the anisotropy of the fiber. A transverse cross section of the structure of a single carbon fiber is shown in Figure IV-C-2. The transverse structure is seen to be similar to that of an onion, while a different structure with different properties results when a longitudinal cross section is made[4]. A theoretical prediction[5] that accounts for fiber anisotropy has been proposed by Levin[6] which relates the transverse composite CTE to the appropriate coefficients of the phases as well as their respective compliances, Equation (3).

$$\bar{\alpha}_{22} = \bar{\alpha}_t + (\alpha_{k\ell}^{(2)} - \alpha_{k\ell}^{(1)}) P_{k\ell rs} (S_{rs22}^* - \bar{S}_{rs22}) \qquad (3)$$

$$P_{k\ell rs} (S_{rsij}^{(2)} - S_{rsij}^{(1)}) = I_{k\ell ij}$$

and
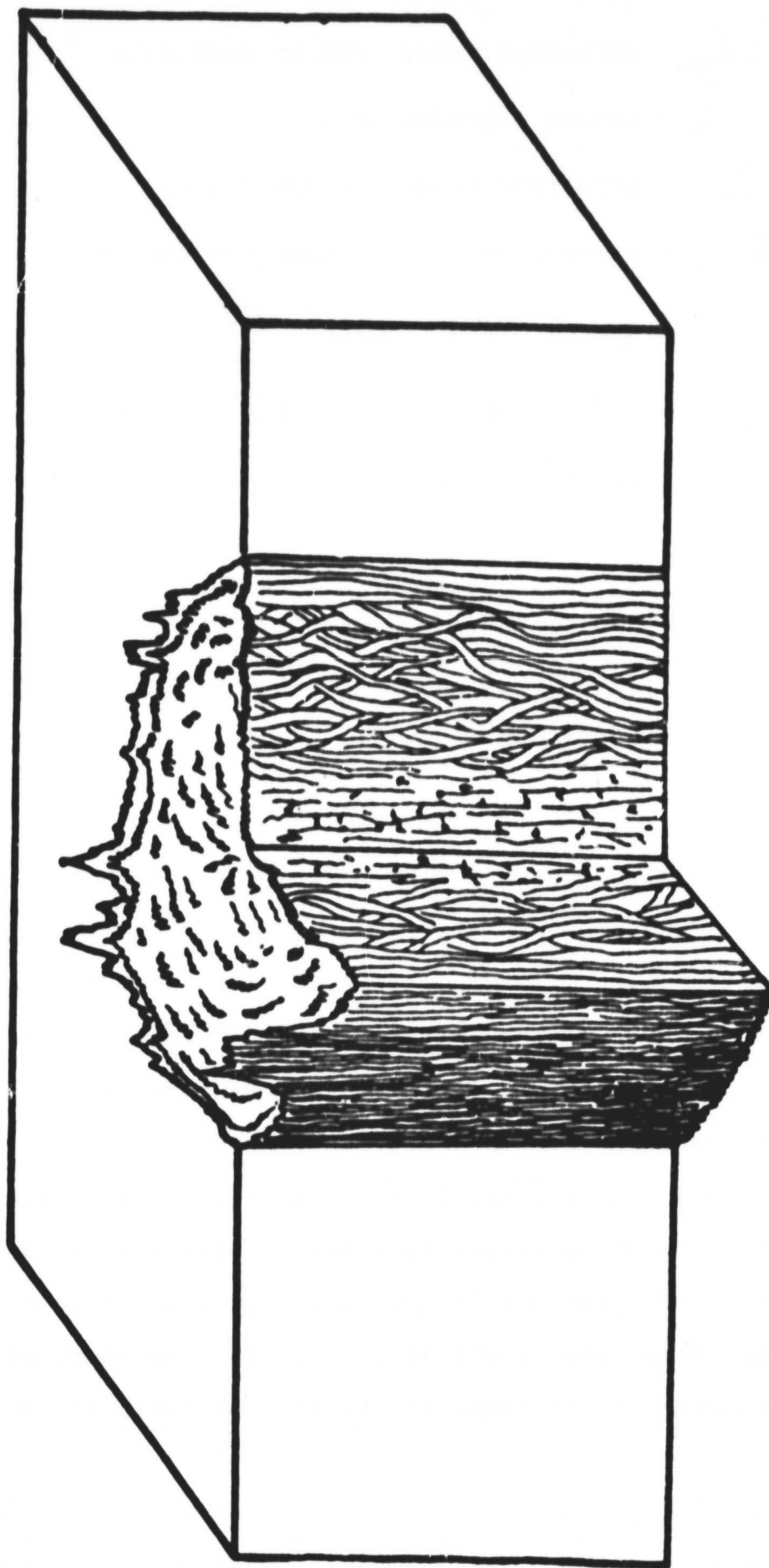
FIGURE IV-C-2

Schematic of Carbon Fiber Section

$\bar{\alpha}_{22}$ = effective trans. CTE of composite

$\bar{\alpha}_t$ = volume fraction etc.

S^*_{rs22} = effective elastic compliancies

$\bar{S}_{rs22}$ = average compliance over the composite

$\alpha^{(q)}_{k\ell}$ = CTE of the qth phase

$S^{(q)}_{rsij}$ = elastic compliance of the qth phase

$I_{k\ell ij}$ = fourth rank symmetric unit tensor

The equation, as is the case with almost all theories predicting transverse behavior, has not been extensively evaluated against experimental data.

1. Status

Several anisotropic fibers are being evaluated so as to establish the overall effectiveness of the Levin theory to generally anisotropic constituents. The fiber types chosen for study are: Thornel pitch 50 million modulus, Thornel 33 6K, Courtauld's HMS 10 K fibers, AS-4 and Kevlar. All fibers were supplied in a prepreg form that consists of fibers in an epoxy resin film twelve inches wide that is only partially cured to insure tackiness. Strips 6" x 12" were cut from the prepreg rolls and laid up into laminates consisting of between 12 and 32 plies. In some cases extra matrix material was added in the form of resin films so as

to vary the filament content. The variation of the resin
content enables a plot of CTE versus fiber volume fraction
to be constructed, from which the transverse coefficient of
the fiber can be determined by extrapolating to 100 per cent
volume fraction. Resin films were chosen over resin in bulk
form for a variety of reasons. First, the reproducible ap-
plication of neat resin in uniform thickness is difficult.
The resin films are more consistent in thickness than could
possibly be attained with bulk resin. Also, there are addi-
tional problems in the application of the neat resin. The
bulk resin nas a very high viscosity which must be reduced
for easy application. A heat source can lower the viscosity
but the resin can become partially cured. A second alterna-
tive is to reduce viscosity with solvents. Unfortunately,
the solvents are difficult to completely remove and they
volatilize off upon curing, leaving voids in the laminate.
The utilization of resin films reduced the void content to a
more acceptable level.

The cure is accomplished by heating up to 250°F at a
controlled rate in an hour, applying pressure for consolida-
tion, and then heating at 250°F for two hours. The pressure
and bleeders (cloths that absorb excess resin) were varied
so as to alter the volume fraction. Table IV-C-1 lists the
various fiber types and the cure process parameters. By
carefully controlling the number of bleeders, applied pres-
sure and amount of excess resin, differences in thicknesses

TABLE IV-C-1
CURE PARAMETERS

Fiberite 2048A1A Thornel Pitch			Fiberite 1048A1E Thornel 300			Fiberite 1248A1A Courtauld HMS			Hercules AS-4* AS			DuPont Kevlar			Number of	
No. of Bleeders	Cure P (psi)	Plate I.D. No.	No. of Bleeders	Cure P (psi)	Plate I.D. No.	No. of Bleeders	Cure P (psi)	Plate I.D. No.	No. of Bleeders	Cure P (psi)	Plate I.D. No.	No. of Bleeders	Cure P (psi)	Plate I.D. No.	Plies	Films
0	0	7	0	0	6	0	0	13	0	0	11	0	0	1	24	---
4	100	10	0	0	9	4	100	14	4	100	12	4	100	2	24	---
8	200	15	8	200	16	8	200	18	8	200	17	8	200	3	27	---
12	300	19	12	300	20	12	300	22	12	300	21	12	300	4	27	---
20	400	23	20	400	24	20	400	26	20	400	25	20	400	5	30	---
---	---	---	30	500	38	30	500	27	30	500	36	30	500	6τ	30	---
0	0	32	0	0	30	0	0	28	---	---	---	---	---	---	21	20
6	150	33	6	150	31+	6	150	29	---	---	---	---	---	---	18	17
2	50	37	2	50	34†	2	50	35	---	---	---	---	---	---	14	26
---	---	---	---	---	---	---	---	---	0	0	40	---	---	---	12	11

---

* — AS-4-32 plies, 40 bleeders, 1000 psi also fabricated as plate 40.

τ — Only 29 plies instead of 30.

† — Seventeen plies with two resin films between plies (total 32).

between plates of different volume fraction can be minimized. This reduces problems with the poor thermal conductivity of the samples during CTE measurements. All lay-ups were cured under a vacuum to avoid the problem of air entrapment in the cured product.

2. Progress During the Report Period

Material was trimmed from each of the fabricated plates using a steel carbide blade to eliminate edge effects such as uneven matrix distribution and nonuniformities in thickness. Twelve samples were then cut from each uniaxial plate; six parallel to the fibers and six transverse to the fibers. The specimens were cut to a length of four inches and a width of one-half inch. A high blade speed with a slow feed rate with slight pressure was used when cutting to minimize edge damage. When the cutting was complete, the group of specimens were identified and stored in a dessicator to minimize moisture absorption. Extra specimens were cut for preliminary mechanical testing. Some of the extra samples were dry sanded by hand with 600 grit sandpaper, while others were sanded on an automatic belt sander with medium grit. Also, a few samples were hand-sanded with 600 grit in addition to belt sanding. A fourth group was cut and not polished in any manner. The motivation behind the preliminary tensile testing was to determine the effect of the various surface finishing techniques on strength and modulus measurements. Testing revealed that all results were well

within the experimental scatter, and it was concluded that
transverse strength measurements are independent of the sur-
face polishing technique when cut as described. Belt sanding
was chosen as the mode of surface treating for the sake of
expediency. Supplemental sanding by hand was performed
where required.

For each of the over 400 samples, seven dimensional
measurements were performed. Fifty per cent of the the
values cluster around the design thickness of 125 mils with
only a few exceeding this value.

An appropriate heating rate has been determined for CTE
measurements, and the temperature range for obtaining the
data is being established. The upper limit of the range may
be limited by the glass transition of the epoxy matrix, but
it may be possible to extend the range. Cured neat resin
was tested in a differential scanning calorimeter to obtain
the glass transition temperature (T_g) of the matrix. The
thermal dimensional stability was found to be lost at
$T \geq 130°C$.

A further cause for concern in establishing the experi-
mental limit is the effect of fibers on the glass transition.
Table IV-C-2a shows a comparison of filled and unfilled
resins for a constant heating rate. Also of importance is
the fact that several different heating rates were run with
the unfilled sample to investigate the effect of scanning
speed. As can be seen, there is an appreciable variation

TABLE IV-C-2A

HEATING RATES USED FOR Tg SAMPLES

Scan Speed °C/min	Tg °C	Additional Comments
10	--	filled[*]
10	140	unfilled[**]
20	100	unfilled[**]
5	140	unfilled[**]

---

[*]Filled samples: AS-4/1908-1
[**]Unfilled samples: Hercules 1908-1

TABLE IV-C-2B

Tg VS. VARYING CURE PROCESS PARAMETERS

Plate Number[*]	Tg °C
11	140
12	140
17	140
21	---
25	140
36	140

---

[*]Plate numbers refer to Table IV-C-1

for different heating rates. The logical extension of this concept is the investigation of T_g for a heating rate close to that of the actual heating rate for CTE experiments. This rate proved too slow for valid results.

As previously mentioned, filled samples have been tested for T_g. A possible correlation between volume fraction (V_f) and T_g (Table IV-C-2b) was not observed, with most of the glass transitions occurring around the same temperature.

Glass transition is not the only possible source of dimensional fluctuation. During testing for CTE, a specimen will be in the atmosphere for a few hours; thus time and humidity effect could be important if not controlled. Using a worst-case situation, one filled and two unfilled resin samples were submerged in water. One unfilled sample was removed after 48 hours and was found to have increased in weight .068 per cent while undergoing no change in any dimension. After 200 hours, the remaining specimens were removed from the water and weighed and measured. The increase in weight for the filled and unfilled samples was .038 per cent and -.013 per cent, respectively. As in the case of immersion for 48 hours, dimensional stability was retained.

3. Plans for Upcoming Period

Future work will be devoted in general to finishing the preliminary studies so that the CTE measurements can be implemented. Investigations are being made to:

a) establish any possible correlation between T_g and V_f or heating rate,

b) determine how these factors influence the range intended for testing and

c) extend the range, if possible, for thermal testing.

The test apparatus is being analyzed for error and finally, techniques are being developed and tested for eliminating noise due to temperature differentials along the test apparatus.

4. References

1) Schapery, R. A., "Thermal Expension Coefficients of Composite Materials Based on Energy Principles", Journal of Composite Materials, Vol. 2, July 1968, p. 380.

2) Larsen, E., et al., "Development of Engineering Data on the Mechanical and Physical Properties of Advanced Composite Materials", Technical Report AFML-TR-74-266, Air Force Materials Lab., Wright-Patterson Air Force Base, Ohio 45433.

3) Khan, K. H., "On the Thermal Expansion of Unidirectional Fibre Composites and Reinforcing Graphite Fibres", Doctoral Thesis, North Carolina State University at Raleigh, North Carolina, 1976.

4) Tokarsky, E. and R. J. Diefendorf, "High-Performance Carbon Fibres", Polymer Engineering and Science, Vol. 15, No. 3, March 1975.

5) Hashin, Z., "Analysis of Properties of Fibrous Composites with Anisotropic Constituents", Journal of Applied Mechanics, Vol. 46, September 1979.

6) Levin, V. M., "Thermal Expansion Coefficients of Heterogeneous Materials", Mekanika Tverdogo Tela, Vol. 2, No. 1, 1967, pp. 88-94.

IV-D FATIGUE IN COMPOSITE MATERIALS

Senior Investigator: E. Krempl[*]

The deformation and failure behavior of graphite epoxy tubes under biaxial (tension, torsion) loading is investigated. The aim of this research is to provide basic understanding and design information on the biaxial response of graphite-epoxy composites.

1. Status

Tests in the elastic range and to failure on thin-walled graphite-epoxy tubes of four layers of $[\pm 45]_s$ showed the following;

For static axial loadings:

- The same effective elastic modulus in tension and compression.
- Equal tensile and compressive strength.
- Time-dependent, nonlinear behavior above 25% of the ultimate strength.
- The development of a hysteresis loop during load controlled, completely reversed loading at a load amplitude of 55% of the ultimate load. Under these conditions, rate of loading is a parameter of significant influence.

For static torsional loadings:

- Departure from linearity of the torque versus angle of twist diagram at approximately 50% of the ultimate torque.

It was further found that the effective elastic and shear modulus were unaffected by combined, completely reversed proportional cycling.

---

[*]RPI graduate student T.-M. Niu

The deformation behavior can therefore be characterized
as quasi-isotropic for the relatively small elastic range
(25% of tensile ultimate), followed by significant time-
dependent behavior. In addition, the time dependence is
more pronounced on the tensile than on the torsion axis, as
might be expected for a $[\pm 45]_s$ laminate.

2. Progress During Report Period

Completely reversed, load-controlled fatigue tests were
performed at three different frequencies for axial loads.
In addition, ultimate strength and elastic properties tests
of the tubes were conducted for torsion. All tests were run
on an MTS servocontrolled hydraulic tension-torsion testing
machine. The results are as follows;

In Axial Fatigue:

The axial fatigue behavior of the tubes at 1, .1 and
.01 Hz was studied using a sine wave forcing function. An
axial (1" or 25.4 mm gage length) and a diametral extenso-
meter were used. The test was terminated automatically when
one of the following three limits was exceeded:

    axial strain   > |4%|
    diametral strain > |3.5%|
    stroke   > |6.35 mm|.

Depending on the location of the failure, any one of these
limits could have been the trigger for the end of the test.

The fatigue tests results are shown in Figure IV-D-1.
The ordinate is the stress amplitude normalized by an average
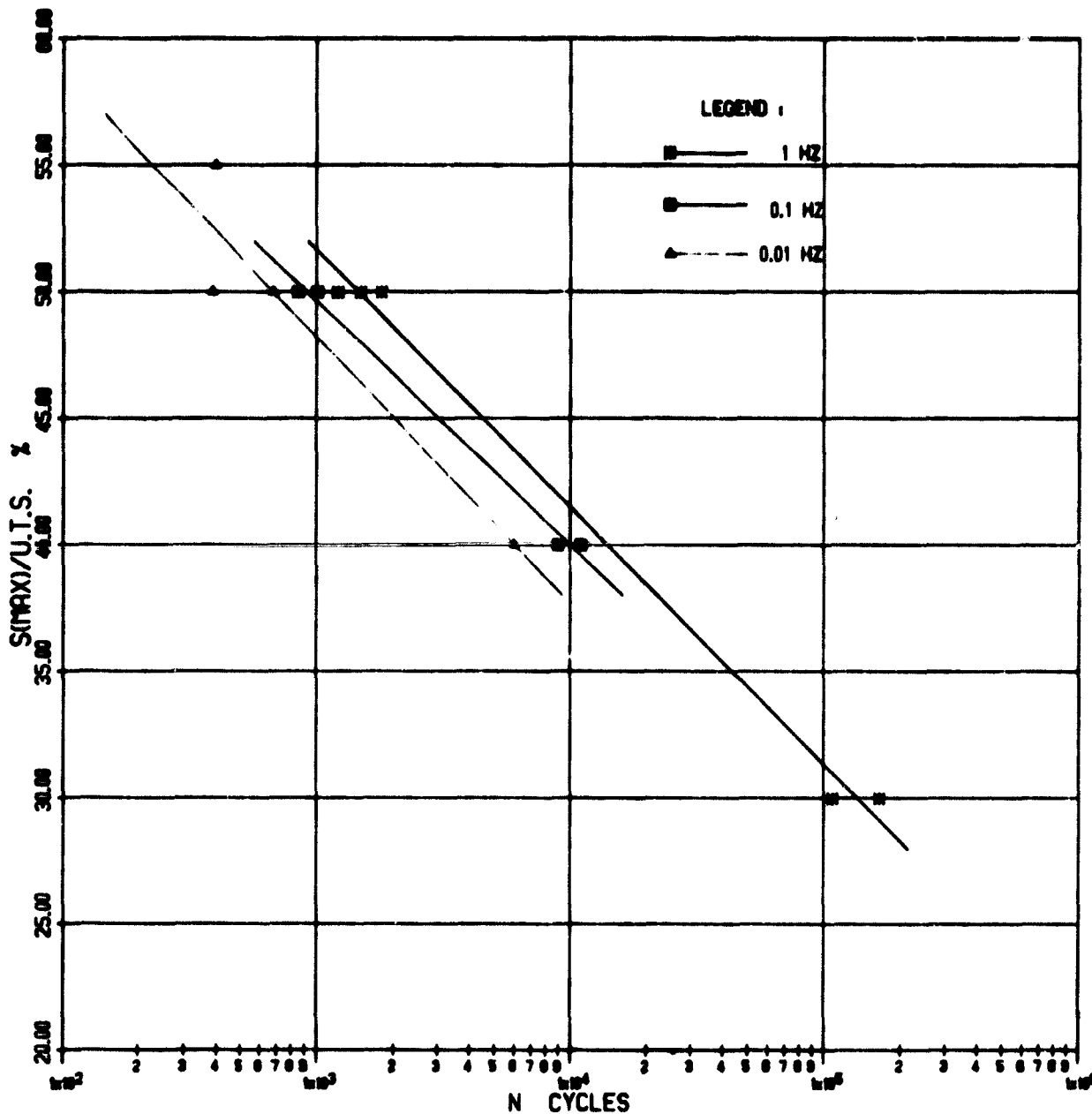
S-N PLOTS FOR TENSION-COMPRESION SINUSOIDAL
FATIGUE OF GRAPHITE EPOXY THIN-WALLED TUBES
(45/-45)S, R RATIO= -1, AT ROOM TEMPERATURE
U.T.S. = 156 MPA

Figure IV-D-1

value of the ultimate tensile strength, obtained from Table
IV-D-1 in Reference 1[*]. The number of cycles, N, are the
cycles-to-failure defined previously. This figure shows
the axial fatigue resistance of these tubes under completely
reversed, load-controlled loading to be poor. At 10^5 cycles
the allowable amplitude is only 30 per cent of the ultimate
strength. Clearly, the deformation of these axially loaded
tubes is matrix-dominated as evidenced by the rate-dependent
hysteresis loops (see Figure IV-D-4 in Reference 1). The
fatigue strength at 10^6 cycles for R = .667 of uniaxial
laminates, shown in Figure 62 in Reference 2, was above 85
per cent of the ultimate tensile strength, and their defor-
mation is fiber dominated. In addition, however, a compari-
son must include the fact that the tubes were also loaded
into compression whereas only tension-tension loading was
used for the laminates.

It appears, therefore, that the low fatigue resistance
of the tubes in axial loading may be caused by the matrix
domination of the deformation and by the compressive loading
of the specimens. Another possible manifestation of the
influence of matrix deformation is the effect of frequency
of loading on the fatigue resistance. As the frequency is
reduced the fatigue resistance is also reduced. The effect
of frequency is not very pronounced but noticeable (see
Figure IV-D-1).

_____

[*]References in this section are listed on page 153.

In Static Torsion:

Table IV-D-1 in Reference 1 lists one value of the ultimate shear strength obtained in torsion. Subsequently, additional tests were performed whose results show that the ultimate shear strength depends on the direction of twist.

Figure IV-D-2 is a diagram of the shear stress versus angle of rotation of the loading ram in the two cases. It is evident that the ultimate shear strength is significantly affected by the direction of torsion. Table IV-D-1 lists further results on the ultimate strength in torsion.

In Figure IV-D-2 and Table IV-D-1, the direction of torsion which stretches the outermost fibers is arbitrarily assigned a negative sign. Under this direction of torsion the average ultimate shear strength is -117 MPa. However, when the outermost fibers are compressed (defined as positive torque) the average ultimate shear strength is 191 MPa.

These results were initially unexpected. However, they are consistent with other data reported earlier (see Reference 3). They can be explained as follows. First, failure is initiated by buckling, as evidenced by separate tests on a model tube. Next note that when outer fibers are in tension, the inner fibers of a $[\pm 45]_s$ tube are in compression. Finally, the bending rigidity, EI, of an element of wall is much greater for cross sections with the outer fibers normal to the cross section. Thus, the rigidity against buckling (the product of modulus and moment of inertia) is
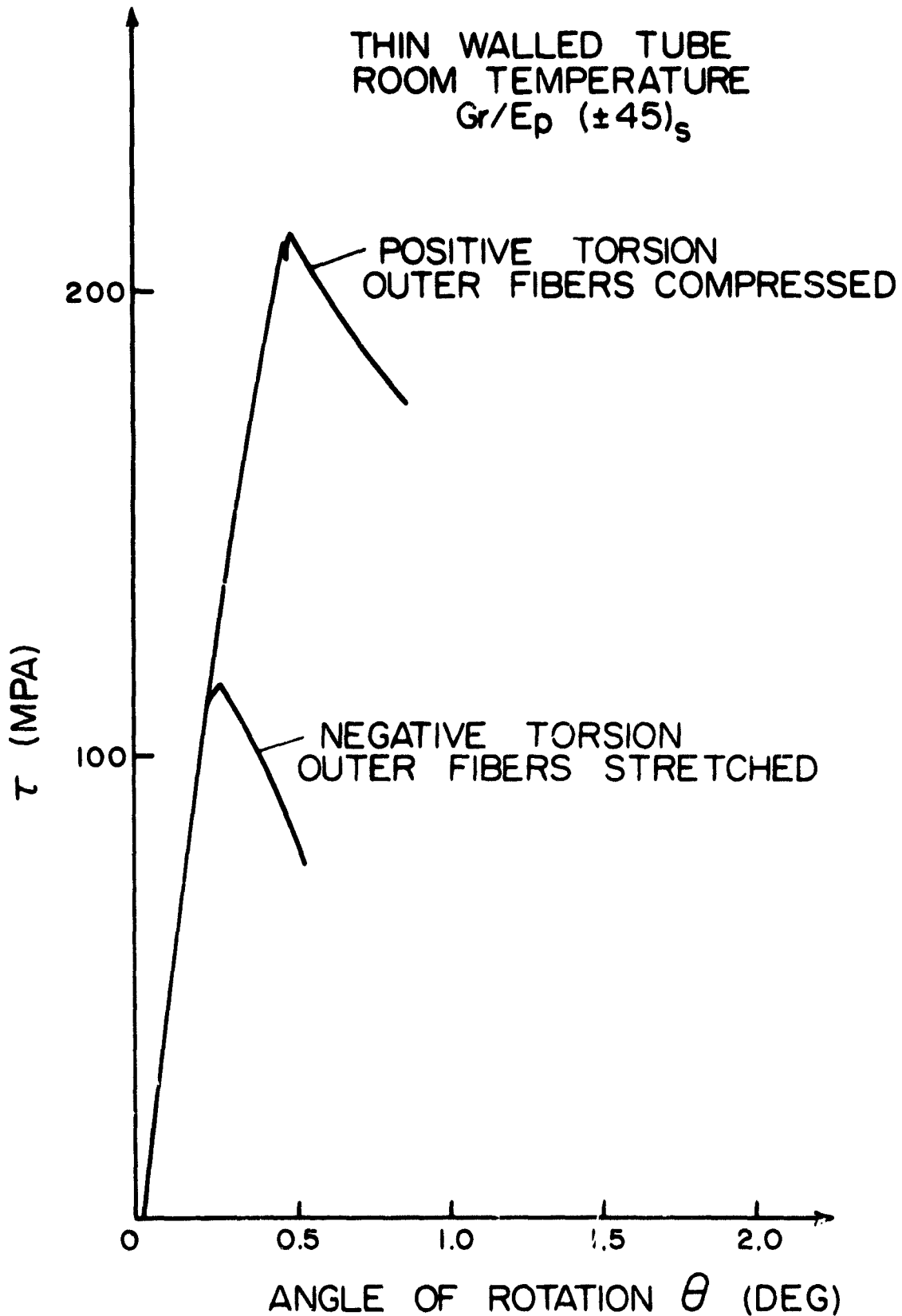
Figure IV-D-2

Effect of Direction of Rotation on Tube Shear Strength

TABLE IV-D-1

TORSION TESTS (ultimate load)

Tube Number	Max. Torque (in-lb)	τ_{max} (MPa)	Remarks
12	+1,120	+180	-------
37	+1,300	+213	-------
38	- 700	-115	-------
39	+1,300	+213	-------
41	- 715	-117	loaded first to +930 in-lbs
42	- 260	--	loaded first to +600 in-lbs
43	- 725	-119	loaded first to +1,000 in-lbs
48	+ 960	+157	-------
Av. Positive Torsion	+1,170	+191	outer fibers compressed
Av. Negative Torsion	- 713	-117	outer fibers stretched

higher when the outer fibers are compressed than when they are stretched. Failures which occur when the outermost fibers are stretched are, therefore, failures in buckling of the inner fibers in compression.

Fracture Appearance:

Figure IV-D-3 shows a photograph of specimens failed in static and fatigue loading (included are two specimens which failed in completely reversed, load-controlled torsional fatigue loading). It is seen that the fractures occur in the gage section by splitting of the plies, and there is some evidence of breakage along the ply bonds. However, no striking differences in appearance are apparent when comparing static with fatigue fractures, neither are there obvious dif-diferences in the appearance of axial versus torsional fatigue fractures. These apparent similarities would seem to complicate failure analysis of static and fatigue fractures of composites.

3. Plans for the Upcoming Period

A new series of tubular specimens will be manufactured. Torsional as well as combined proportional and out-of-phase tests are scheduled. Deformation measurements using the Instron biaxial extensometer are planned to determine the time-dependent behavior of the tubes under combined loading.
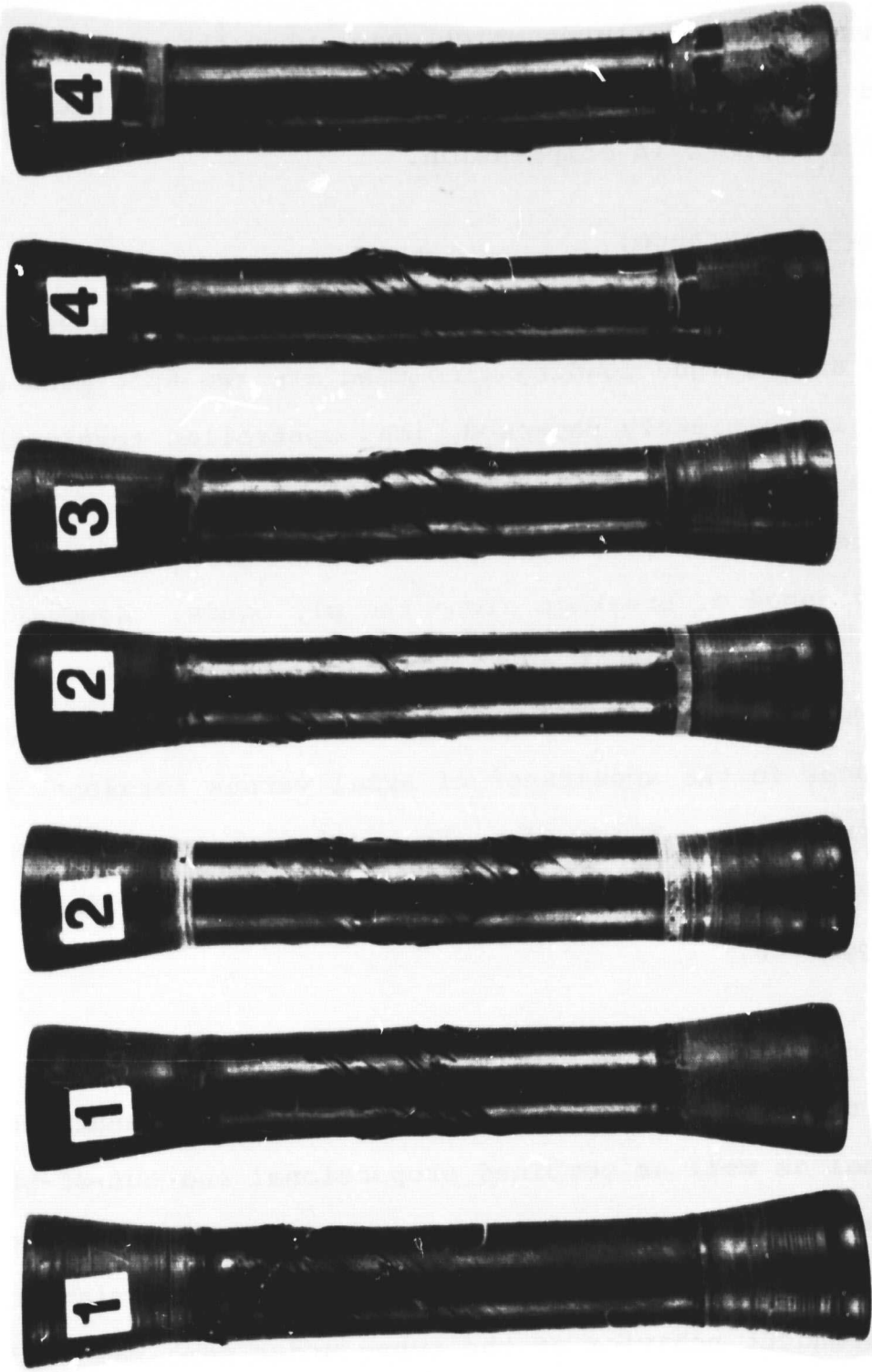
Figure IV-D-3

Fractured Graphite Epoxy Tubes: 1 left, monotonic tension,
1 right, monotonic compression, 2 completely reversed axial
fatigue, 3 monotonic torsion, 4 completely reversed torsional fatigue.

4. References

1) 39th Semi-Annual Progress Report, "Composite Structural Materials", January 1981.

2) 38th Semi-Annual Progress Report, "Composite Structural Materials", June 1980.

3) Marlowe, D. E., Shushinsky, G. F. and Dexter, H.B.,"Elastic Torsional Buckling of Thin-Walled Composite Cylinders", ASTM STP 546, American Society for Testing and Materials, 1974, pp. 84-108.

5. Current Publications or Presentations by Professor Krempl on this Subject

1) "Inelastic Constitutive Equations and Phenomenological ngical Laws of Damage Accumulation for Structural Metals"

   Published in Proc. IUTAM Symposium on Physical Non-linearities in Structural Analysis, J. Hult and J. Lemaitre, editors, Springer Verlag 1981, pp. 117-129.

2) "Some Remarks on the Identification of Damage"

   Presented at the Workshop on Continuum Mechanics Approach to Damage and Life Prediction, General Butler State Lodge, Carrollton, Kentucky, May 1980.

   Published in University of Cincinnati Report, 1981, pp. 134-137.

IV-E ACOUSTIC EMISSION OF COMPOSITE MATERIALS

Senior Investigator: H. A. Scarton[*]

The Acoustic Emission (AE) technique has been shown to be useful in monitoring composite material fracture for both monotonically increasing loads[1,2][**] and fluctuating loads with a large static component[3]. Monotonic and cyclic tests both exhibit consistent acoustic behavior, with the lowest signal amplitude arising from matrix cracking; the intermetidate amplitude with delamination, interfacial fiber matrix debonding and fiber pullout; and the largest amplitude from fiber breakage. The current research dealt with the practical application of the AE technique to monitor the failure process in an actual component part: the Boeing 727 Elevator Actuator Attachment. Discussion of this test occurs in the CAPCOMP section of this report. The remainder of this section deals with the other main activity implemented during the reporting period - the selection of new AE monitoring equipment.

1. Status

In the past, acoustic emission test and data analysis have been performed successfully for composite materials using Dunegan/Endevco 3000 series equipment.

---

[*] RPI graduate students C.-M. Chang and G. Bobal and undergraduate student J. Crowell

[**] Bracketed numbers in this section refer to the references listed on page 156.

2. Progress During the Report Period

Since the Dunegan/Endevco 3000 series equipment, although reliable, is not as "state-of-the-art" as newer acoustic emission equipment, a careful search for replacement acoustic emission equipment was carried out. The subsequent equipment acquisition was funded by a Sloan Foundation grant. The major equipment vendors considered were Dunegan/Endevco, Bruël and Kjaer Instruments , Physical Acoustics Corp. and Acoustic Emission Technology Corp. The latter three vendors were invited to participate in an acoustic emission experiment at RPI. The first vendor was not invited since we were in possession of, and have used, a version of that equipment. Results of the successful AET test are discussed in the CAPCOMP section of this report. Our earlier experiments[1,2,3] were carried out using Dunegan/ Endevco equipment. Our final equipment selection was based upon many factors including: cost, utility, speed, high and "state-of-the-art" technology, and adaptibility to other RPI facilities. A Physical Acoustic Corporation (PAC) Model 3400 Four-Channel Acoustic Emission/Analyzer/Locator was selected. This sophisticated computer-based system represents the most advanced instrument available for the cost. The unit can be coupled to other computers such as the RPI Interactive Computer Graphics System for additional data monitoring.

3. Plans for Upcoming Period

When the new PAC AE equipment arrives, extensive tests applying AE to the diagnosis of various composite materials under load will be carried out. It is also anticipated that the second Boeing 727 elevator actuator attachment, fabricated using revised curing techniques, will be monitored during its ultimate failure test.

4. References

1) Otsuka, H. and H. A. Scarton, "Variation in Acoustic Emission between Graphite and Glass-Epoxy Composites", Journal of Composite Materials, Accepted for publication.

2) Otsuka, H. and H. A. Scarton, "Acoustic Emission Testing of Composite Tensile Specimens", NASA/AFOSR 38th Semi-Annual Report, Composite Structural Materials, June 1980, pp. 133-139.

3) Otsuka, H. and H. A. Scarton, "Acoustic Emission of Composite Materials Undergoing Fatigue", NASA/AFOSR 39th Semi-Annual Report, Composite Structural Materials, January 1981, pp. 167-178.

IV-F VISCOELASTIC CHARACTERIZATION OF IN SITU RESINS AND NEAT RESINS

Senior Investigator: S. S. Sternstein[*]

This project is concerned with those properties of high performance composites which are strongly dependent on the physical properties of the matrix resin. To date, the research has involved the precise viscoelastic characterization of epoxy neat resins, interlaminar failure of composites and the inhomogeneous swelling of and the effects of moisture on composites.

1. Status

The viscoelastic properties of carbon-epoxy laminates (CEL) and neat resins have been studied as a function of temperature, frequency and moisture content. Twelve-ply laminates of various stacking sequences were prepared from prepreg supplied by Fiberite and designated HY-E10408A1E. Disc samples of one inch nominal diameter were cut from master sheets of the laminates and tested in the centro symmetric deflection (CSD) mode as described in the previous report. Briefly, the disc is supported around its perimeter and a central load is applied via a ball bearing nosepiece. Dynamic tests were performed on a Dynastic (T.M.) mechanical spectrometer.

---

[*]RPI graduate students C. Altman, P. Herbert, D. Taggart and P. Yang

2. Progress During the Report Period

The results reported here were conducted at a static load of 3 kg with a superposed 1 kg amplitude load of various frequencies, using the same techniques as developed and described in the earlier periods.

The laminate stacking sequences reported here are as follows:

Nominal Designation	Stacking Sequence
90 degree	$[0/90/0/90/0/90]_s$
45 degree	$[0/45/90/135/0/45]_s$
30 degree	$[0/30/60/90/120/150]_s$

A typical temperature sweep at a constant frequency of 6.5 Hz is shown in Figure IV-F-1 for a 90 degree sample. The storage (or in-phase) modulus M' and loss (or out-phase) modulus M'' are shown versus temperature and indicate clearly the matrix glass transition at about 160°C. Temperature sweeps at various fixed frequencies from 0.1 Hz to 40 Hz are shown in Figure IV-F-2 for M' and Figure IV-F-3 for M''. Defining the glass transition temperature as the temperature of maximum loss (the peak of M'') for each frequency, then one obtains Figure IV-F-4. T_g changes linearly with log frequency about 8°C per decade, and this emphasizes strongly the necessity of obtaining dynamic data at fixed frequency.

The storage and loss modulii are shown versus frequency at constant temperature in Figures IV-F-5 and -6, respectively. When these curves are appropriately shifted
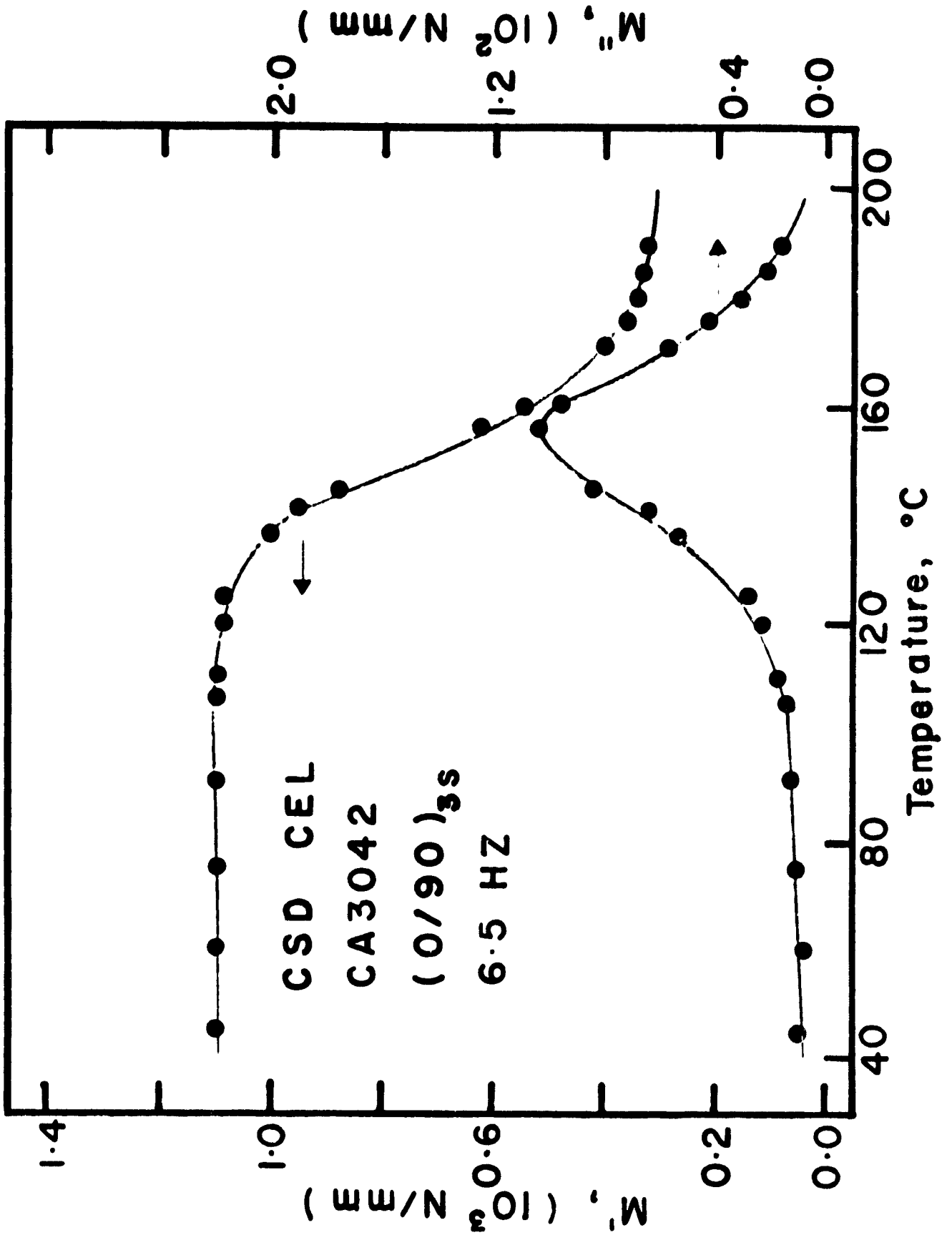
Figure IV-F-1

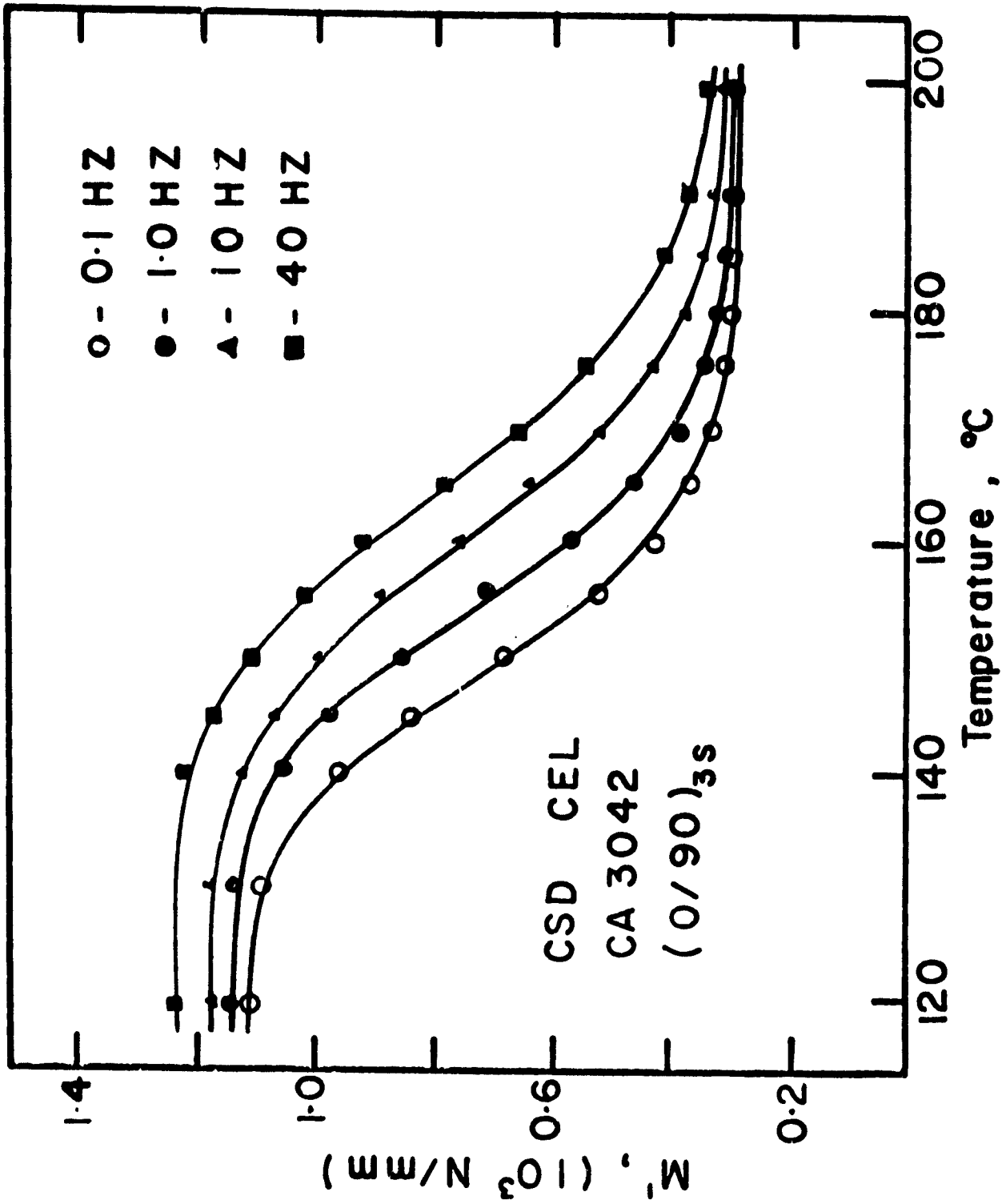Storage and Loss Moduli vs Temperature at Constant Frequency

Figure IV-F-2

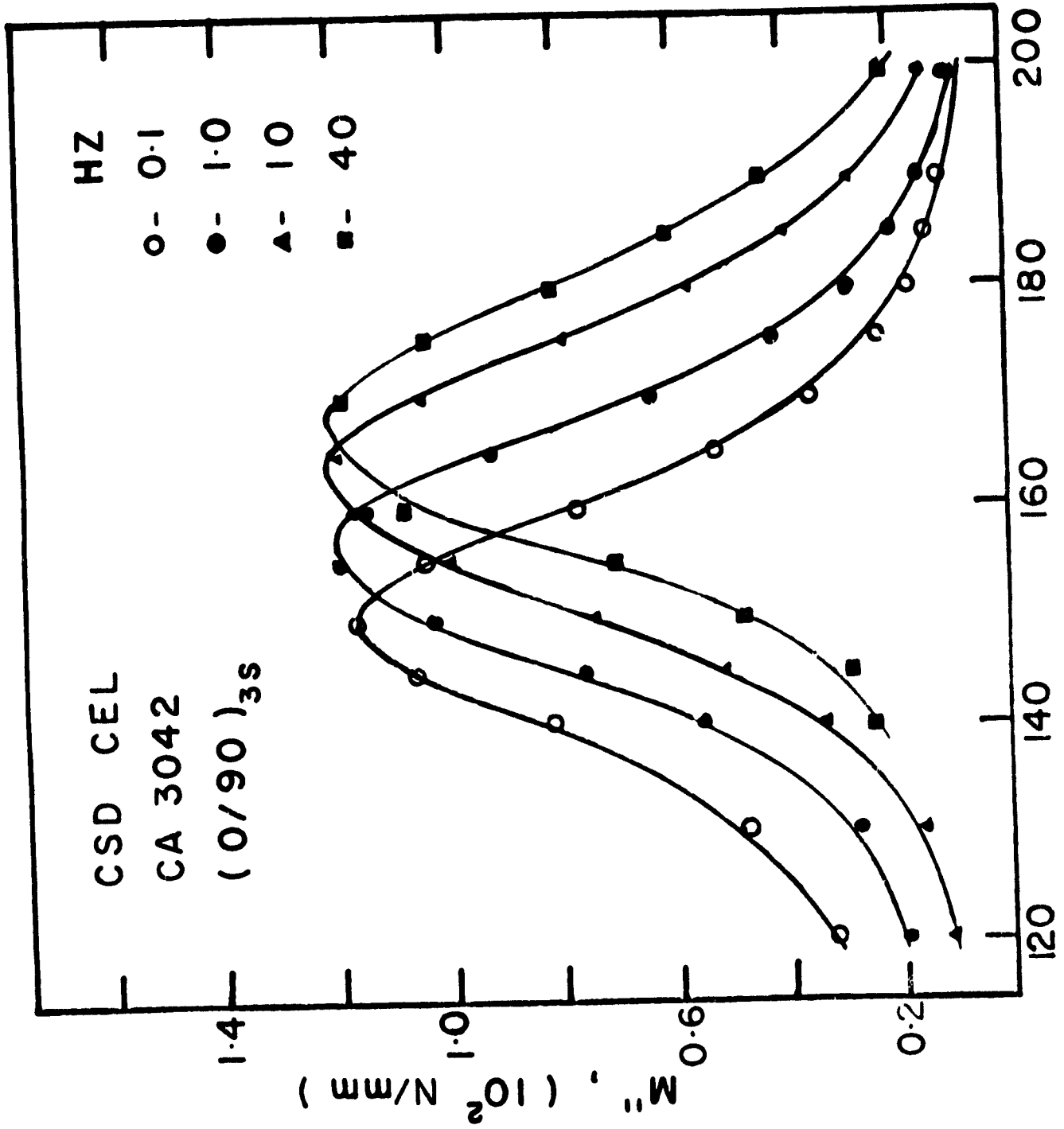Storage Modulus vs Temperature at Various Fixed Frequencies

Figure IV-F-3
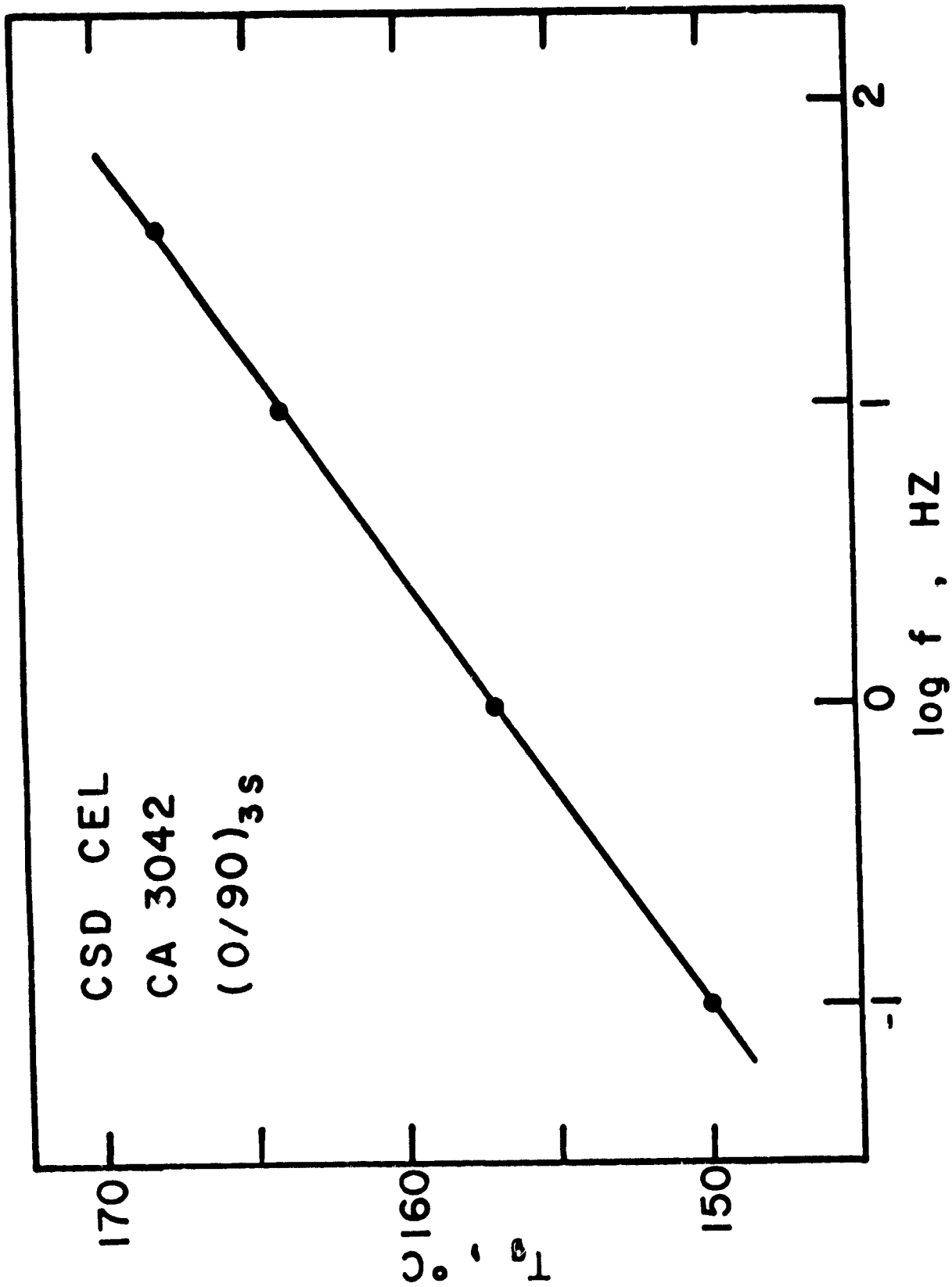Loss Modulus vs Temperature at Various Fixed Frequencies

Figure IV-F-1

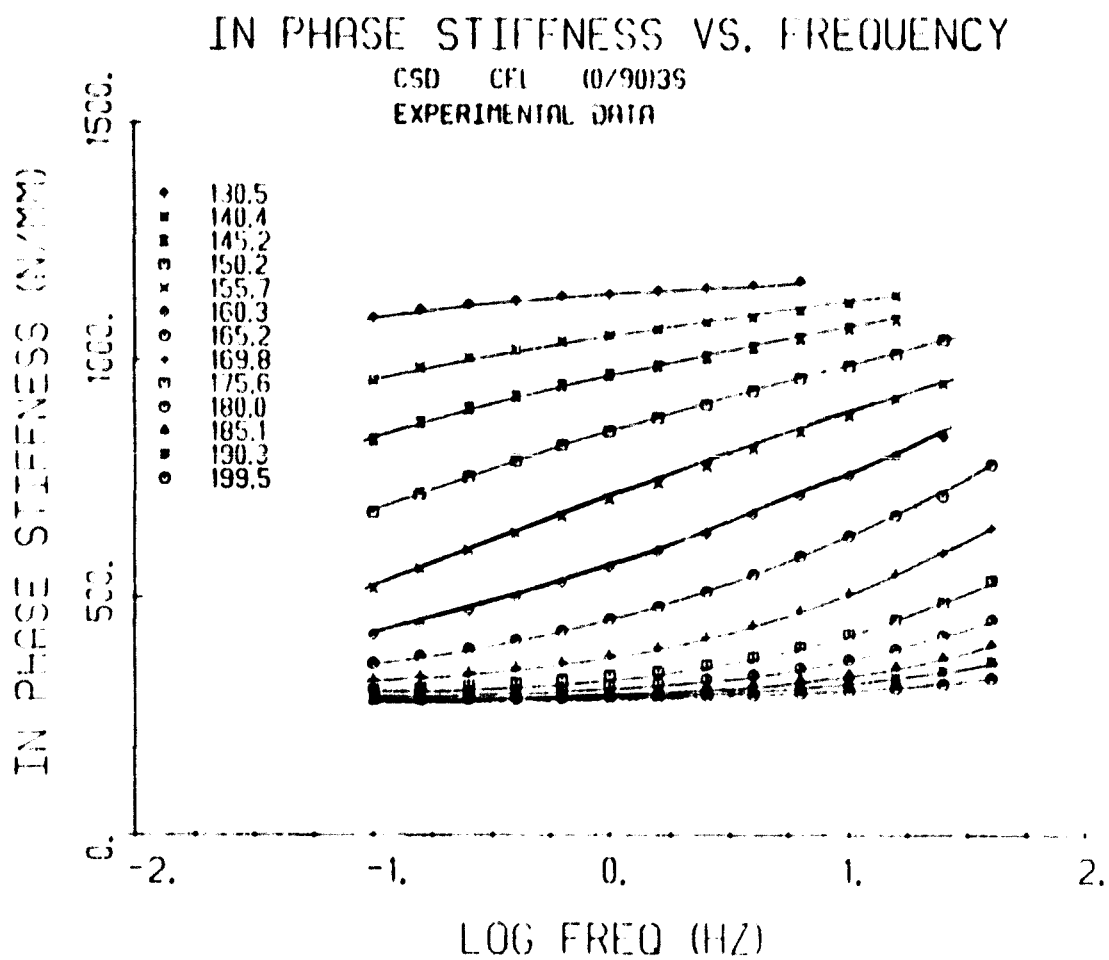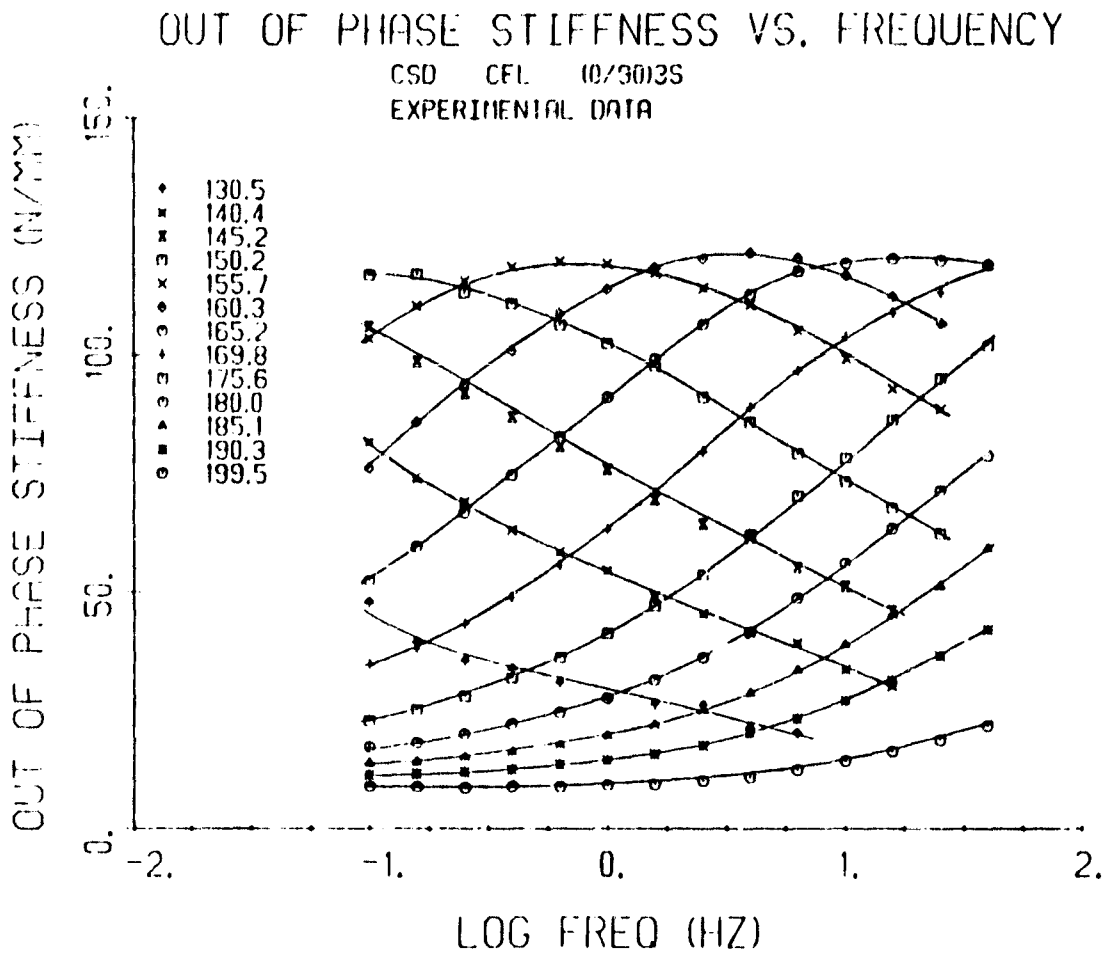Glass Transition Temperature as a Function of Frequency

Figure IV-F-5

164

OUT OF PHASE STIFFNESS VS. FREQUENCY
CSD   CFL   (0/30)3S
EXPERIMENTAL DATA

Figure IV-F-6

horizontally on the log frequency axis, the master curves of Figures IV-F-7 and -9 are obtained. These master curves show clearly that time-temperature superposition is obeyed by the in situ resin. The shift factor required to obtain the master curves is shown versus temperature in Figure IV-F-9. Below about 170°C, the independently obtained shift factors for M' and M'' are identical in value. Above 170°C, the shift factors for M' and M'' are distinct. This is due to the micromechanics of the composite structure which alters the internal stress distribution when one phase (the matrix) softens with respect to the second phase (the fibers) w ch is unaffected by temperature.

It is interesting to note that our preliminary studies on neat resins show that the shift factors for M' and M'' are identical at all temperatures. Thus, the diverging shift factors for M' and M'' is seen only in the composite. This is one reason why torsional braid techniques for polymer resin evaluation can lead to difficulties in interpretation of data. In the torsional braid method, the resin is coated on a supporting glass braid. One would expect that the micromechanics problem presented in this report would be significant.

Experiments have also been performed on laminates having the 30 and 45 degree stacking sequences. Master curves similar to Figures IV-F-7 and -8 have been obtained. When the storage modulus master curves (e.g., Figure IV-F-7) are

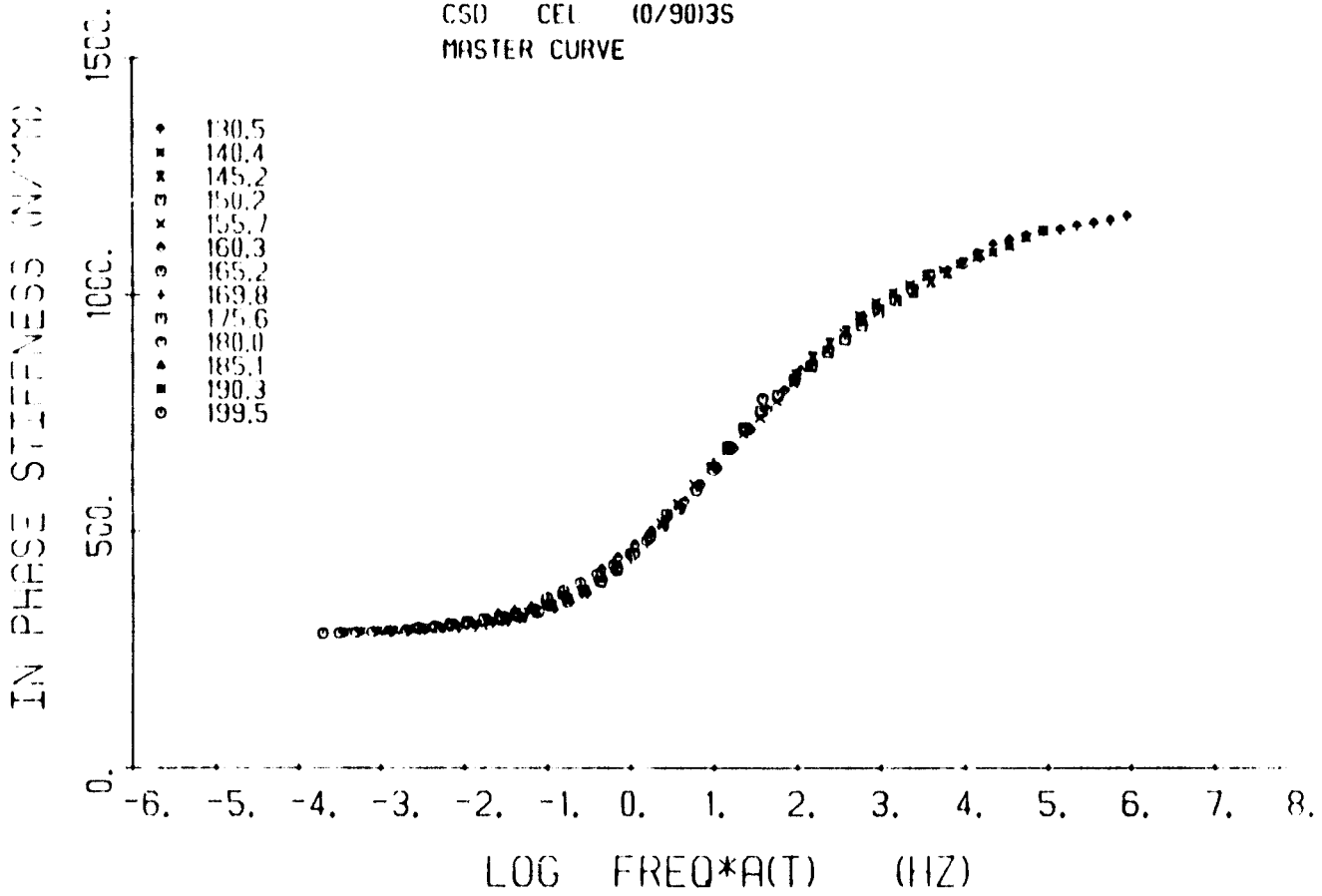IN PHASE STIFFNESS VS. FREQUENCY

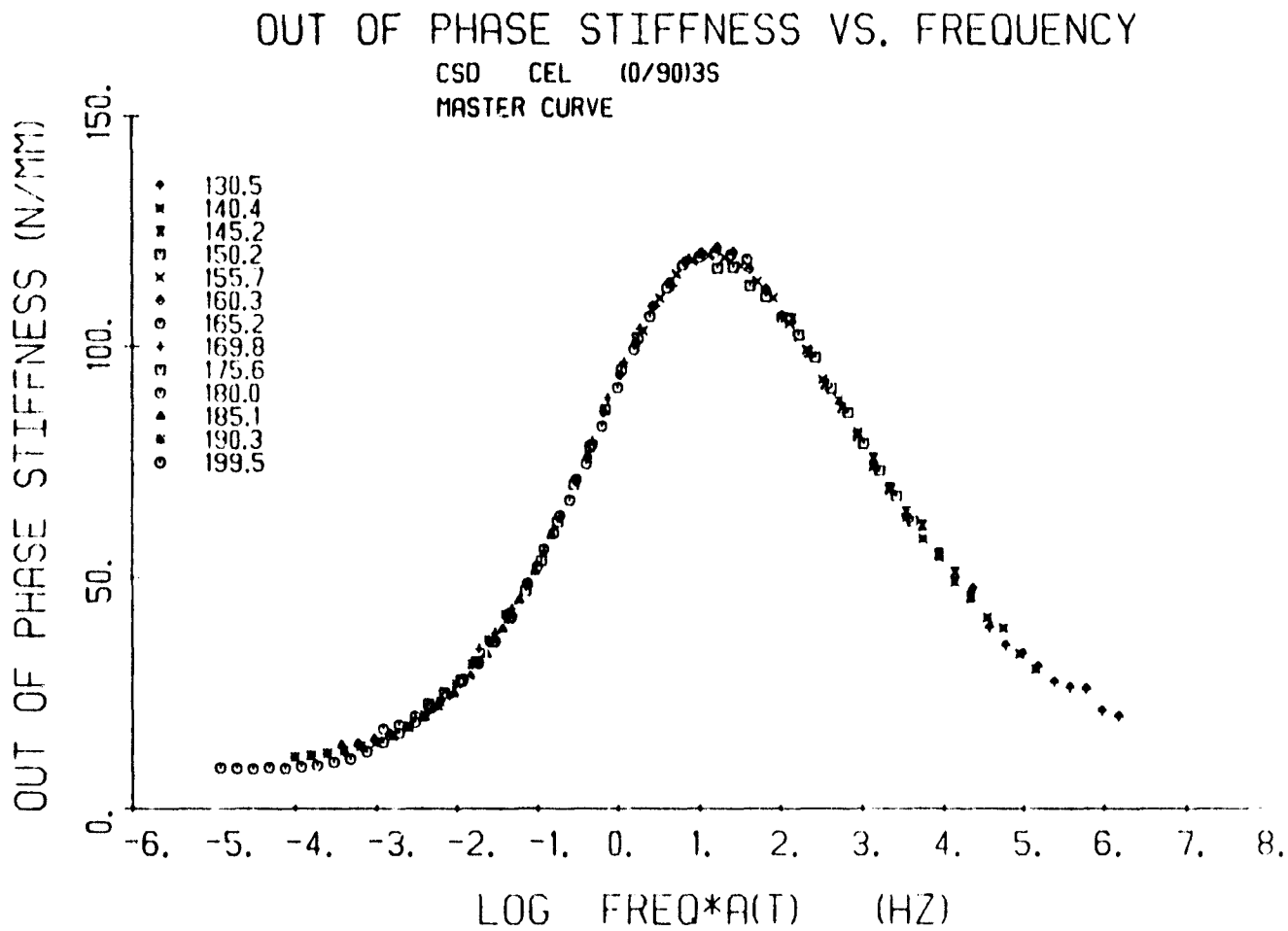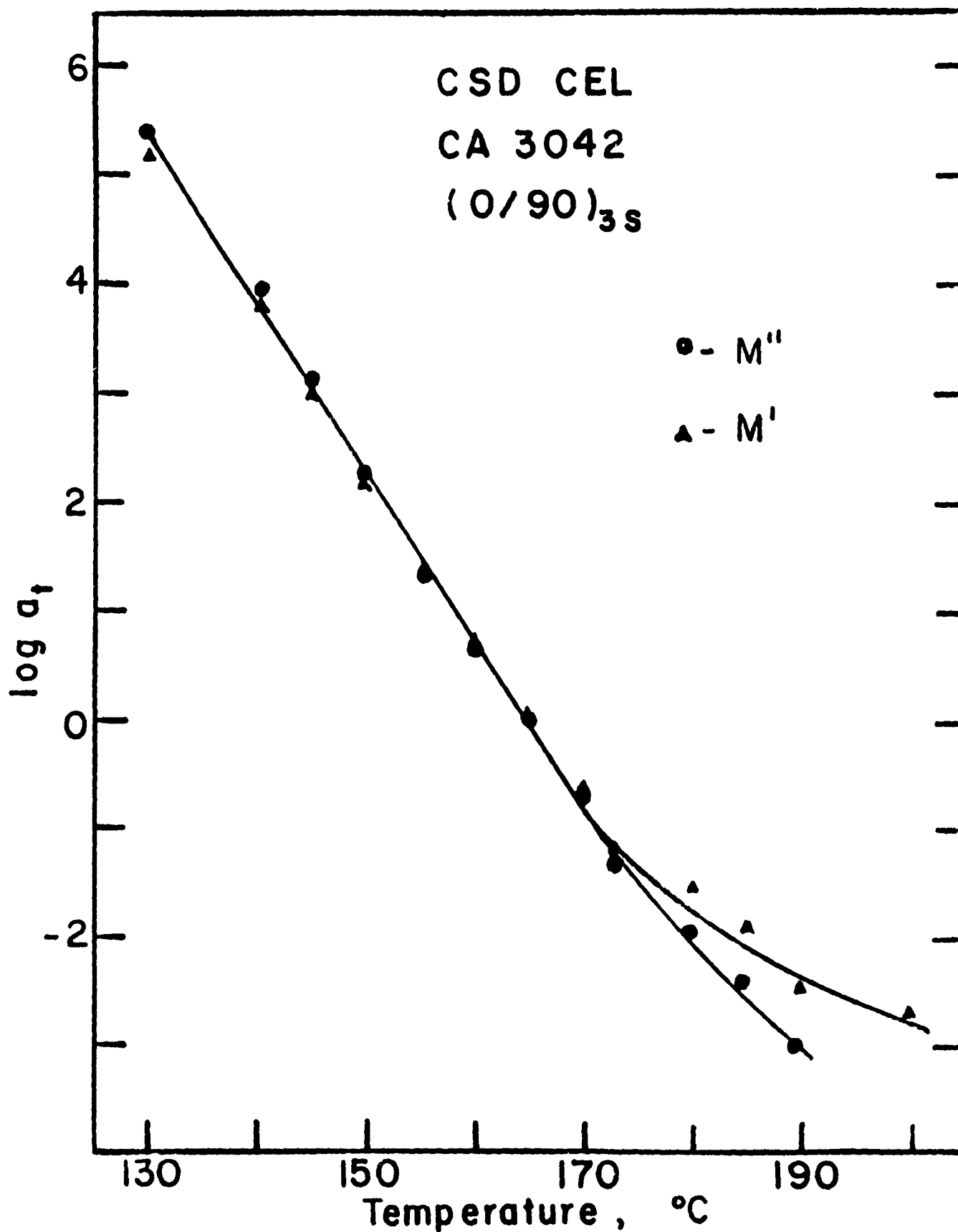CSD   CEL   (0/90)3S

MASTER CURVE

Figure IV-F-7

Figure IV-F-8

Figure IV-F-9

Shift Factor vs Temperature

"scaled" such that the dispersion region low frequency asymp-
tote is set equal to unity, then it is found that all stack-
ing sequency samples (90°, 45° and 30°) fall on a single
curve as shown in Figure IV-F-10.

Similarly, when the loss modulus master curves (e.g.,
Figure IV-F-8) are scaled such that the loss maximum (M'')
is set equal to unity, then all samples fall on a single
curve as shown in Figure IV-F-11.

The similarly scaled epoxy neat resin results are also
shown in Figures IV-F-10 and -11. Except for the high fre-
quency side of the dispersion peak, it appears that the neat
resin behavior is equivalent to that of the in situ resin.
However, the neat resin data in Figures IV-F-10 and -11 were
superposed with respect to a reference temperature of 150°C
(i.e., the temperature at which the shift factor is unity)
whereas the composites were superposed with respect to a
reference temperature of 165°C. Thus, the dispersion char-
acteristics of the neat resin and in situ resin are compar-
able, but the in situ resin has a glass transition tempera-
ture some 12°C higher than that of the neat resin.

Finally, the effects of moisture on the glass transition
temperature of in situ resin can be conveniently studied
using mechanical spectroscopy. The loss moduli (M'') for
samples containing 0.7% and 0.3% water as well as a dry sam-
ple are shown in Figure IV-F-12. The change in glass transi-
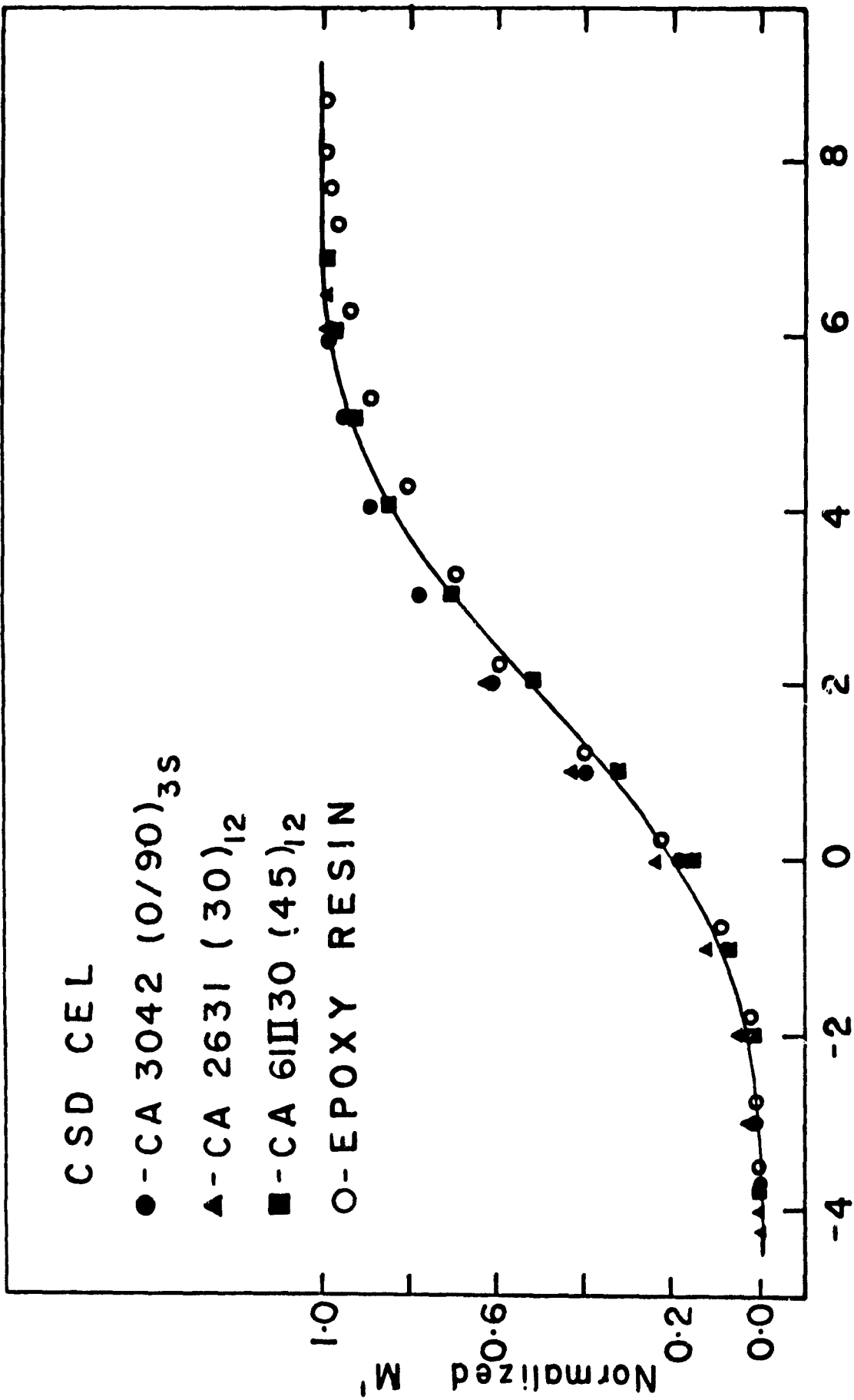tion is very significant and has been found to be reversible.

Figure IV-F-10
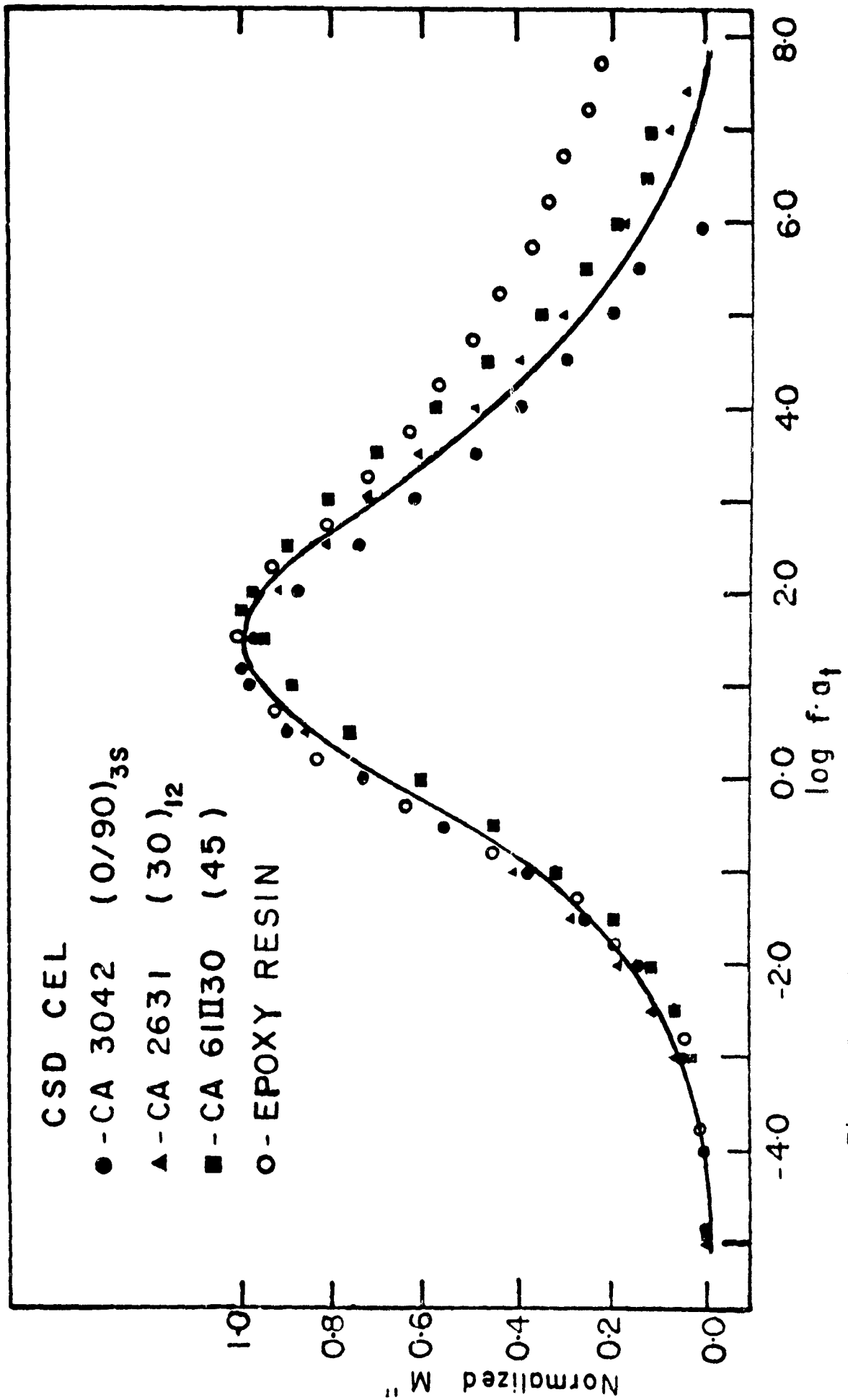Normalized Storage Modulus vs Frequency

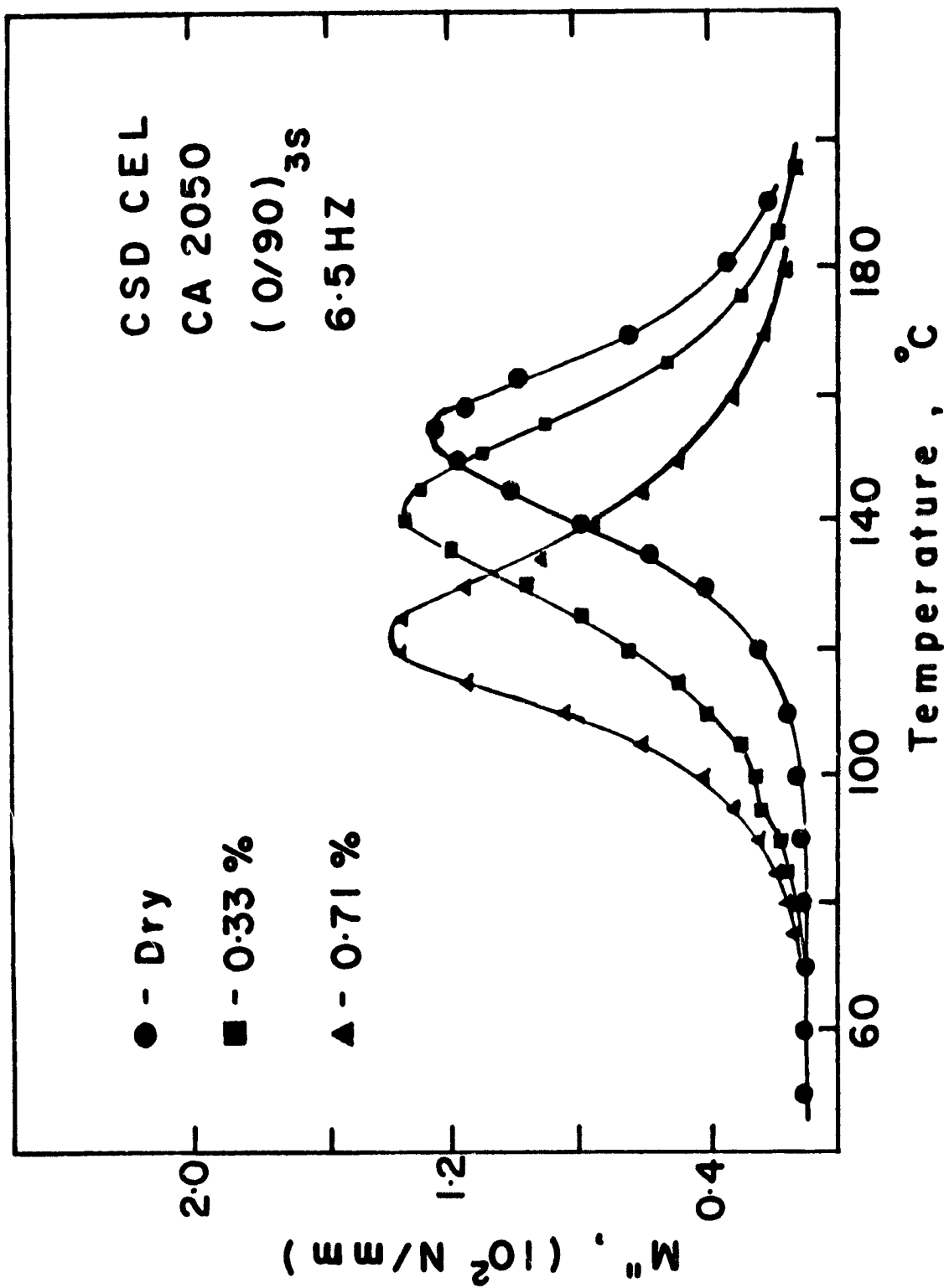Figure IV-F-11   Normalized Loss Modulus vs Frequency

Figure IV-F-12

Loss Modulus vs Temperature

3. Plans for the Upcoming Period

Similar experiments to those reported here are being conducted on other resins such as Narmco 5208 and will be reported on during the next period.

4. Current Publications or Presentations by Professor Sternstein on this Subject

1) "Delamination Failure in Carbon-Epoxy Laminates"

   Presented at the Society of Rheology Meeting, Williamsburg, Virginia, February 23-25, 1981.

2) "Viscoelastic Characterization of Solids"

   Presented at the National A.C.S. meeting, Atlanta, Georgia, March 30, 1981.

PART V

PERSONNEL

AUTHOR INDEX

PERSONNEL

Senior Investigators

Brunelle, E. J., Jr., Sc.D.
(Aeroelastic and structural
design and analysis, applied
mechanics of composite
structures, research)*

Associate Professor of
Aeronautical Engineering

Bundy, F., Ph.D.
(Physical chemistry and
CAPGLIDE)*

Research Professor of Materials
Engineering

Das, P. K., Ph. D.
(Non-destructive evalua-
tion, research)*

Professor of Electrical and
Systems Engineering

Diefendorf, R. J., Ph.D.
(Fabrication, CAPGLIDE,
fiber behavior, research)*

Professor of Materials
Engineering

Feeser, L. J., Ph.D.
(Computer applications and
graphics, computer aided
design, optimization)*

Professor of Civil Engineering

Goetschel, D. B., Ph.D.
(Structural analysis and
design, CAPCOMP)*

Assistant Professor of
Mechanical Engineering

Hagerup, H. J., Ph.D.
(Aerodynamics, configura-
tion, pilot accommodation,
CAPGLIDE)*

Associate Professor of
Aeronautical Engineering

Hoff, N. J., Ph.D.
(Structural design and
analysis, CAPGLIDE)*

John A. Clark and Edward T.
Crossan Professor of Engineer-
ing

Krempl, E., Dr.Ing.
(Fatigue studies,
research)*

Professor of Mechanics and
Director of Cyclic Strain
Laboratory

Scarton, H., Ph.D.
(Acoustic emission NDE)*

Associate Professor of Mechan-
ical Engineering and Mechanics

---

*Fields of Speciality

Senior Investigators

Shephard, M., Ph.D.
(Computer graphics, finite
element methods)*

Assistant Professor of Civil
Engineering

Sternstein, S. S., Ph.D.
(Failure analysis, matrix
behavior, research)*

William Weightman Walker
Professor of Polymer Engineer-
ing

Tiersten, H. F., Ph.D.
(Non-destructive evaluation
theory, research)*

Professor of Mechanics

Research Staff

Manager & Master Technician, Composites Laboratory
Paedelt, Volker

Research Associate
Carlsson, Leif, Ph.⌐

Graduate Assistants

Altman, Carl, B.A.	Niu, Tyan-Min, M.S.
Bobal, G., M.E.	Oyibo, Gabriel, M.S.
Chang, Chi-Min, M.S.	Taggart, David, B.S.
Chen, Shu-Ping, B.S.	Uzo, Cyprian, B.S.
Helmer, James, B.S.	Yang, Phillip, B.S.
Herbert, Paul, B.S.	Valicenti, Raymond, B.S.
Kim, Wonsub, B.S.	Winckler, Steven, B.S.
Lumban Tobing, Frida, M.S.	Yehia, Nabil, M.S.
Muser, Christoph, Dipl.Mech.Ing.	

Undergraduate Assistants - Seniors

Beck, William	Dalzell, Scott
Bidlack, Thimothy	Davidson, Thomas
Brown, Maureen	DeTaranto, Francis
Burnett, Eric	Ellis, Craig
Cawthorne, Matthew	Gorman, John
Crowell, John	Grant, Peter

---

*Fields of Speciality

Undergraduate - Seniors (continued)

Kappeyne Van Decoppello, Michael

Merritt, Mark

Morizio, Thomas

Murawski, Michael

Ryan, Kenneth

Thomas, John

Vinopal, Timothy

Ward, Stephen

Werner, Ross

Wetzel, Eric

Undergraduate - Juniors

Applewhite, Keith

Argintar, Donald

Bertolazzi, Andrew

Blake, William

Bristol, Brian, P.

Cackett, Matthew

Cox, Mary

Fachon, Eric

Fairchild, Kendall

Fisher, Steven

Gray, Bruce, M.

Ives, Douglas

Melendez, Hermenegildo

Niederer, Melvin

Novoa, Raul

Snyder, David

Staniorski, Anthony

Vaney, Phillippe R.

Watrous, Donald

Undergraduate - Sophomore

DeMint, Thomas

Ficarra, Robert

Kalmes, Donald

Kuntsmann, Debra

Lafreniere, Suzanne

Michael, Thomas

Symmes, Jeffrey

AUTHOR INDEX